TECHNICAL NOTE

D-636

A WIND-TUNNEL INVESTIGATION OF A TRANSONIC-TRANSPORT CONFIGURATION UTILIZING DRAG-REDUCING DEVICES AT MACH NUMBERS FROM 0.20 TO 1.03

By Donald L. Loving

Langley Research Center
Langley Field, Va.

NATIONAL AERONAUTICS AND SPACE ADMINISTRATION

WASHINGTON

March 1961

NATIONAL AERONAUTICS AND SPACE ADMINISTRATION

TECHNICAL NOTE D-636

A WIND-TUNNEL INVESTIGATION OF A TRANSONIC-TRANSPORT CONFIGURATION UTILIZING DRAG-REDUCING DEVICES AT MACH NUMBERS FROM 0.20 TO 1.03

By Donald L. Loving

SUMMARY

The static longitudinal stability and control and lateral characteristics of a transonic-transport model, incorporating recent drag-reducing devices, has been investigated in the Langley 8-foot transonic pressure tunnel. The wing was cambered, had a thickened root and a taper ratio of 0.3. Wing sweepback angles of 45° and 40° were investigated with corresponding aspect ratios of 7 and 8, respectively. Modifications to the model for reducing the drag were: a forward fuselage addition and special bodies (four big enough to house jet engines) added to the upper surface of the wing. Other components and changes investigated included an empennage, a wing-tip body, wing fences, wing trailing-edge flaps, horizontal-tail settings, and wing dihedral angle. The investigation covered the Mach number range from 0.20 to 1.03 for the angle-of-attack range from -5° to 15.4°, and a sideslip angle of -5°, in the Reynolds number range from 0.52×10^6 to 1.94×10^6 based on the wing mean aerodynamic chord.

The various fuselage and wing additions delayed the drag-rise Mach number and greatly reduced the drag beyond the drag rise. The wing bodies markedly alleviated unstable pitch tendencies throughout the test Mach number range. At low landing speeds, the wing bodies exhibited little interference with the ability of trailing-edge flaps to increase the lift near maximum lift coefficient; and the use of fences greatly reduced the severe longitudinal instability trend at landing attitudes. The model with a 6° dihedral angle exhibited positive lateral and directional stability characteristics in the presence of the fuselage and wing additions. An increase in drag-rise Mach number associated with the fuselage and wing additions on the 40° sweptback wing combination was similar to that for the comparable 45° combination. These additions did, however, reduce the drag of the 40° sweptback configurations more than the 45° configurations in the transonic speed range.

INTRODUCTION

Increased cruise speeds can result in a number of important advantages for jet-propelled transports. Presently, for these airplanes, cruise speed is limited by the severe drag rise encountered as the speed of sound is approached. This drag rise is primarily associated with shock-induced boundary-layer separation, particularly at lifting conditions, on the upper surface of the relatively thick cambered wings generally used in such airplane design. Of the numerous investigations made toward reducing the shock-induced boundary-layer separation on the wing, the methods for reducing the strength of the shock wave, with a resulting alleviation of separation, have provided the largest reductions of shock-induced separation. These methods include wing modifications, fuselage changes, and additions to the wing. A brief review of these investigations is given in reference 1.

The present investigation was made to determine the aerodynamic characteristics at transonic speeds that could be obtained for a new transport design incorporating several of the latest drag-reducing devices. This transport configuration was investigated with wing aspect ratios of 7 and 8 for wing sweepback angles of 45° and 40°, respectively. Special bodies, similar to those of reference 2 were added to the upper surface of the wing. Four of these wing bodies were made large enough to house jet engines. A forward fuselage addition, based on the information of reference 3, and an empennage made up the complete configuration. The wing was cambered on the basis of linear theory; and most of the results were obtained with the wing swept back 45°. This amount of sweepback is considerably greater than that on current transports. The results of reference 2 indicated that significant alleviation of the pitch-up (a nonlinearity of the pitching-moment coefficient curve indicating instability) of sweptback wings was provided by special bodies added to the wing. This alleviation considerably relaxes the limitation on wing sweep previously imposed by the instability trend. The effects of the various primary components and additions on the aerodynamic characteristics of the model were determined separately. The effects of wing fences, wing dihedral, wing trailing-edge flaps, and changes in horizontal-tail settings also have been explored. Configurations were tested primarily in pitch with various horizontal-tail settings and in yaw at a single sideslip angle. The Mach number range extended from 0.20 to 1.03.

COEFFICIENTS AND SYMBOLS

The stability system of axes used for the presentation of the data, together with an indication of the positive direction of forces, moments, and angles, is presented in figure 1. All moments are referred to the 37.5-percent-chord point of the mean aerodynamic chord.

A	cross-sectional area, normal to longitudinal axis
a	vertical transfer distance from fuselage center line to radius center of fuselage addition
b	wing span
c	chord of wing parallel to free stream
$\bar{c}$	mean aerodynamic chord of wing, $\frac{2}{S}\int_0^{b/2} c^2 dy$
D	diameter
M	Mach number
q	free-stream dynamic pressure, $\frac{\rho V^2}{2}$
R	Reynolds number based on $\bar{c}$
r, r_1, r_2	radii of fuselage, fuselage additions, and wing bodies, respectively
S	wing planform area
t	thickness of wing
V	free-stream velocity
x, x_1	distance rearward either from model nose or reference origin, and from wing leading edge along center line of wing body, respectively
y	distance spanwise from fuselage center line
z, z_1	distance vertically from reference origin and center line of wing body, respectively
α	angle of attack of fuselage reference line
β	angle of sideslip of fuselage reference line
Γ	angle of dihedral referred to horizontal
δ_f	trailing-edge flap angle of deflection relative to wing lower surface reference line (see fig. 9)

ϵ	effective downwash angle
Λ	angle of sweepback of wing quarter-chord line
ρ	free-stream air density
i_t	angle of incidence of horizontal tail
C_D	drag coefficient, $\frac{\text{Drag}}{qS}$
C_L	lift coefficient, $\frac{\text{Lift}}{qS}$
C_m	pitching-moment coefficient, $\frac{\text{Pitching moment}}{qS\bar{c}}$
C_l	rolling-moment coefficient, $\frac{\text{Rolling moment}}{qSb}$
C_n	yawing-moment coefficient, $\frac{\text{Yawing moment}}{qSb}$
C_Y	lateral-force coefficient, $\frac{\text{Lateral force}}{qS}$
$\frac{L}{D}$	lift-drag ratio
$C_{L,(L/D)_{max}}$	lift coefficient corresponding to $\left(\frac{L}{D}\right)_{max}$
C_{L_α}	lift-curve slope, $\frac{\partial C_L}{\partial \alpha}$ per degree
$C_{m_{i_t}}$	stabilizer effectiveness parameter, $\frac{\partial C_m}{\partial i_t}$ per degree
$C_{m_{C_L}}$	static-longitudinal-stability parameter or stability level, $\frac{\partial C_m}{\partial C_L}$

C_{l_β} effective-dihedral derivative, $\frac{\partial C_l}{\partial \beta}$ per degree

C_{n_β} directional-stability derivative, $\frac{\partial C_n}{\partial \beta}$ per degree

C_{Y_β} lateral-force derivative, $\frac{\partial C_Y}{\partial \beta}$ per degree

$\frac{\partial \epsilon}{\partial \alpha}$ effective downwash, per degree

Subscripts:

max maximum

min minimum

Model components:

E empennage (horizontal tail and vertical tail)

F fuselage

F_A original fuselage addition

F_{A_a} modified fuselage addition

W wing

W_B wing bodies

APPARATUS AND MODELS

Tunnel

The investigation was conducted in the Langley 8-foot transonic pressure tunnel, which is a rectangular, slotted-throat, single-return wind tunnel. This tunnel is designed to obtain aerodynamic data through the speed of sound without the usual effects of choking and blockage. The tunnel operates at stagnation pressures ranging from 0.25 to 2.00 times atmospheric pressure. A more complete description of the tunnel can be found in reference 4.

Model

A three-view drawing of the basic model is given as figure 2. Photographs of the model without and with drag-reducing devices on the fuselage and wing are shown as figure 3. The wing is mounted in a low position on the fuselage, and an all-movable horizontal tail is located on the center line of the fuselage. A vertical tail is located such that its maximum cross-sectional thickness is slightly forward of that for the horizontal tail. The geometric characteristics of the model are presented in figure 2. Consideration of the area rule of reference 5 was given throughout the entire design, and the axial development of the cross-sectional area distribution for the complete basic model is shown in figure 4. The construction of the model was such that various components could be tested in combination.

Fuselage.- The basic fuselage has an overall extended fineness ratio of approximately 13. This fuselage, truncated to accommodate a sting support, has a fineness ratio of 11.6 and is divided into three integral longitudinal sections, for which ordinates are given in table I. The forward fuselage section has a fineness ratio of 3. The middle section is cylindrical, beginning approximately 4 inches ahead of the leading edge of the wing-fuselage juncture and extending rearward 5.6 fuselage maximum diameters. The rear portion of the fuselage has a fineness ratio of about 3 (based on the truncated length) and is indented to provide improvements of the total area development in the region of the vertical and horizontal tails. The maximum diameter of the basic fuselage is 4.06 inches. The ratio of the fuselage maximum cross-sectional area to the wing planform area is 0.045. Other details and dimensions are given in figure 2.

Fuselage additions.- The fuselage additions investigated were designed to be concentrated on the upper forward part of the fuselage. Their purpose is to provide a practical means of obtaining a desired fuselage camber, as well as improving the area distribution of the configuration, as pointed out in reference 3. The cross sections were laid out as shown in figure 5. As also indicated in figure 5, these components will be referred to as the original and modified additions. The original addition was tested on the fuselage with the wing at dihedral angles of 0° and 6°. The modified addition was tested on the fuselage with the wing at a dihedral angle of 6°. The shape of the original fuselage addition was determined by the relatively simple procedure outlined in reference 3 for a thick wing. The shape of the addition arrived at by this procedure provides approximately the most satisfactory improvements of the area developments for a Mach number of the order of 1.1. The maximum height of this original addition is approximately 0.28 times the fuselage maximum diameter. Further details of the design of this original addition are shown in figure 5.

The modified addition was obtained by decreasing the cross-sectional areas of the original addition by 30 percent. It was thought that the appearance of the configuration could be improved by such a measure while at the same time not too adversely affecting the drag reduction obtained from use of the original fuselage addition.

Wing.- The wing is twisted and cambered to obtain a lift distribution which should provide good high-speed characteristics at a lift coefficient of about 0.3. The camber lines over the inboard sections were designed for a Mach number of 1.2 by use of the supersonic theory of reference 6. It was considered that at high free-stream subsonic speeds the local velocities will be supersonic over the relatively thick inboard sections of the wing. The method used in reference 7 to design wing camber for sonic velocity was used in the design of the extreme outboard sections of the wing. Camber lines between the two regions of the wing were faired together in the vicinity of the 70-percent-semispan station. The resulting streamwise camber ordinates are shown in figure 6. The wing was given an additional amount of twist to add to the calculated spanwise distribution of twist to offset anticipated changes in section incidence angles due to wing bending under the design static load condition (C_L = 0.3; M = 0.9; and q = 700 lb/sq ft). This wing, as originally designed, had 40° sweepback of the 0.25 chord line, an aspect ratio of 8, and a taper ratio of 0.3. The airfoil sections parallel to the free stream were the NACA 64A series. The wing thickness ratio streamwise varied linearly from 0.12 at the root to 0.08 at the 0.50-semispan station and remained 0.08 from that station to the tip. The sweepback angle of this wing was increased to 45° for most of the investigation. This increase was accomplished simply by rotating the 40° sweptback wing about the intersection of the 0.50 chord line and the fuselage center line until the 0.25 chord line was swept back 45°. The following dimensional characteristics evolved: aspect ratio is about 7, which is approximately the value for most current transports; taper ratio is still 0.3; the wing thickness ratio varies from 0.115 at the root to approximately 0.074 at the midsemispan station with a thickness of 0.074 from that station to the tip. The variation of thickness ratio with semispan station is shown in figure 7. Also shown in figure 7 is the twist distribution adjusted for deflection due to load, which was used for the 40° sweptback wing construction, as it appears after the wing was swept back to 45°. The forward part of the wing tip was rounded off, in the plane of the wing, to minimize the effect of the wing-tip shock wave.

Provision was made for the wing to be tested at angles of incidence of 0° and 2°. The investigation, however, was made primarily with the wing at an angle of incidence of 2°. A number of configurations were tested at the beginning of the investigation with the wing at a dihedral angle of 0°. Most of the investigation, however, was made with the wing

set at a dihedral angle of 6°. The purpose of this modification was to provide needed additional lateral stability and to ensure more satisfactory ground clearance for take-off and landing. Other details of the wing are shown in figure 2.

Wing bodies.- As a practical means of significantly delaying the onset of shock-induced boundary-layer separation on the outer sections at lifting conditions, a series of six special bodies were added to the upper surface of the wing. These bodies, which will be referred to as wing bodies, are similar to those reported in reference 2. The wing bodies are entirely above the wing, as shown in the cross sections in figure 8, and extend from near the leading edge of the wing to beyond the trailing edge. These bodies were yawed out 3° by rotating the center line of the body about the wing trailing edge. Each body was initially circular in cross section. When these bodies were mounted on the wing, the maximum body radius was placed at the trailing edge in such a way that the distance from the wing surface to the center of the cross section is about 0.10 inch less than the maximum radius. (See fig. 8.) The lower portion of the bodies is faired to match the contour of the airfoil sections. The center line of the bodies is tilted up, at the rear, from 5° to 7.5° relative to the local chord line. The four inner bodies, located at the 0.33- and 0.57-semispan stations, have been made sufficiently large to enclose jet engines. The maximum diameter of these bodies is equal to 22.6-percent mean aerodynamic chord. The afterbodies extend 2.5 maximum diameters downstream of the trailing edge and are truncated to simulate a jet exit. Air inlets for engines placed in these bodies would be on the lower surface of the wing. Inlets, however, are not incorporated in any of the configurations investigated. The two outboard bodies are located at the 0.80-semispan station. The maximum diameter is equal to 15.5 percent mean aerodynamic chord. These wing bodies are ogival in shape and have an afterbody fineness ratio of 3.63.

During the investigation, another smaller body was placed at the tip of the wing in a manner very similar to the inboard bodies. The forebody shape was determined by the contour of the wing tip. Dimensions of this body are given in figure 8. The purpose of the wing-tip body is to utilize the configuration shock that extends out beyond the wing tip at transonic speeds. It was reasoned that the pressure rise behind the configuration shock should act on the converging afterpart of the body and produce a small force in the thrust direction. At the same time the wing-tip body will provide an end-plate effect. The radii of all wing bodies are given in table II.

Fences.- Chordwise wing fences were located from the wing leading edge rearward along the forward portion of the six wing bodies. It was intended that these fences should provide additional improvements in lift and stability at the higher angles of attack and low speeds by alleviating the pitch-up characteristics of the sweptback wing encountered

during landing conditions. These fences have a maximum height of approximately 0.25 inch and are faired tangent to the top of the wing bodies, as shown in figure 8. The forward portion of each fence was angled out approximately 6° with the free stream. To the rear, they curved gently to become alined with the center line of the wing bodies (which were yawed out at 3°, as mentioned earlier). (See fig. 8 and table II.)

Flaps.- Two sets of plain trailing-edge flaps were investigated on the wing and in combination with the six wing bodies with and without fences. One set covered the inboard span of the wing from 0.077 semispan to 0.33 semispan. (It should be noted that the fuselage maximum diameter extends to 0.103 semispan.) The second set extended the region covered by the first set of flaps out to the 0.57-semispan location. The chords of the flaps are 0.25 local wing chord. The flap deflection angle measured relative to the wing lower surface reference line and perpendicular to the wing trailing edge is 30°. Along a line parallel to the fuselage plane of symmetry, this flap deflection is approximately 25°. A sketch of the flaps and the pertinent dimensions are given in figure 9.

Empennage.- An all-movable horizontal tail with NACA 65A006 airfoil sections, streamwise, is mounted on the fuselage center line. The 0.25 chord line is swept back 45°. The aspect ratio is 3.0, the taper ratio is 0.3, and the tail volume ratio is 0.45. Horizontal-tail incidences were accomplished by pivoting the horizontal tail about a line approximately through the 0.145 mean aerodynamic chord point of the horizontal tail. A sketch of this tail is shown in figure 2.

The vertical tail was not deflected during the investigation. The 0.25 chord line is swept back 45°. The aspect ratio is 1.5 and the taper ratio is 0.26. As in the case of the horizontal tail, NACA 65A006 airfoil sections, streamwise, are used. This vertical tail is located slightly forward on the fuselage relative to the horizontal tail to improve the total longitudinal area developments. A sketch of the vertical tail is shown in figure 2.

TESTS

Reynolds Number

The investigation was conducted over a range of Reynolds numbers. In order not to exceed the design strength of the model wing, limits were imposed on the maximum Reynolds number at which the model could be tested safely for the different phases of the investigation. At test conditions that generally would permit the determination of maximum values of lift-drag ratio, the average Reynolds number, based on the

wing mean aerodynamic chord, varied from 1.45×10^6 at a Mach number of 0.6 to 1.85×10^6 at a Mach number of 1.03. Some performance data were obtained at Mach numbers of 0.2 and 0.4 at Reynolds numbers extending from 0.55×10^6 to 1.05×10^6. These data are included among the basic data but not in the analysis figures. Data at $M = 0.6$ generally reflect conditions at these lower speeds. In the stability and control phase, during which data were obtained to cover adequately the high-lift range at low speeds and the pitch-up range at high speeds, the average Reynolds number varied from 1.4×10^6 at a Mach number of 0.2 to 0.9×10^6 at a Mach number of 1.03. These Reynolds numbers, based on the mean aerodynamic chords of the 45° and 40° sweptback wings, are shown in figure 10 as a function of Mach number.

Transition Strip

The investigation was conducted with fixed transition on the model by applying 1/10-inch-wide strips of No. 60 carborundum around the nose of the fuselage 10 percent of fuselage length back from the nose and along the 10-percent chord line of all surfaces of the wing and horizontal and vertical tails. (See fig. 3(a).)

Measurements

Lift, drag, pitching-moment, lateral-force, rolling-moment, and yawing-moment data were obtained by means of an electrical strain-gage balance located inside the fuselage. The model and the accompanying balance were supported by a sting attached to the support strut which changed the angle of attack in such a way that the model was kept close to the tunnel center line. In general, performance measurements were taken for an angle-of-attack range from -5° to 2°. Stability data were obtained at angles of attack from -5° to 14°. Lateral measurements were made at an angle of sideslip of -5° for angles of attack from -4° to as high as 15.4°.

Flow Visualization

Observations of the flow in the boundary layer of the wing upper surface were made for several configurations by using the fluorescent-oil-film method of reference 8. During this phase of the investigation, the model was oriented with the wings in the vertical plane of the tunnel. This orientation permitted the flow patterns to be observed and photographed through the tunnel sidewall windows. Force measurements were

made simultaneously with the flow visualization near the wing design lift coefficient. A schlieren system was used to observe and photograph shock waves in the flow about several configurations.

Corrections and Accuracy

Corrections to the free-stream Mach number and dynamic pressure for the effects of model and wake blockage are not necessary for tests in the slotted test section of the Langley 8-foot transonic pressure tunnel. (See ref. 4.) All data presented are essentially free of reflected disturbances up to a Mach number of 1.00. From consideration of the results of reference 4, it is believed that for Mach numbers up to approximately 1.03 the effects of reflected compressions and expansions from the test-section boundary on the measurements made in the present investigation are negligible.

The drag data have been adjusted to the condition of free-stream static pressure at the base of the fuselage. A further adjustment has been made for sting interference on the drag, based on the results of reference 9.

Cylindrical extensions were fitted to the base of the four inboard wing bodies during that part of the performance phase of the investigation devoted exclusively to obtaining data for the various configurations with bodies added to the wings. The drag data for this part of the investigation have been adjusted for skin friction associated with the wetted area of these extensions and also have been adjusted to the condition of free-stream static pressure at the base of the extensions. For the stability phase of the investigation, the chord force has been adjusted to the condition of stream static pressure at the base of the wing bodies. Only the two inboard cylindrical extensions or wing bodies on one wing panel were instrumented. The extensions were alined parallel to the fuselage center line in the vertical and horizontal planes. They extended 10 inches downstream from the base of the wing bodies; this condition essentially placed the effective bases of the wing bodies in a region of relatively undisturbed airflow. The diameters of the extensions and of the base of the wing bodies were the same (1.1 inches).

The angles of attack and sideslip are estimated to be accurate to within $\pm 0.1^{\circ}$. The estimated accuracy of the data, based on static calibrations and repeatability of the data, is:

M	± 0.005
C_L	± 0.010
C_D	± 0.0010

C_m	±0.004
C_l	±0.0003
C_n	±0.0005
C_Y	±0.0030

No corrections have been made for wing aeroelasticity.

PRESENTATION OF RESULTS

A number of model changes were made during the investigation reported herein. The configuration having the basic components, fuselage with original fuselage addition, the wing with wing bodies at 0.33, 0.57, and 0.80 semispan stations, and the empennage is referred to as the basic model. (See fig. 3(b).) The original fuselage addition and the six wing bodies together are referred to as the basic additions. In order to simplify data identification keys on some of the figures, symbols are used instead of the names of components.

Photographs of the fluorescent-oil-film pattern observed on several of the 45° configurations at a Mach number of 0.96 are shown as figures 11 to 15. Schlieren photographs of shock waves about some of these same configurations are shown as figures 16 and 17 for Mach numbers of 0.96 and 1.00, respectively.

The basic longitudinal characteristics of the various configurations are presented as functions of lift coefficient. The basic lateral data are presented as functions of angle of attack. Most of the analysis data are presented as functions of Mach number. The longitudinal parameters C_{L_α} and $C_{m_{C_L}}$ were obtained for a lift-coefficient range from 0 to 0.4. The lateral-stability parameters were determined by assuming a linear variation of lateral characteristic with sideslip angle up to $\beta = -5°$.

The basic data and the associated analytical results are presented in figures 18 to 56. An index to the figures is presented as table III.

RESULTS AND DISCUSSION

The displacement of the separated flow behind the blunt bases of the four inboard wing bodies differs substantially from that of a jet

emanating from such bases as would be the case for a real airplane. This difference in the flow displacement would cause significant increases in the drag of the test model, compared with a configuration with jets, particularly at transonic speeds. In order to simulate the effect of jets emanating from nacelles on the flow about the model, cylindrical extensions were attached to the base of the four inboard wing bodies during the performance phase of the investigation. As is pointed out in reference 9, for gradually contoured afterbodies of the type used on the present wing bodies, a practical extension shape can be made which will produce the same drag as the jet at a given pressure ratio. A cylindrical extension was chosen for the present investigation as an approximation to the shape of the jet, instead of using differently shaped extensions for each of a number of different pressure ratios. Such a cylinder obviously provides the simplest solution to the problem of obtaining drag measurements. Forces acting on these solid extensions, which would be transmitted directly to the model, are minimized by the cylindrical shape of the extensions and the low angles of attack involved during their use. The effects of these forces are small and do not require any adjustment to the lift or drag other than the skin-friction and base-pressure corrections mentioned earlier. In all applications of the area rule to specific airplane models without air flow through nacelles, it has been suggested that a constant stream-tube area be added following the base of the nacelle area to simulate an exhausting jet (ref. 10). The cylindrical extensions physically provide this added area to the model of the present investigations. (See fig. 4.)

Drag Characteristics for Low Angles of Attack at High Speed; $\Lambda = 45^\circ$

Basic components.- The effects of the basic components (empennage, original fuselage addition, and six wing bodies) on the wing-fuselage drag characteristics with a wing geometric dihedral angle of 6° are shown in figure 18.

Comparisons of the variation of drag coefficient with Mach number from 0.6 to 1.03 for lift coefficients of 0.2 and 0.4 are shown in figure 26. The addition of the empennage to the wing-fuselage combination increases the drag at all Mach numbers, as would be expected.

Addition of the original fuselage addition results in a delay of the drag rise similar to that reported in reference 3. At $C_L = 0.4$, the drag-rise delay of 0.035 in Mach number is an indication of the effectiveness of this addition at lifting conditions. The addition of the six wing bodies produces the same type of drag-rise delay and large reductions in drag at transonic speeds that were shown originally for the optimum-sized wing bodies of reference 2. Drag reductions are realized at Mach

numbers above 0.92 for $C_L = 0.2$ and above $M = 0.87$ for $C_L = 0.4$. The drag rise for $C_L = 0.4$ is delayed approximately 0.06 in Mach number by these wing bodies. At this same lift coefficient, the wing bodies reduce the drag coefficient approximately 0.0135 at Mach numbers between 0.96 and 1.03.

The reduction in the separated-flow region on the wing resulting in this important reduction in drag, for approximately the design lift coefficient of 0.3, is illustrated by a comparison of the fluorescent-oil-film photographs of figures 11 and 12 for a Mach number of 0.96. The accumulation of and spanwise spread of the oil over the rear portion of the wing (fig. 11) is indicative of the separated flow region. This separation is all but eliminated when the bodies are added to the wing; the oil moves smoothly rearward to the trailing edge (fig. 12).

The reductions of shock-wave strength resulting from the addition of the six wing bodies are shown in the schlieren photographs of figure 16 for test conditions similar to those for the fluorescent-oil-film presentation and in figure 17 for a Mach number of 1.00. The strong shock wave on the wing (figs. 16(a) and 17(a)) is replaced by several weaker shocks when the wing bodies are added (figs. 16(b) and 17(b)). In addition to reducing the strength of drag-producing shock waves and attendant separation on the wing, the wing bodies have the added advantage of eliminating the drag of engine installations in the underslung location in current use. This drag may be relatively large at the higher subsonic speeds.

Fences and dihedral.- Figure 19 includes the drag characteristics of the basic model with and without fences. Figure 27 shows the comparison of the drag characteristics for the same configurations at $C_L = 0.2$ and 0.4. The small drag penalty associated with the fences at the highest test Mach numbers is not deemed prohibitive when consideration is given to beneficial effects which may be gained from the fences at the design low speeds. The conclusion that the fences do not have a detrimental effect on the flow is verified by noting the similarity of the fluorescent-oil-film photographs for the fences off and on in figures 12 and 13.

Figure 18 includes the drag characteristics of the basic model with 6° dihedral. Figure 20 includes the same data for the basic model with 0° dihedral. Comparisons of the drag-coefficient variation with Mach number for the basic model with these two different dihedral angles are shown in figure 28. The increase in dihedral angle results in a decrease in drag coefficient between Mach numbers of 1.00 and 1.03.

Variations.- During a preliminary part of the investigation, the wing was tested on the model at angles of incidence of 0° and 2°. It

was determined that an angle of incidence of 2° had a strong influence in reducing the drag at lifting conditions and improving the values of maximum lift-drag ratio $\left(\frac{L}{D}\right)_{max}$. The 2° angle of incidence, therefore, was made a basic feature of the investigation.

The drag characteristics of the configuration (basic model with fences) with and without bodies added to the wing tips are included in figure 19. The drag characteristics of the basic model with and without the 0.80b/2 wing bodies are included in figure 20. The effects of the wing-tip bodies and the 0.80b/2 wing bodies on the variation of drag coefficient with Mach number are shown in figure 29. The small favorable effect of the wing-tip bodies indicates that the skin friction is more than compensated for by favorable end-plate and interference effects between the configuration shock and the wing-tip bodies.

The addition of the 0.80b/2 wing bodies accounts for approximately 17 percent of the drag-rise delay associated with all six wing bodies at $C_L = 0.4$. (See figs. 26 and 29.) Also, about 30 percent of the drag reduction produced by the six wing bodies results from the influence of the 0.80b/2 wing bodies at $M = 0.98$ and $C_L = 0.4$. The effect of the 0.80b/2 wing body on the separated-flow region on the outer panel of the wing is shown in the fluorescent-oil-film photographs of figures 14 and 15.

The drag characteristics of the basic model with the original and modified fuselage additions are compared in figures 19 and 30. Reducing the cross-sectional area (modified fuselage addition) of the fuselage addition has a detrimental effect on the drag coefficient, as would be expected.

Horizontal tail.- Figure 21 shows the drag characteristics of the basic model with various horizontal-tail incidences. For lift coefficients of 0.2 and 0.4, as shown in figure 31, the lowest values of drag coefficient throughout the test Mach number range are produced by the configuration with $i_t = 2°$. A horizontal-tail setting of 2°, therefore, has been chosen as the basic horizontal-tail setting for the configurations of the investigation involving the empennage.

Maximum untrimmed lift-drag ratios.- The maximum untrimmed lift-drag ratios and the lift coefficient at maximum untrimmed lift-drag ratio are presented in figure 32 for various configurations of the basic model components. The drag reductions at transonic speeds which result from the original fuselage addition and the six wing bodies are reflected as improvements in maximum values of untrimmed lift-drag ratio.

Lift and Pitching-Moment Characteristics for Low Angles of Attack at High Speeds; $\Lambda = 45^\circ$

Basic components.- Figure 22 shows the effect of the empennage, original fuselage addition, and six wing bodies on the variation of angle of attack and pitching-moment coefficient with lift coefficient for the basic wing-fuselage combination. Of the additions tested, the six bodies added to the wing provide the most predominant influence on the lift and pitching-moment characteristics, especially at transonic speeds. (See fig. 33.) Above a Mach number of 0.90 these wing bodies substantially increase the lift-curve slope by approximately 25 percent and result in a significant increase in stability as manifested by a rearward shift in the aerodynamic-center location equivalent to about 15 percent of the mean aerodynamic chord. These changes are associated with an increase in lift over the aft portion of the wing with the wing bodies present.

The original fuselage addition produces only minor changes in the lift-curve slope which show up as a slight reduction in longitudinal stability in the transonic range. (See fig. 33.) The effects of the horizontal tail on lift, pitching moment, and longitudinal stability are about as expected.

Horizontal-tail effectiveness.- The effectiveness of the horizontal tail for the basic model is shown in figure 34. The effectiveness was determined from the effects of the horizontal-tail deflections on the aerodynamic characteristics in pitch shown in figure 25. The wing dihedral angle was 0° for these configurations. Included also in figure 25 are data for the $i_t = 2^\circ$ condition at the two different Reynolds numbers used in the performance and stability phases of the investigation. (See fig. 10.) These data are used to make Reynolds number adjustments to other data herein. Tests of similar horizontal-tail settings were not made for the wing with 6° dihedral angle, since it is believed that the horizontal-tail effectiveness would be little affected by the change in dihedral angle. The horizontal-tail effectiveness, averaged for an angle-of-attack range from -4° to 3°, increases gradually with increase in Mach number from a value of -0.0175 at a Mach number of 0.60 to a value of -0.021 at the highest test Mach number of 1.03.

Effective downwash.- The pitching-moment results for the various horizontal-tail deflections, as well as for the horizontal tail off, have been used to determine the experimental values of effective downwash for two arbitrary stability levels, $C_{m_{C_L}} = -0.05$ and -0.10 (both measured near zero lift at a Mach number of 0.8). (See fig. 34.) At the intersections of the horizontal-tail-off curve with the horizontal-tail-on curves (where the tail provides no pitching moment), it is

assumed that the tail is alined with the local stream direction; hence, the downwash angle can be determined from the relation $\epsilon = \alpha + i_t$. The $\partial\epsilon/\partial\alpha$ values are in the acceptable range and compare favorably with those from tests of other similar models.

Longitudinal Characteristics for High Angles of Attack at High Speeds; $\Lambda = 45^\circ$

Basic components.- The basic wing of the present investigation experiences the high lift instability commonly referred to as pitch-up, which is characteristic of sweptback wings. An examination of figure 22 indicates that addition of the horizontal tail has little effect on this pitch-up characteristic. Neither is the lift coefficient for pitch-up significantly altered by the forward fuselage addition. This instability tendency, however, is markedly delayed to higher lift coefficients by the addition of the wing bodies. For instance, the pitch-up occurs at a lift coefficient 0.3 higher at a Mach number of 0.90 when the wing bodies are added. At Mach numbers from 0.60 to 0.90 the effects of the wing bodies are much greater than for fences investigated in the past, particularly at the higher speeds. This greater effect results from the fact that the wing bodies produce a pressure gradient which improves the overall flow rather than a simple barrier to outward flow, as has been discussed in reference 2. Attendant with the alleviation of instability is an increase in lift coefficient as shown in figure 22.

Fences and dihedral.- Adding the fences to the forward part of the six wing bodies delays the pitch-up at $M = 0.60$, but the effect steadily diminishes with increase in Mach number and becomes nil above $M = 0.90$. (See fig. 23.) Changing dihedral angle from 0° to 6° has no effect on the instability. (Compare fig. 24 with fig. 22.)

Variations.- The effect of the 0.80b/2 wing bodies on pitch-up (fig. 24) is similar to that of the fences (fig. 23) in that the delaying effect diminishes above a Mach number of 0.6. The modified fuselage addition and wing-tip body have a negligible effect on the pitch-up tendency (fig. 23).

Longitudinal Trim Characteristics; $\Lambda = 45^\circ$

In the determination of the longitudinal trim characteristics only the basic configuration was considered. The maximum trim values of lift-drag ratio L/D are shown in figure 35 for two stability levels of $C_{m_{C_L}} = -0.05$ and -0.10 (at $M = 0.80$) and for a Reynolds number of

approximately 1.9×10^6. These values were obtained by adjusting the data presented in figures 21 and 25 for Reynolds number and for wing-body extensions on and off, where needed. Where values of maximum trim L/D occurred for control deflections other than those tested, the values were obtained by assuming a linear variation of pitching moment with control deflection. The results also are shown adjusted to a Reynolds number approximately corresponding to flight conditions ($R \approx 100 \times 10^6$).

The maximum trim values of L/D are relatively insensitive to a change in stability level from $C_{m_{C_L}} = -0.05$ to -0.10 in the design operating speed range from $M = 0.96$ to 1.03. These values of trim $\left(\frac{L}{D}\right)_{max}$ vary from about 12.5 at a Mach number of 0.96 to 8.0 at a Mach number of 1.03. The corresponding values at the assumed flight Reynolds number are 14.8 and 8.8, respectively. It is interesting to note that no loss in $\left(\frac{L}{D}\right)_{max}$ occurs at a Mach number of 0.96 when the basic model is trimmed. (See fig. 32.) The lift coefficient associated with the experimental values of trim $\left(\frac{L}{D}\right)_{max}$ varies between approximately 0.4 and 0.45. The assumed flight conditions would require slightly lower lifts.

Figure 36 indicates that the horizontal-tail setting for trim conditions is affected by Mach number, lift coefficient, and stability level. At a Mach number of 0.96 and a stability level of -0.05, at $M = 0.80$, a horizontal-tail setting of approximately 2° is indicated for a lift coefficient of the order of 0.45 (the lift coefficient associated with trim $\left(\frac{L}{D}\right)_{max}$ at $M = 0.96$, as shown in fig. 32).

Landing Conditions; $\Lambda = 45^\circ$

Basic components.- An examination of figures 22(a) and 40(a) indicates that for Mach numbers of 0.20 and 0.40 the fuselage addition has very little effect on the landing characteristics of the model. The wing bodies, however, show pronounced favorable effects for the basic model. The wing additions result in an increase of the order of 0.05 in lift coefficient in the region of maximum lift and a delay in the onset of instability of as much as 0.6 in lift coefficient at $M = 0.20$.

Trailing-edge flaps.- In order to explore the possibility of higher values of the low-speed lift coefficient and reasonable landing attitudes, plain partial-span trailing-edge flaps (fig. 9) were investigated.

Although they are not the most sophisticated of flaps, those used give an indication of the effect of the wing bodies on flap effectiveness. The basic lift and pitching-moment data are shown in figures 37 and 38. The data of figure 39 show the effect of the flap configurations on the lift coefficient at the average maximum angle of attack tested, $\alpha = 14^{\circ}$ (considered to be near the region of maximum lift).

At landing speeds the trailing-edge flaps result in an expected increase in lift near maximum lift for the basic model with wing bodies off. (See figs. 37(a) and 39(a).) The lift increase associated with the 0.33 semispan flap is approximately doubled by extending the flap out to 0.57 semispan. In general, the wing bodies have little apparent influence on flap effectiveness. Primarily, these wing additions provide an increase in lift in the presence of the flaps of about the same magnitude as for the flaps-off case. (See figs. 39(a) and 39(b).) The pitch-up tendency of the wing without wing bodies is delayed by the trailing-edge flaps. (See fig. 38(a).) At a Mach number of 0.20 the delay amounts to approximately 0.4 in lift coefficient for the 0.57-semispan flap. This delay is extended about another 0.4 in lift coefficient by the addition of the wing bodies in the presence of the flap. (See fig. 38(b).)

Fences.- At low Mach numbers, the small wing fences which extend over the forward portion of the wing bodies provide an increase in lift coefficient comparable to that associated with the wing bodies. (See figs. 37(c) and 39(c).) In addition, the fences extend the lift coefficient for instability almost to the lift coefficient obtained at the maximum allowable test angle of attack. (See figs. 23, 38(b), and 38(c).) When the fences are used in combination with the trailing-edge flaps, the pitch-up tendency is essentially eliminated and a marked increase in stability occurs in its place, as shown in figure 38(c).

It is of significance to note that the largest increases in lift and most acceptable pitching-moment characteristics are obtained with the flap extended out to 0.57 semispan on the basic model with fences.

Lateral and Directional Characteristics; $\Lambda = 45^{\circ}$

The longitudinal aerodynamic characteristics for various combinations of components of the test model in sideslip ($\beta = -5^{\circ}$) are presented in figures 40 and 42.

Basic components.- Figure 41 shows the effect on the lateral and directional aerodynamic characteristics of various additions on the wing-fuselage combination having a dihedral angle of 6°. All combinations exhibit positive effective dihedral (that is, negative C_{l_β}) in the angle-of-attack range of the design lift. (See fig. 44(a).) The

most noticeable effect on C_{l_β} is produced by the addition of the wing bodies. In this instance the positive effective dihedral is reduced slightly in the subsonic speed range; generally, between Mach numbers of 0.9 and 1.0, a reduced dihedral effect associated with the model without wing bodies is reversed, as shown in figure 46. The basic configuration with the vertical tail exhibits positive directional stability (positive C_{n_β}) throughout the test Mach number range for lift coefficients of 0.2 and 0.4. This stable directional stability characteristic is not significantly altered by either the fuselage addition or the wing bodies. (See figs. 44(b) and 46.)

Dihedral.- Figure 43 shows the effect of dihedral angle on the lateral and directional aerodynamic characteristics of the model. The basic model with 0° geometric dihedral indicates negative effective dihedral at low lift coefficients ($\alpha < -2°$) and all test Mach numbers as shown in figures 45(a) and 47. With an increase in lift coefficient, however, this basic model becomes laterally stable. A change in dihedral angle to 6° provides an expected and desired positive dihedral effect throughout the test angle-of-attack and Mach number ranges. An increase in lift coefficient from 0 to 0.4 produces similar increments in C_{l_β} as for the 0° dihedral case. (See fig. 47.)

Longitudinal Aerodynamic Characteristics; $\Lambda = 40°$

The basic aerodynamic data for the 40° sweptback wing-fuselage-empennage configuration without and with the original fuselage addition and six wing bodies are shown and compared with those for the 45° sweptback wing in combination with identical components in figures 48 to 53. The variation with Mach number of the drag coefficient at $C_L = 0.2$ and 0.4, maximum lift-drag ratio $\left(\frac{L}{D}\right)_{max}$, and lift coefficient for $\left(\frac{L}{D}\right)_{max}$, the lift-curve slope C_{L_α}, and of the static longitudinal-stability parameter $C_{m_{C_L}}$ for the configurations of figures 48 to 53 are shown for a Mach number range from 0.60 to 1.03 in figures 54 to 56 for the analysis.

The drag coefficients of the transonic-transport model without or with the basic additions are affected in the classical manner by the change in wing sweepback angle. At a given lift coefficient, the drag is lower at the low Mach numbers for the 40° sweptback wing and lower in the high Mach number range for the 45° sweptback wing. The drag-rise Mach number is changed approximately 0.03 at a lift coefficient of 0.4 by the change in sweepback angle. (See figs. 54(a) and 55(a).)

The increase in drag-rise Mach number of approximately 0.06 for the fuselage addition and wing bodies on the 40° sweptback-wing combination (fig. 56(a)) is similar to that obtained for the comparable 45° sweptback-wing combination. (See fig. 26.) The actual reduction in drag coefficient at transonic speeds $\left(0.025 \text{ at } C_L = 0.4 \text{ and } M = 0.96\right)$ is greater, however, for the additions on the 40° sweptback-wing combination, probably mainly because of the more extensive separated-flow region on the 40° sweptback wing. The reduction associated with the comparable 45° configuration was an incremental drag coefficient of 0.019.

The reduction in drag at the higher Mach numbers due to change in sweepback angle from 40° to 45° produces increases in $\left(\frac{L}{D}\right)_{max}$ at Mach numbers above 0.84 for the wing-fuselage-empennage configuration (fig. 54(b)) and above $M = 0.87$ for the complete basic model (fig. 55(b)).

The combined effects of increase in sweepback angle from 40° to 45° and use of the original fuselage addition and six wing bodies on the wing-fuselage-empennage combination result in an increase in drag-rise Mach number of about 0.09. (See figs. 26 and 54(a).) At a Mach number of 0.96, the increased sweepback angle and basic additions together produce a decrease in drag coefficient of approximately 0.032 at a lift coefficient of 0.4. (See figs. 26 and 54(a).) An increase in untrimmed maximum lift-drag ratio of the order of 6.0 also is obtained. (See figs. 32 and 54(b).)

As might be expected, pitch-up generally occurs at higher lift coefficients for the 40° sweptback configurations than for the 45° configurations (figs. 51 and 52). In addition, the severity of pitch-up for the basic configuration is considerably less for the 40° sweptback case. (See fig. 52.) The ability of the basic additions to alleviate the pitch-up problem, as shown for the 45° sweptback wing in figure 22, is even more effective for the 40° configuration. (See fig. 53.)

Changes in C_{L_α} and $C_{m_{C_L}}$ due to the change in sweepback angle are summarized in figures 54(c) and 55(c). The relative effect of the fuselage addition and wing bodies on these parameters for the 40° and 45° sweptback-wing configurations are about as expected, as shown in figures 33 and 56(c).

CONCLUSIONS

The wind-tunnel investigation of a transonic-transport configuration utilizing recent drag-reducing devices at Mach numbers from 0.20 to 1.03 has produced the following conclusions:

1. The various fuselage and wing additions delay the drag-rise Mach number and greatly reduce the drag beyond the drag rise.

2. The wing bodies markedly alleviate the unstable pitch tendencies throughout the test Mach number range.

3. At the landing speeds, the wing bodies show little interference with the ability of trailing-edge flaps to increase lift near $C_{L_{max}}$, and the use of fences on the wing bodies greatly reduces the severe longitudinal instability trend at high angles of attack.

4. The various configurations with 6° dihedral exhibit positive effective dihedral in the design lift range. Addition of the vertical tail provides positive directional stability in the design lift range which is not significantly affected by either the fuselage addition or the wing bodies.

5. The combination of the fuselage addition and wing bodies reduces the drag of the 40° sweptback-wing configurations more than the 45° configurations in the transonic range.

6. The increase in drag-rise Mach number associated with the combination of the fuselage and wing additions on the 40° sweptback-wing combination is similar to that obtained for the comparable 45° sweptback-wing combination.

Langley Research Center,
National Aeronautics and Space Administration,
Langley Field, Va., September 23, 1960.

REFERENCES

1. Whitcomb, Richard T., and Heath, Atwood R., Jr.: Several Methods for Reducing the Drag of Transport Configurations at High Subsonic Speeds. NASA MEMO 2-25-59L, 1959.

2. Whitcomb, Richard T.: Special Bodies Added on a Wing To Reduce Shock-Induced Boundary-Layer Separation at High Subsonic Speeds. NACA TN 4293, 1958.

3. Whitcomb, Richard T.: A Fuselage Addition To Increase Drag-Rise Mach Number of Subsonic Airplanes at Lifting Conditions. NACA TN 4290, 1958.

4. Wright, Ray H., Ritchie, Virgil S., and Pearson, Albin O.: Characteristics of the Langley 8-Foot Transonic Tunnel With Slotted Test Section. NACA Rep. 1389, 1958. (Supersedes NACA RM L51H10 by Wright and Ritchie and RM L51K14 by Ritchie and Pearson.)

5. Whitcomb, Richard T.: A Study of the Zero-Lift Drag-Rise Characteristics of Wing-Body Combinations Near the Speed of Sound. NACA Rep. 1273, 1956. (Supersedes NACA RM L52H08.)

6. Tucker, Warren A.: A Method for the Design of Sweptback Wings Warped To Produce Specified Flight Characteristics at Supersonic Speeds. NACA Rep. 1226, 1955. (Supersedes NACA RM L51F08.)

7. Heath, Atwood R., Jr.: Longitudinal Aerodynamic Characteristics of a High-Subsonic-Speed Transport Airplane Model With a Cambered 40° Sweptback Wing of Aspect Ratio 8 at Mach Numbers to 0.96. NASA TN D-218, 1960.

8. Loving, Donald L., and Katzoff, S.: The Fluorescent-Oil Film Method and Other Techniques for Boundary-Layer Flow Visualization. NASA MEMO 3-17-59L, 1959.

9. Cahn, Maurice S.: An Experimental Investigation of Sting-Support Effects on Drag and a Comparison With Jet Effects at Transonic Speeds. NACA Rep. 1353, 1958. (Supersedes NACA RM L56F18a.)

10. Whitcomb, Richard T.: Some Considerations Regarding the Application of the Supersonic Area Rule to the Design of Airplane Fuselages. NACA RM L56E23a, 1956.

TABLE I.- FUSELAGE AND FUSELAGE ADDITION COORDINATES

[All dimensions are in inches; see fig. 5]

	Fuselage	Original addition		Modified addition			Fuselage	Original addition		Modified addition	
x	r	a	r_1	a	r_1	x	r	a	r_1	a	r_1
0	0	0	0	0	0	21.000	2.030	0.550	1.690	0.510	1.690
.100	.230	0	0	0	0	22.000	2.030	.430	1.710	.415	1.710
.200	.350	0	0	0	0	22.500	2.030	.360	1.740	.36	1.740
.400	.550	0	0	0	0	23.000	2.030	.300	1.770	0	1.770
.600	.690	0	0	0	0	23.500	2.030	.230	1.800	0	0
.800	.800	0	0	0	0	24.000	2.030	0	0	0	0
1.000	.910	0	0	0	0	24.000	2.030	0	0	0	0
1.500	1.100	0	0	0	0	24.500	2.030	0	0	0	0
2.000	1.260	0	0	0	0	25.000	2.030	0	0	0	0
2.500	1.380	0	0	0	0	26.000	2.030	0	0	0	0
3.000	1.480	.200	1.300	0	1.300	27.000	2.030	0	0	0	0
4.000	1.630	.240	1.460	.220	1.460	28.000	2.030	0	0	0	0
5.000	1.750	.305	1.570	.150	1.570	29.000	2.030	0	0	0	0
6.000	1.840	.370	1.660	.320	1.660	30.000	2.028	0	0	0	0
7.000	1.910	.470	1.720	.400	1.720	31.000	2.024	0	0	0	0
8.000	1.950	.575	1.765	.480	1.765	32.000	2.019	0	0	0	0
9.000	1.990	.680	1.810	.560	1.810	33.000	2.012	0	0	0	0
10.000	2.010	.800	1.830	.655	1.830	34.000	2.000	0	0	0	0
11.000	2.020	.925	1.855	.740	1.855	35.000	1.980	0	0	0	0
12.000	2.030	1.060	1.860	.830	1.860	36.000	1.963	0	0	0	0
12.500	2.030	1.120	1.860	.870	1.860	37.000	1.933	0	0	0	0
13.000	2.030	1.180	1.860	.920	1.860	38.000	1.896	0	0	0	0
13.500	2.030	1.245	1.850	.960	1.860	39.000	1.849	0	0	0	0
14.000	2.030	1.300	1.840	1.005	1.860	40.000	1.788	0	0	0	0
14.500	2.030	1.330	1.840	1.050	1.850	41.000	1.710	0	0	0	0
15.000	2.030	1.320	1.840	1.045	1.850	42.000	1.618	0	0	0	0
15.500	2.030	1.290	1.840	1.000	1.845	43.000	1.502	0	0	0	0
16.000	2.030	1.260	1.830	.945	1.835	44.000	1.375	0	0	0	0
16.500	2.030	1.200	1.815	.900	1.825	45.000	1.261	0	0	0	0
17.000	2.030	1.130	1.800	.850	1.810	46.000	1.176	0	0	0	0
18.000	2.030	.950	1.765	.750	1.765	47.000	1.130	0	0	0	0
19.000	2.030	.770	1.740	.650	1.690	47.140	1.128	0	0	0	0
20.000	2.030	.660	1.690	.510	1.690						

TABLE II.- WING BODY RADII AND FENCE COORDINATES

[All dimensions are in inches; see fig. 8]

	Station 0.33b/2		Station 0.57b/2		Station 0.80b/2		Station 0.98b/2
x_1	Wing body r_2	Fence z_1	Wing body r_2	Fence z_1	Wing body r_2	Fence z_1	Wing body r_2
0	0	0	0	0	0	0	0
.100	0	.134	0	.150	0	.115	.034
.203	0	.222	0	.250	.060	.198	.065
.268	0	.265	.124	.290	.068	.240	.085
.500	0	.380	.172	.400	.102	.350	.150
.781	.188	.456	.239	.473	.149	.423	.220
1.000	.212	.485	.282	.500	.178	.445	.267
1.250	.244	.508	.336	.528	.215	.460	.310
1.500	.274	.520	.387	.548	.252	.468	.345
2.000	.337	.548	.482	.586	.327	.483	.386
2.500	.400	.576	.570	.625	.400	.500	.400
3.000	.462	.605	.644	.665	.469	.517	.380
3.500	.525	.634	.704	.705	.524	.533	.332
3.750	.555	.649	.725	.725	.540	.540	.298
4.000	.587	.663	.741	0	.549	.549	.255
4.500	.650	.678	.767	0	.549	0	.158
5.000	.704	.720	.783	0	.533	0	.038
5.150	.718	.728	.787	0	.515	0	0
5.500	.748	.749	.790	0	.500	0	0
5.750	.763	.763	.790	0	.475	0	0
6.000	.778	0	.789	0	.446	0	0
6.500	.791	0	.780	0	.375	0	0
7.000	.799	0	.765	0	.282	0	0
7.500	.800	0	.740	0	.166	0	0
8.000	.795	0	.705	0	.022	0	0
8.061	.794	0	.700	0	0	0	0
8.500	.782	0	.660	0	0	0	0
9.000	.761	0	.601	0	0	0	0
9.350	.740	0	.550	0	0	0	0
9.500	.729	0	0	0	0	0	0
10.000	.686	0	0	0	0	0	0
10.500	.630	0	0	0	0	0	0
11.000	.565	0	0	0	0	0	0
11.100	.550	0	0	0	0	0	0

TABLE III.- INDEX TO FIGURES

Basic aerodynamic data			Analytical results		
Primary configuration	Data plotted	Figure	Primary configuration	Data plotted	Figure
Drag characteristics for low angles of attack at high speed; $\Lambda = 45^\circ$					
Basic components	C_D against C_L	18	Basic components	C_D against M Untrimmed $\left(\frac{L}{D}\right)_{max}$ against M	26 32
Fences	C_D against C_L	19	Fences	C_D against M	27
Dihedral angle	C_D against C_L	20	Dihedral angle	C_D against M	28
Wing-tip bodies	C_D against C_L	19	Wing-tip bodies and 0.80b/2 wing bodies	C_D against M	29
0.80b/2 wing bodies	C_D against C_L	20			
Modified fuselage addition	C_D against C_L	19	Modified fuselage addition	C_D against M	30
Horizontal-tail incidence	C_D against C_L	21	Horizontal-tail incidence	C_D against M	31
Lift and pitching-moment characteristics for low angles of attack at high speeds; $\Lambda = 45^\circ$					
Basic components	α against C_L C_m against C_L	22	Basic components	C_{L_α} against M $C_{m_{C_L}}$ against M	33
Fences, wing-tip bodies, and modified fuselage addition	α against C_L C_m against C_L	23			
Dihedral angle and 0.80b/2 wing bodies	α against C_L C_m against C_L	24			
Horizontal-tail incidence	α against C_L C_m against C_L	25	Horizontal-tail effectiveness Effective downwash	$C_{m_{i_t}}$ against M $\frac{\partial \epsilon}{\partial \alpha}$ against M	34

TABLE III.- INDEX TO FIGURES - Continued

Basic aerodynamic data			Analytical results		
Primary configuration	Data plotted	Figure	Primary configuration	Data plotted	Figure
Longitudinal trim characteristics; $\Lambda = 45^\circ$					
Horizontal-tail incidence	C_D against C_L α against C_L C_m against C_L	21 25	Basic model	Trimmed $\left(\frac{L}{D}\right)_{max}$ against M Trim i_t against M	35 36
Longitudinal characteristics for high angles of attack at high speeds; $\Lambda = 45^\circ$					
Basic components	α against C_L C_m against C_L	22	Basic components	α against C_L C_m against C_L	22
Fences, wing-tip bodies, and modified fuselage addition	α against C_L C_m against C_L	23	Fences, wing-tip bodies, and modified fuselage addition	α against C_L C_m against C_L	23
Dihedral angle and 0.80b/2 wing bodies	α against C_L C_m against C_L	24	Dihedral angle and 0.80b/2 wing bodies	α against C_L C_m against C_L	24
Landing conditions; $\Lambda = 45^\circ$					
Basic model 0.33b/2 flap 0.57b/2 flap	C_L against α	37	Conditions near maximum lift	C_L against M $\alpha = 14^\circ$	39
Basic model 0.33b/2 flap 0.57b/2 flap	C_m against C_L	38			

TABLE III.- INDEX TO FIGURES - Concluded

Basic aerodynamic data			Analytical results		
Primary configuration	Data plotted	Figure	Primary configuration	Data plotted	Figure
Lateral and directional characteristics; $\Lambda = 45^\circ$					
Basic components	α against C_L C_m against C_L	40	Basic components	C_{l_β} against α C_{n_β} against α C_{Y_β} against α	44
	C_l against α C_n against α C_Y against α	41		C_{l_β} against M C_{n_β} against M C_{Y_β} against M	46
Dihedral angle	α against C_L C_m against C_L	42	Dihedral angle	C_{l_β} against α C_{n_β} against α C_{Y_β} against α	45
	C_l against α C_n against α C_Y against α	43		C_{l_β} against M C_{n_β} against M C_{Y_β} against M	47
Longitudinal aerodynamic characteristics; $\Lambda = 40^\circ$					
Basic additions off; $\Lambda = 40^\circ$ and 45°	C_D against C_L	48	Basic additions off; $\Lambda = 40^\circ$ and 45°	C_D against M Untrimmed $\left(\frac{L}{D}\right)_{max}$ against M	54
Basic additions on; $\Lambda = 40^\circ$ and 45°	C_D against C_L	49	Basic additions on; $\Lambda = 40^\circ$ and 45°	C_D against M Untrimmed $\left(\frac{L}{D}\right)_{max}$ against M	55
Basic additions off and on; $\Lambda = 40^\circ$	C_D against C_L	50	Basic additions off and on; $\Lambda = 40^\circ$	C_D against M Untrimmed $\left(\frac{L}{D}\right)_{max}$ against M	56
Basic additions off; $\Lambda = 40^\circ$ and 45°	α against C_L C_m against C_L	51	Basic additions off; $\Lambda = 40^\circ$ and 45°	C_{L_α} against M $C_{m_{C_L}}$ against M	54
Basic additions on; $\Lambda = 40^\circ$ and 45°	α against C_L C_m against C_L	52	Basic additions on; $\Lambda = 40^\circ$ and 45°	C_{L_α} against M $C_{m_{C_L}}$ against M	55
Basic additions off and on; $\Lambda = 40^\circ$	α against C_L C_m against C_L	53	Basic additions off and on; $\Lambda = 40^\circ$	C_{L_α} against M $C_{m_{C_L}}$ against M	56

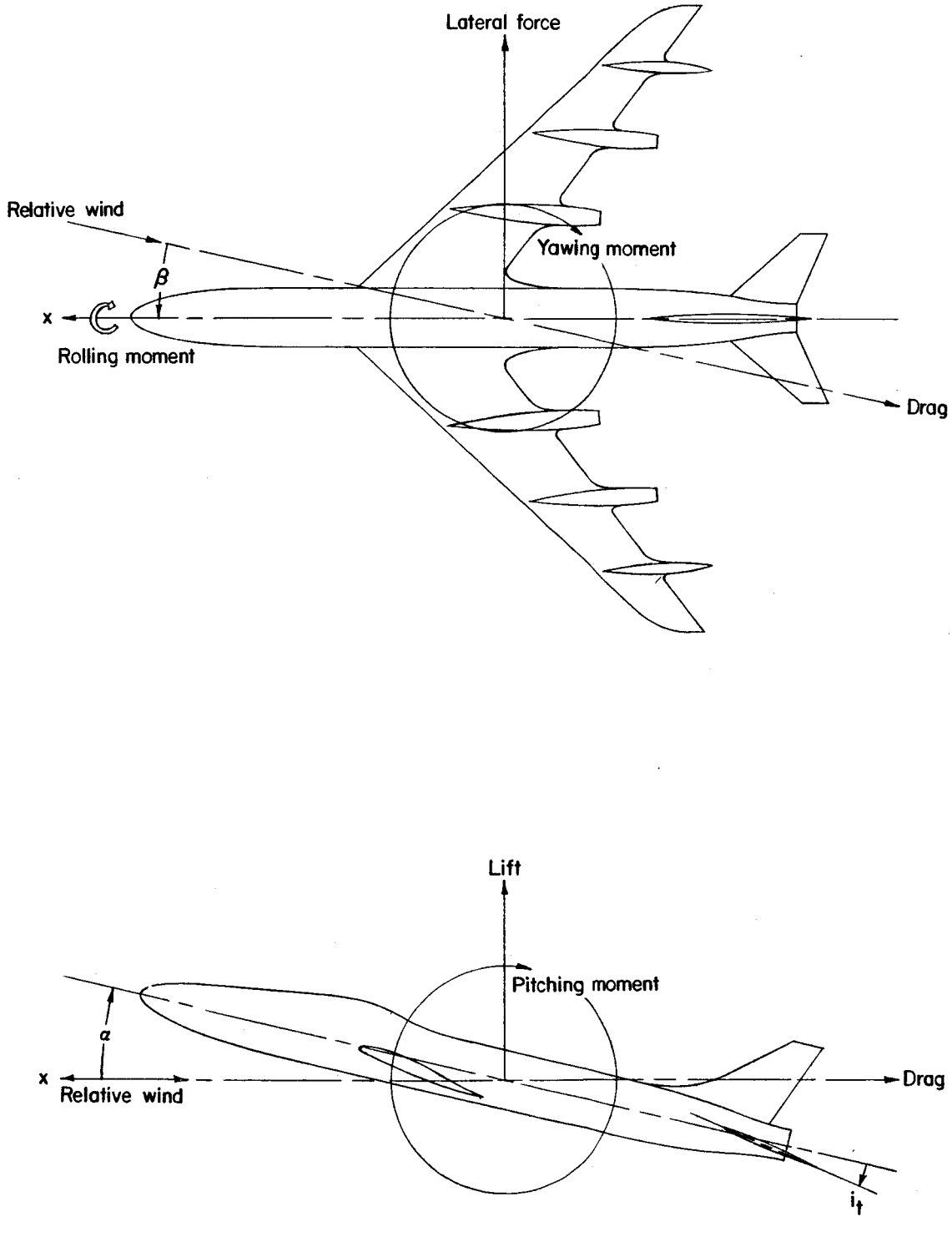

Figure 1.- Coordinate system of stability axes used.

GEOMETRIC CHARACTERISTICS OF MODEL

	45° Configuration	40° Configuration
Wing:		
Airfoil section parallel to plane of symmetry for $\Lambda = 40^\circ$	NACA 64A series	NACA 64A series
Area, sq ft	2	2
Aspect ratio	7	8
Taper ratio	0.3	0.3
Sweepback of quarter-chord line, deg	45	40
Incidence, deg	2	2
Dihedral, deg	6	0 and 6
Wing thickness streamwise:		
Root	0.115	0.12
Midsemispan to tip	.074	.08
Horizontal tail:		
Airfoil section	NACA 65A006	NACA 65A006
Area, sq ft	0.33	0.33
Aspect ratio	3.0	3.0
Taper ratio	0.3	0.3
Sweepback of quarter-chord line, deg	45	45
Vertical tail:		
Airfoil section (4.0 in. above fuselage reference line)	NACA 65A006	NACA 65A006
Area (without dorsal), sq ft	0.25	0.25
Aspect ratio	1.5	1.5
Taper ratio	0.26	0.26
Sweepback of quarter-chord line, deg	45	45

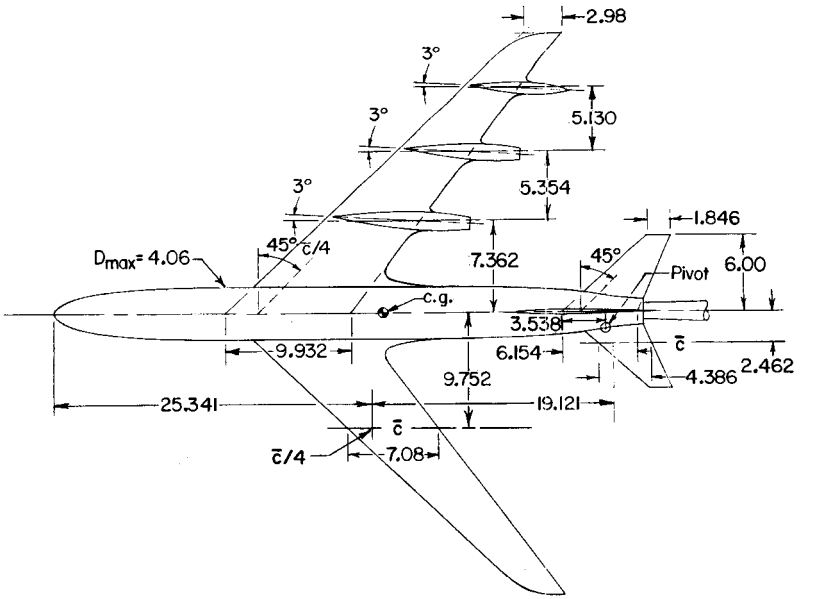

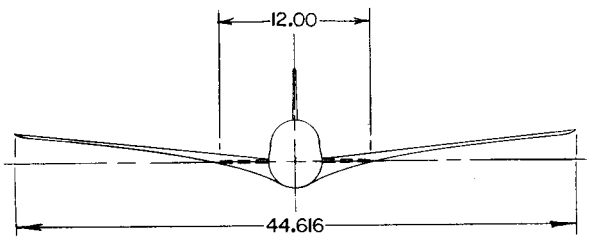

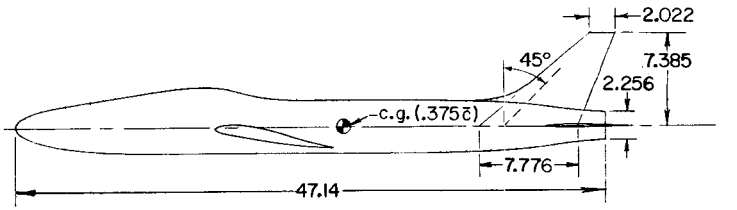

Figure 2.- Sketch and geometric details of transonic-transport model. All dimensions are in inches unless otherwise noted.

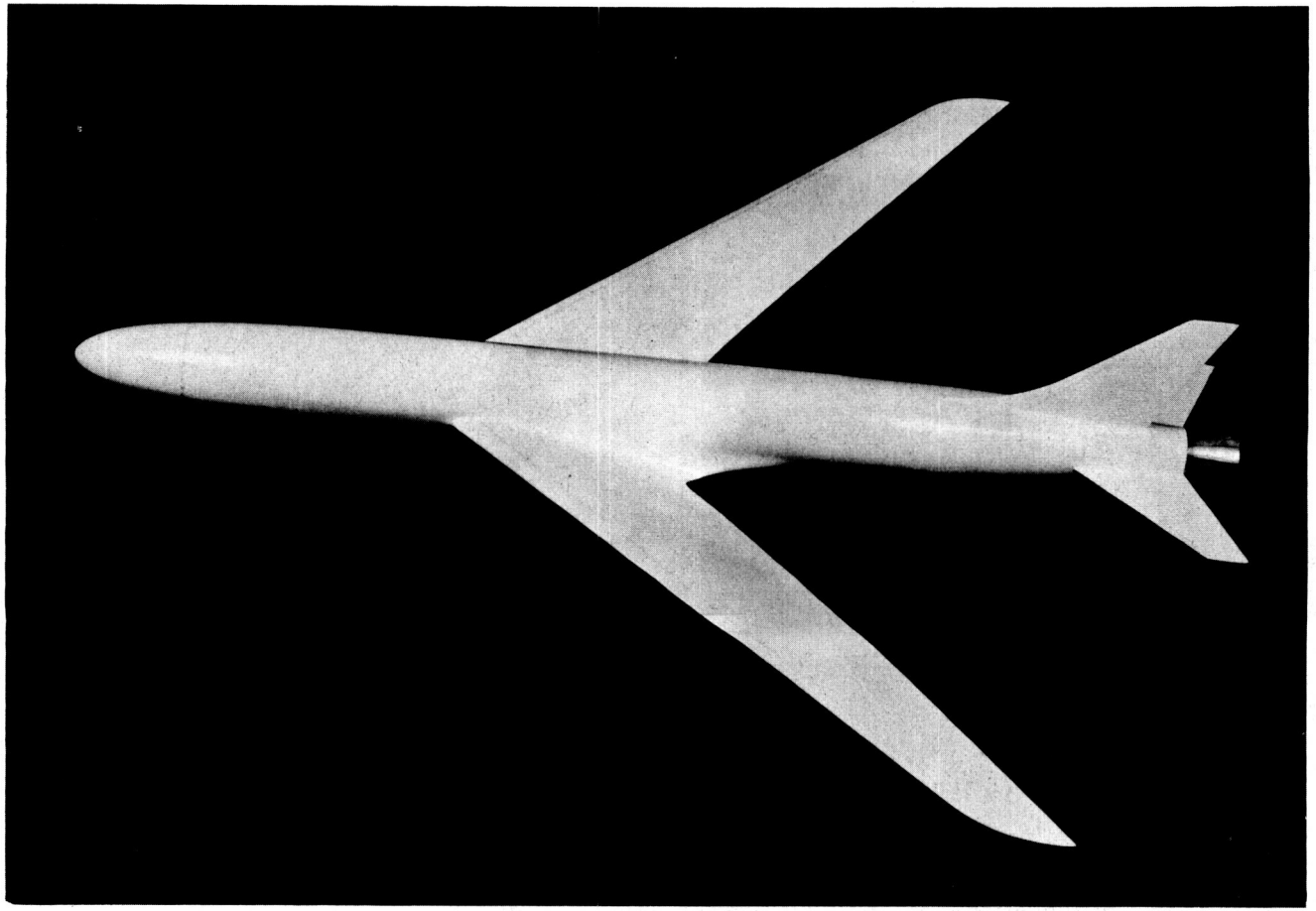

(a) Basic model without basic additions; transition fixed. L-59-2922

Figure 3.- Photograph of transonic-transport model investigated in Langley 8-foot transonic pressure tunnel. $\Lambda = 45^{\circ}$; $\Gamma = 6^{\circ}$; $i_t = 2^{\circ}$.

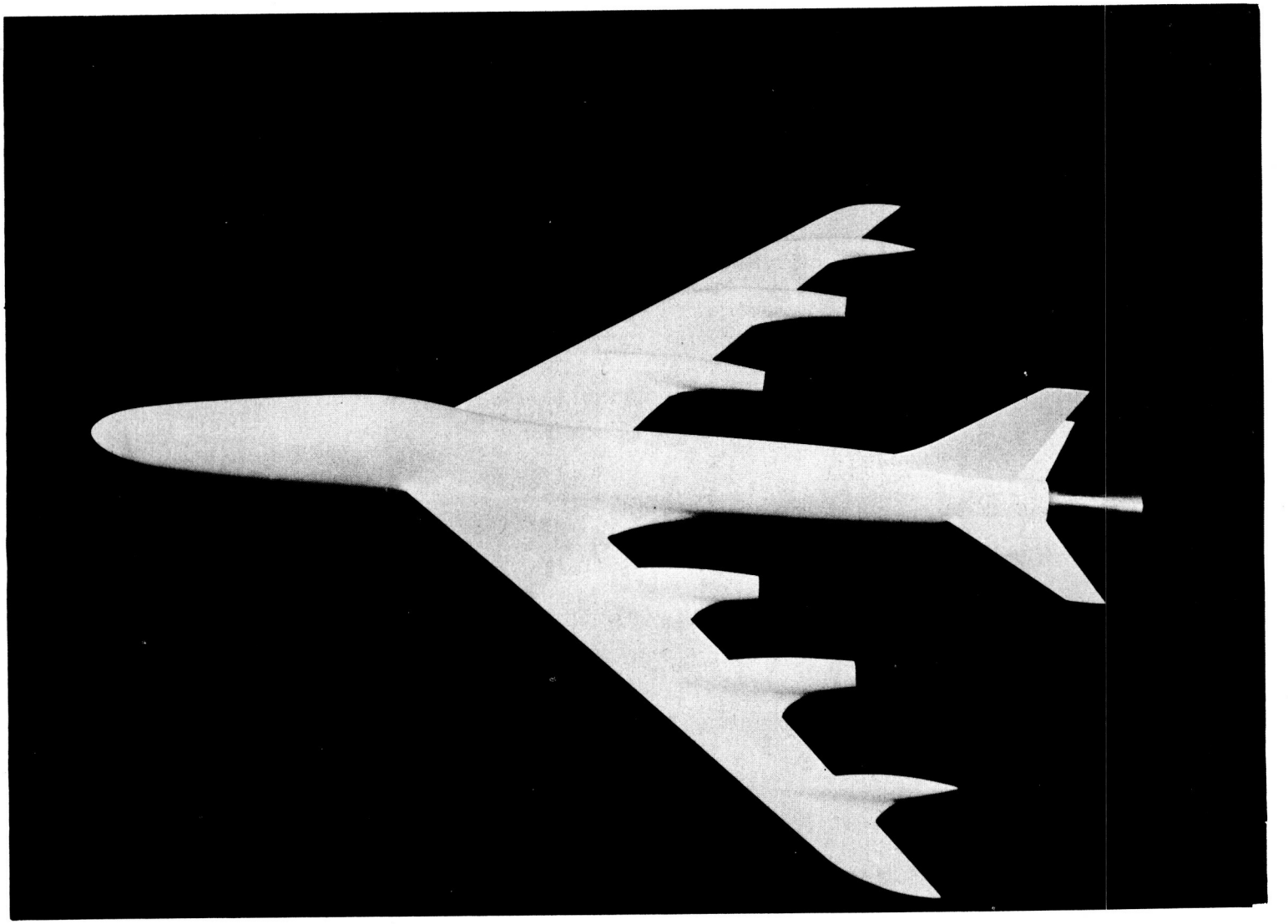

(b) Basic model. L-59-5125

Figure 3.- Concluded.

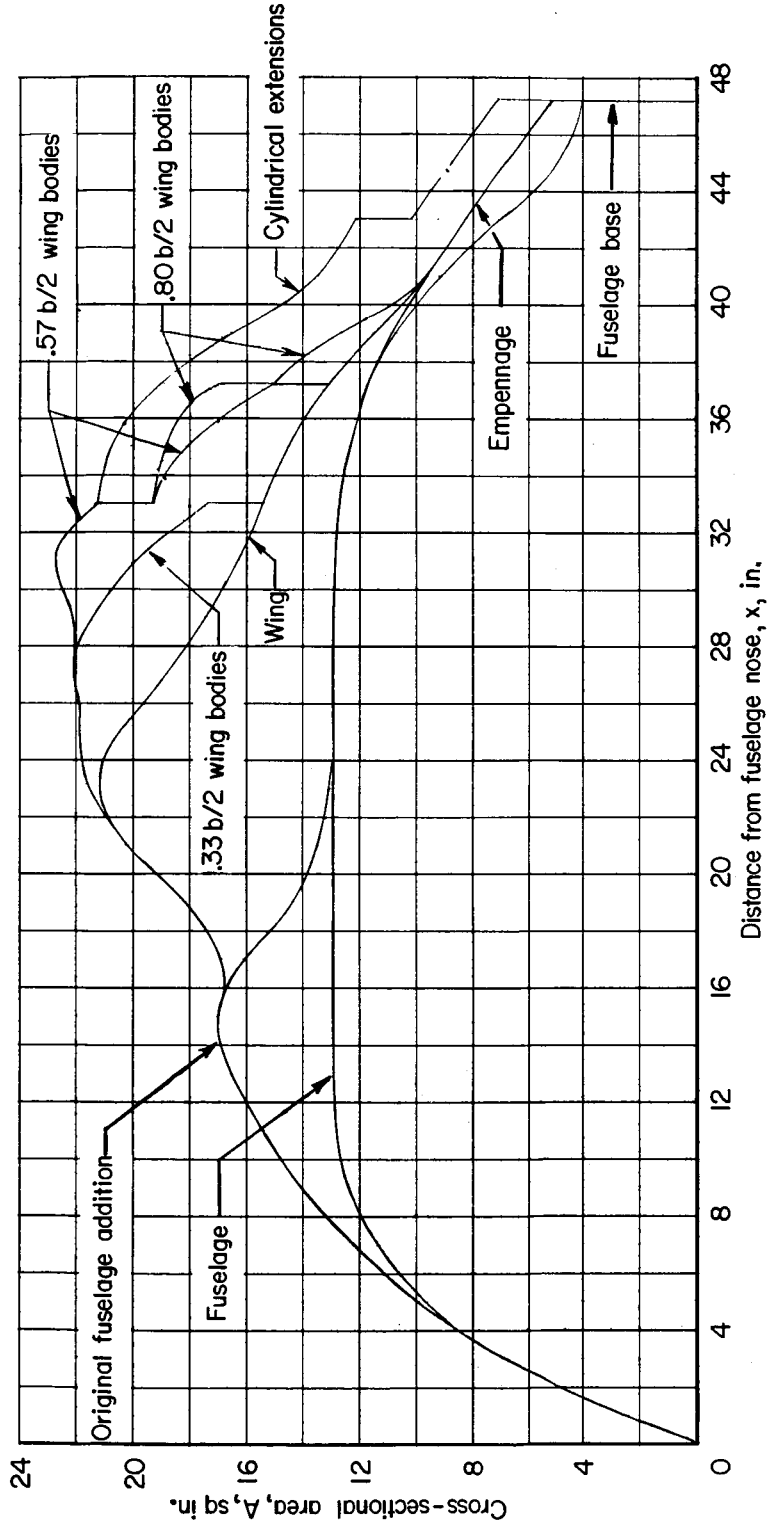

Figure 4.- Axial development of cross-sectional area distribution for basic model.

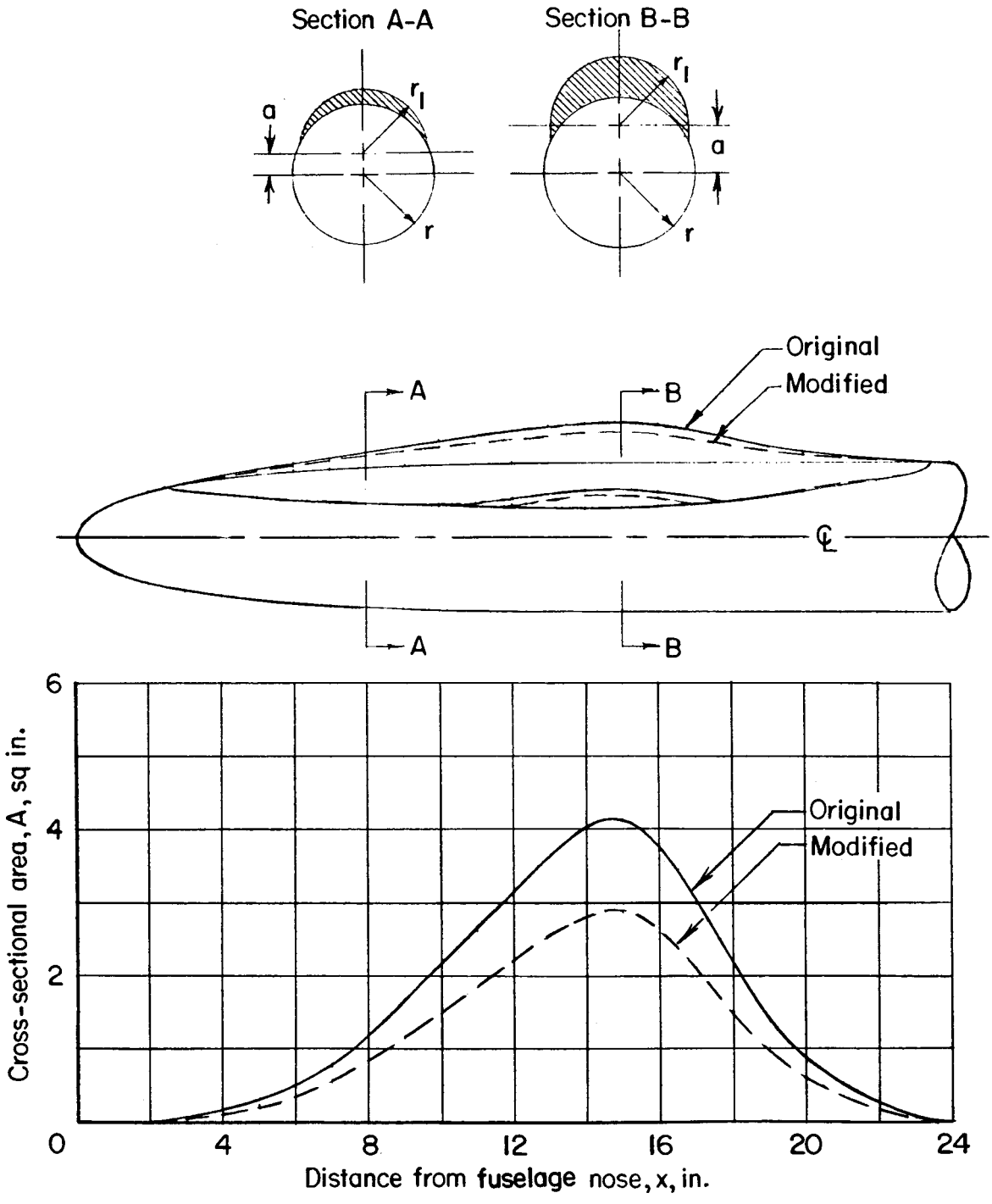

Figure 5.- Sketch of details of fuselage additions.

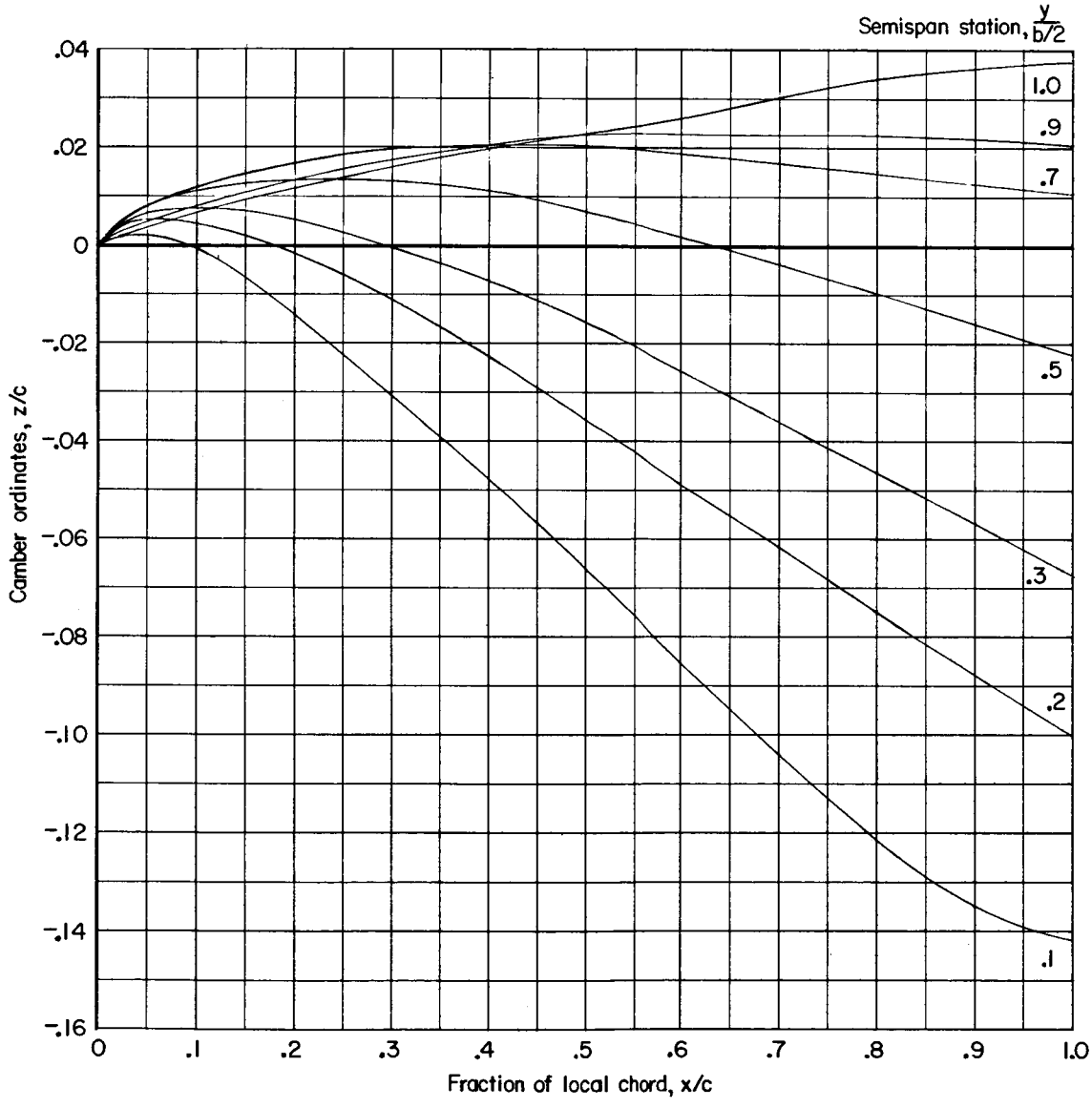

Figure 6.- Streamwise camber ordinates of transonic-transport model wing. $\Lambda = 40^{\circ}$.

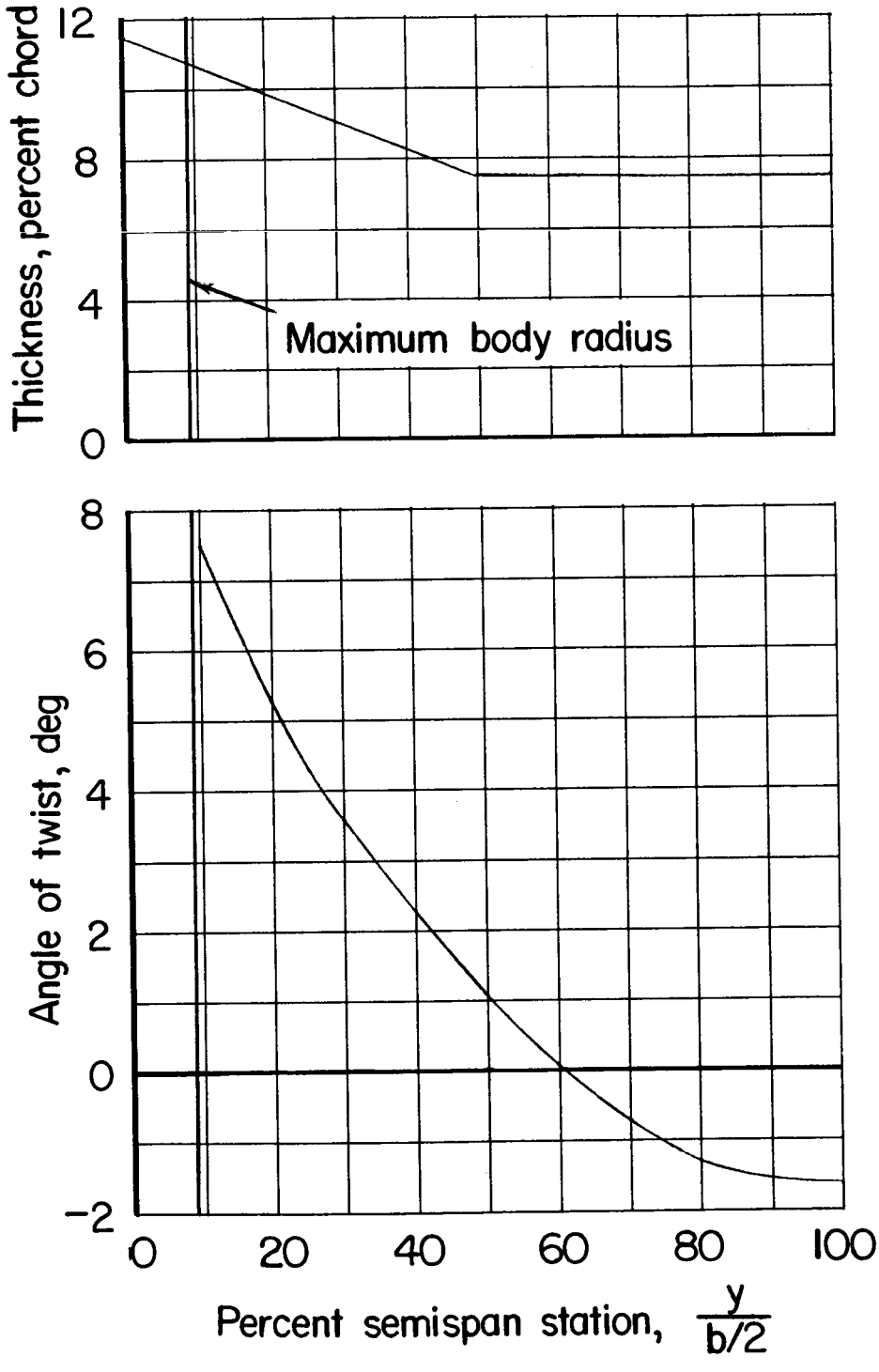

Figure 7.- Thickness ratio and twist distribution of transonic-transport model wing. $\Lambda = 45^{\circ}$.

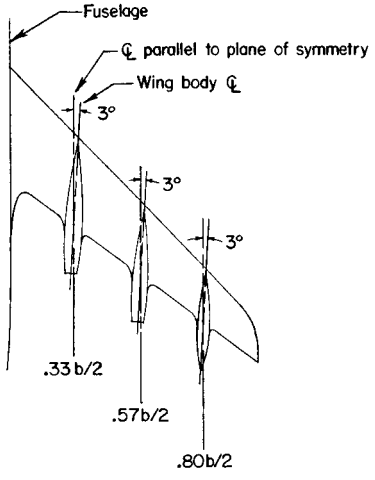

(a) Basic-model wing-body arrangement.

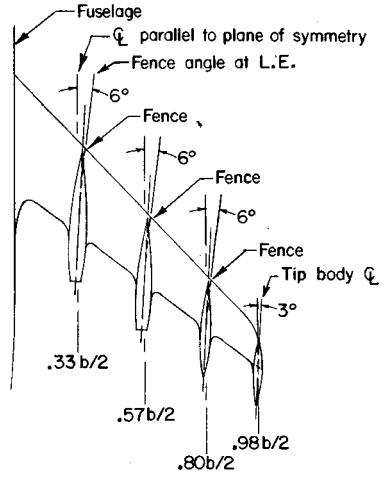

(b) Wing with basic wing bodies, wing-tip body, and fences.

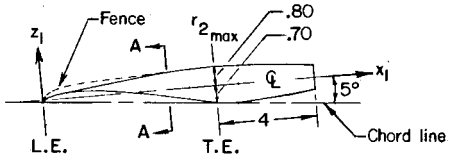

Station 0.33 b/2

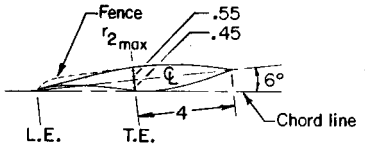

Station 0.80b/2

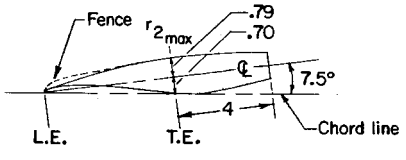

Station 0.57 b/2

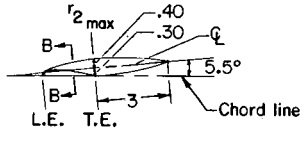

Station 0.98b/2

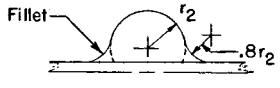

Section A-A (typical)
(Not to scale)

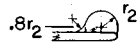

Section B-B
(Not to scale)

(c) Profiles of wing bodies and fences and typical cross sections of wing bodies.

Figure 8.- Sketch and geometric details of wing bodies and fences on model wing.

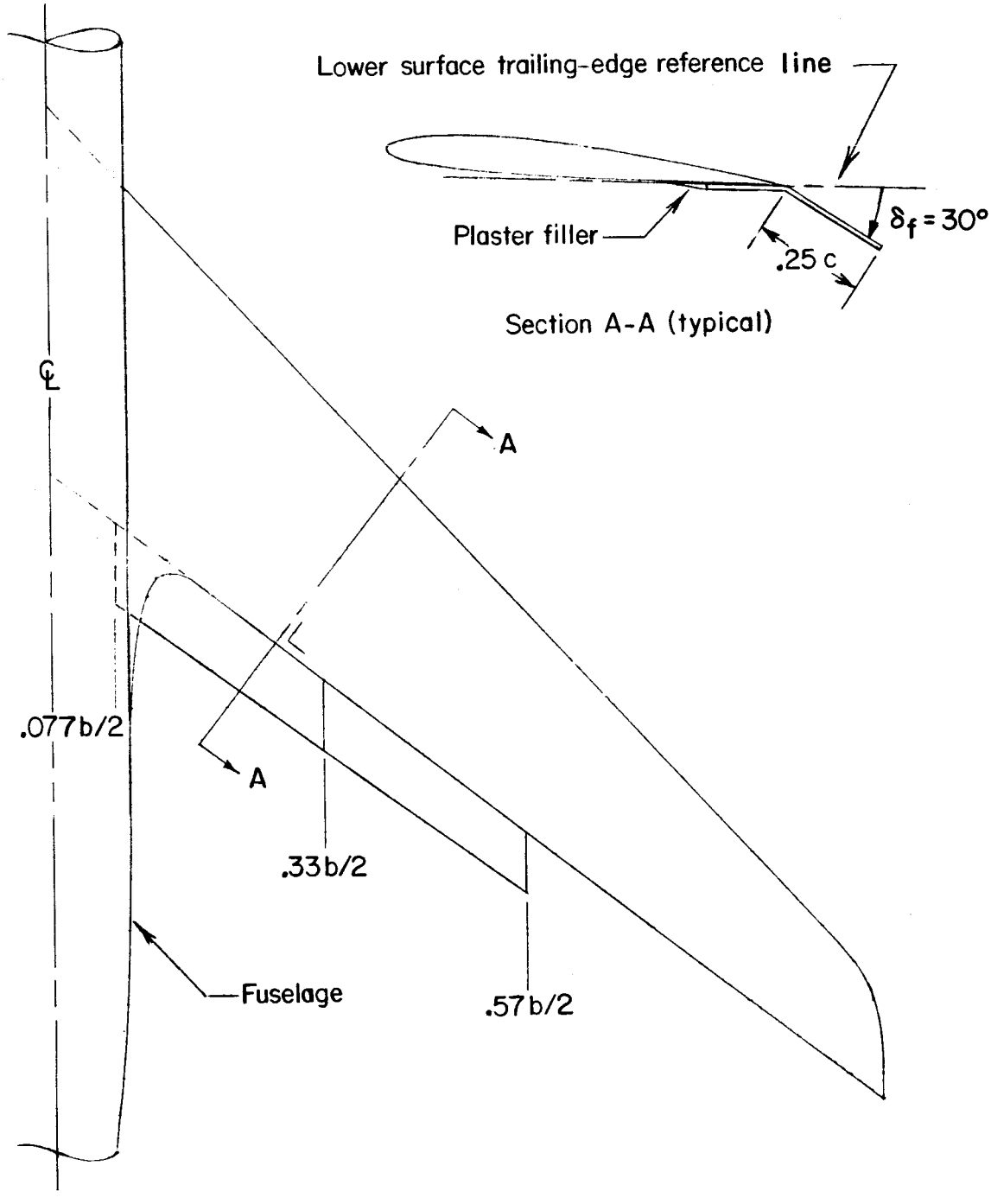

Figure 9.- Sketch of details of wing trailing-edge flaps.

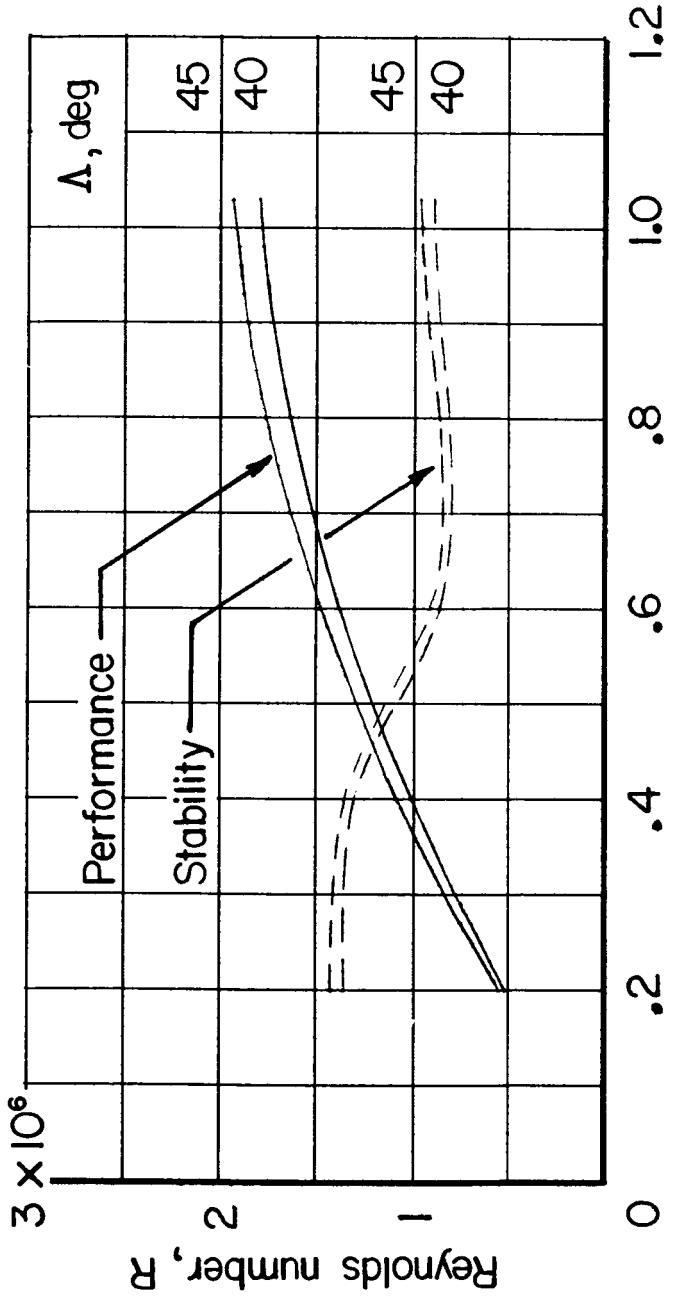

Figure 10.- Variation with Mach number of Reynolds number for transonic-transport model in Langley 8-foot transonic pressure tunnel.

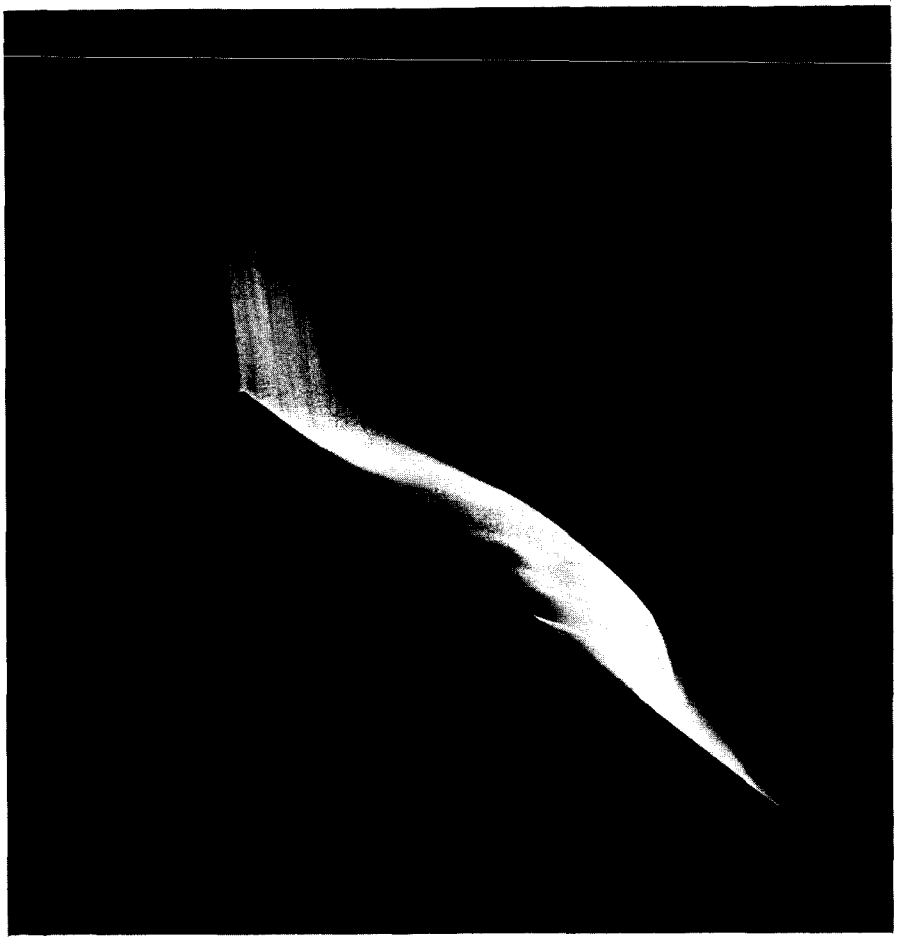

L-60-5585

Figure 11.- Photograph of fluorescent-oil-film pattern on transonic-transport model wing. $\Lambda = 45^{\circ}$; $\Gamma = 6^{\circ}$; $M \approx 0.96$; $C_L \approx 0.3$.

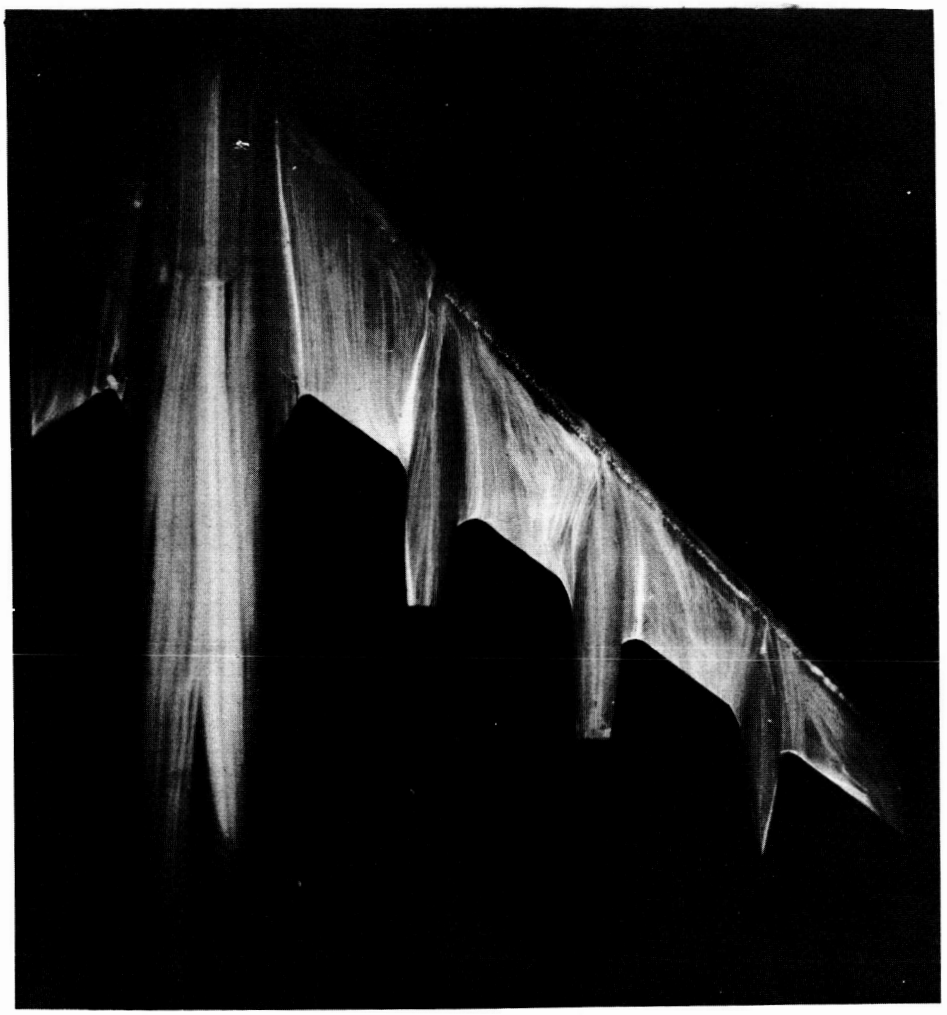

L-60-5586.1

Figure 12.- Photograph of fluorescent-oil-film pattern on transonic-transport model wing with wing bodies (basic model). $\Lambda = 45^\circ$; $\Gamma = 6^\circ$; $M \approx 0.96$; $C_L \approx 0.3$.

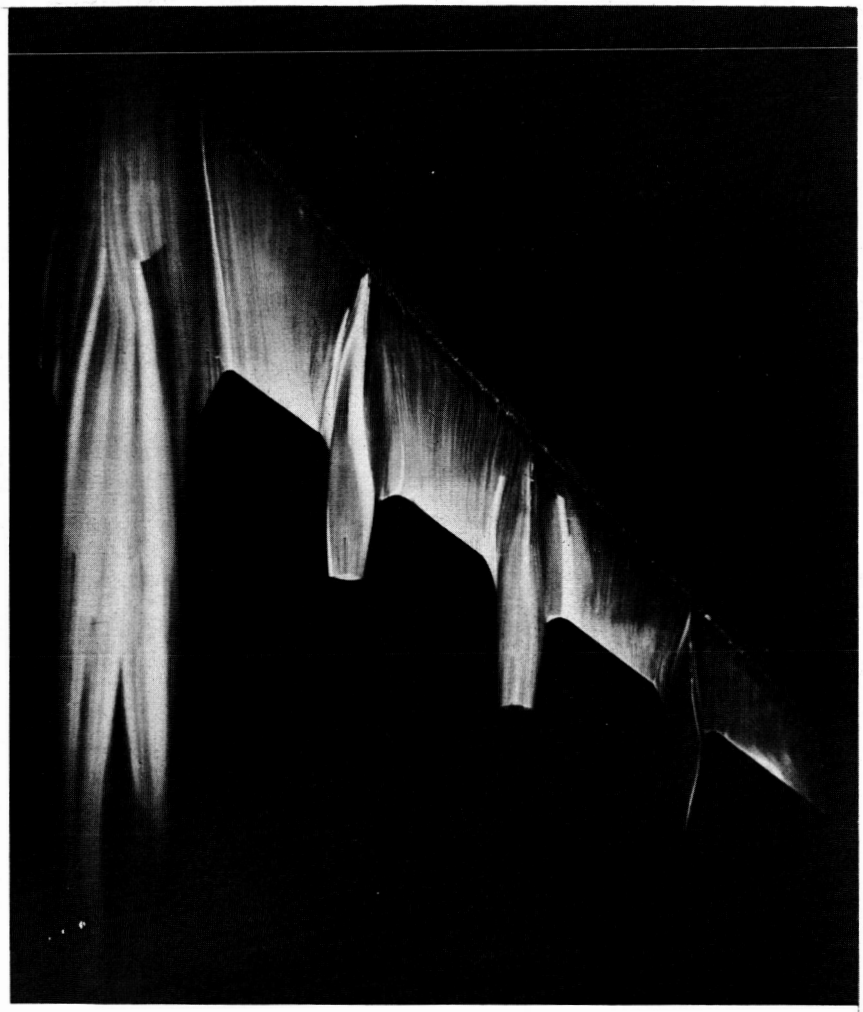

L-60-5587

Figure 13.- Photograph of fluorescent-oil-film pattern on transonic-transport basic model with fences. $\Lambda = 45^{\circ}$; $\Gamma = 6^{\circ}$; $M \approx 0.96$; $C_L \approx 0.3$.

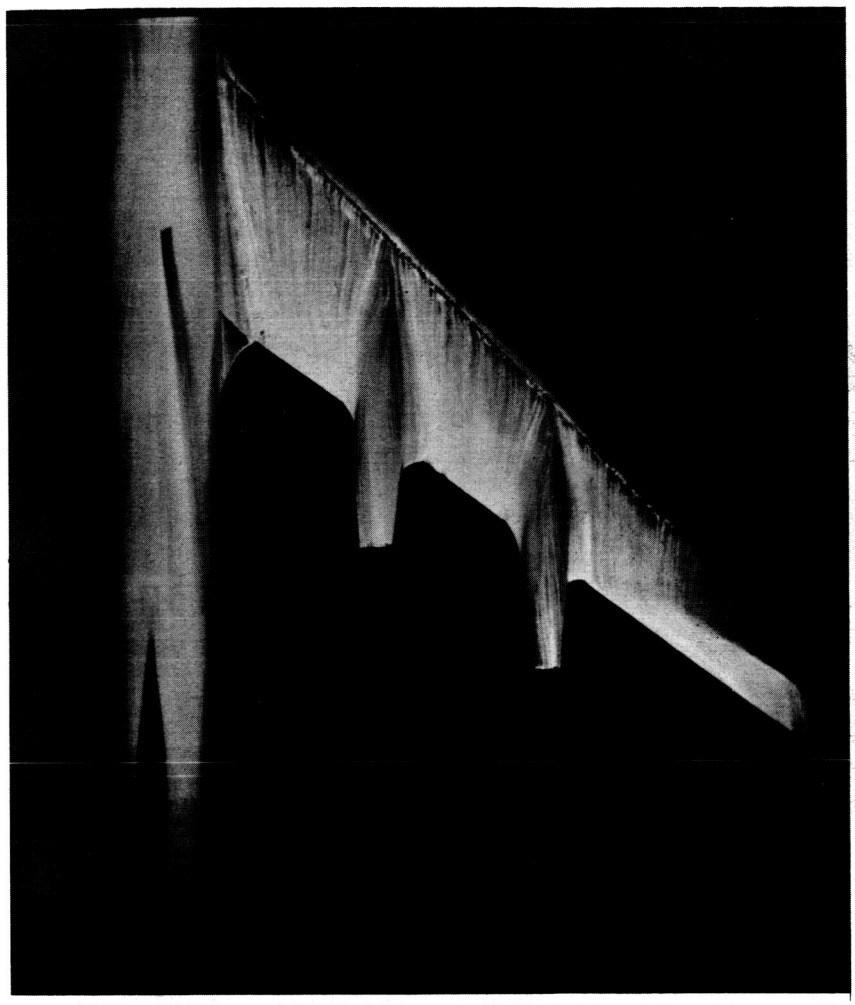

L-60-5588

Figure 14.- Photograph of fluorescent-oil-film pattern on transonic-transport basic model without 0.80b/2 wing body. $\Lambda = 45^{\circ}$; $\Gamma = 0^{\circ}$; $M = 0.96$; $C_L \approx 0.3$.

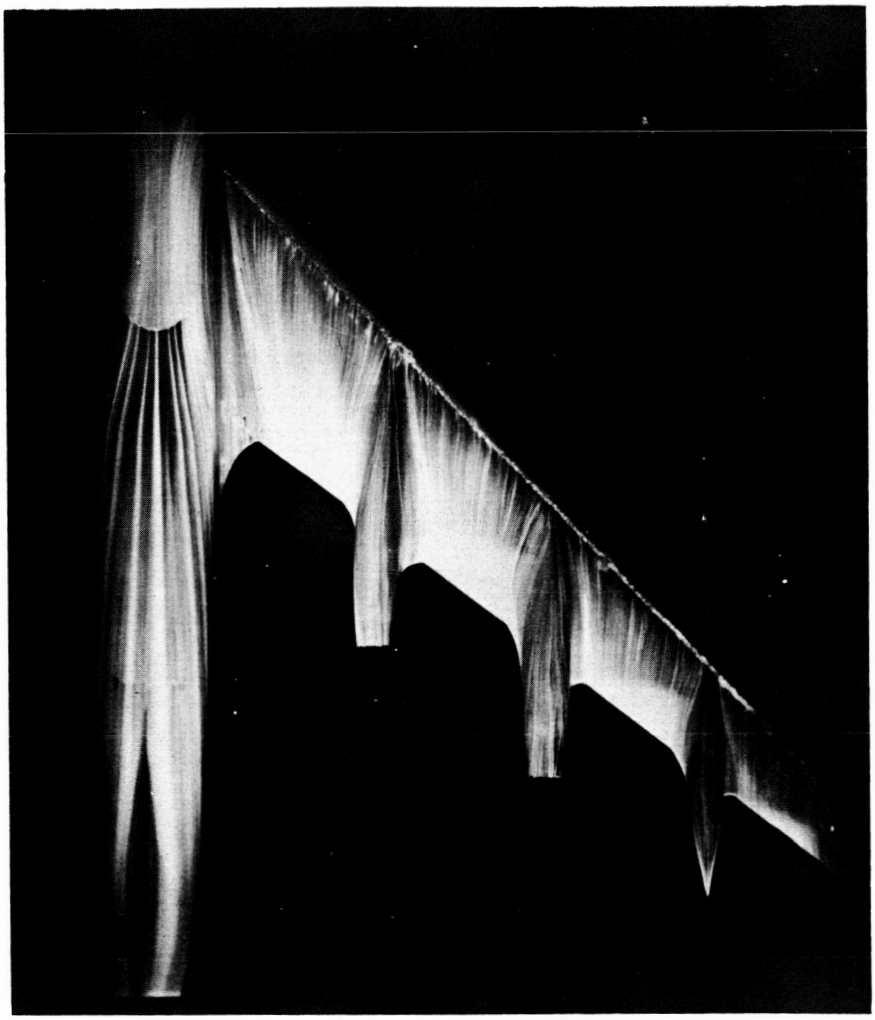

L-60-5589

Figure 15.- Photograph of fluorescent-oil-film pattern on transonic-transport basic model with 0.80b/2 wing body. $\Lambda = 45^{\circ}$; $\Gamma = 0^{\circ}$; $M = 0.96$; $C_L \approx 0.3$.

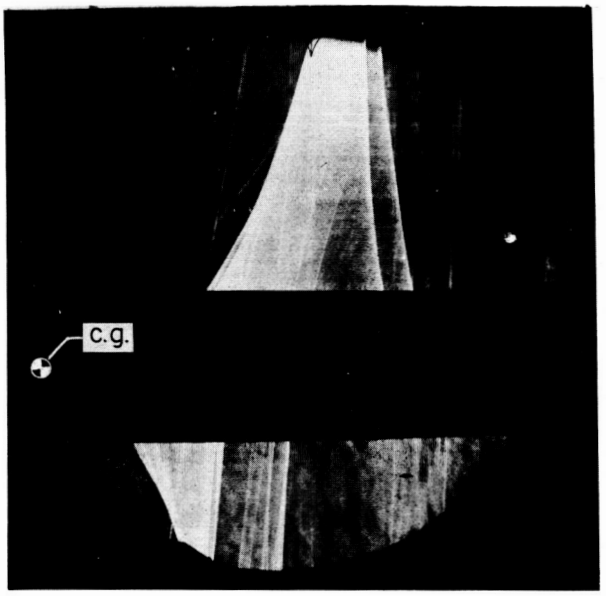

(a) Without wing bodies.

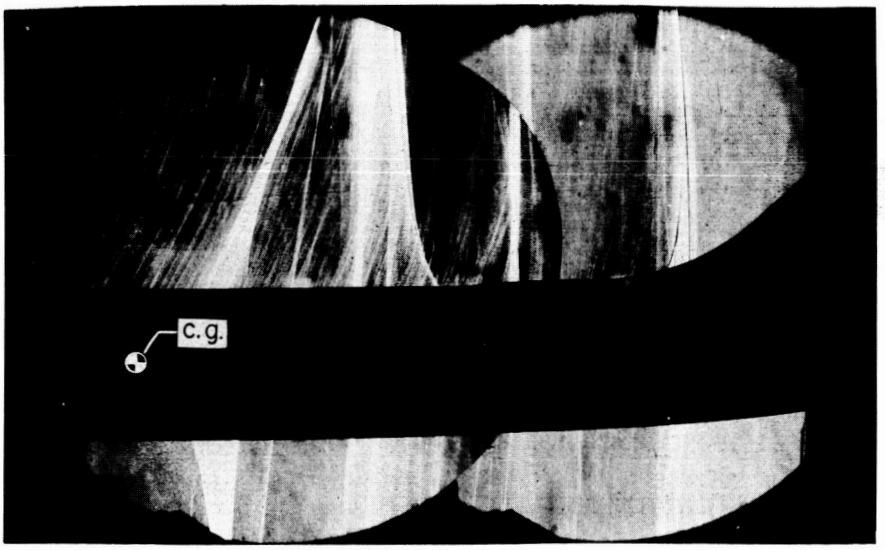

(b) With wing bodies. L-60-5590.1

Figure 16.- Schlieren photographs of shock waves in the flow about transonic-transport basic model. $\Lambda = 45^{\circ}$; $\Gamma = 6^{\circ}$; $M = 0.96$; $C_L \approx 0.3$.

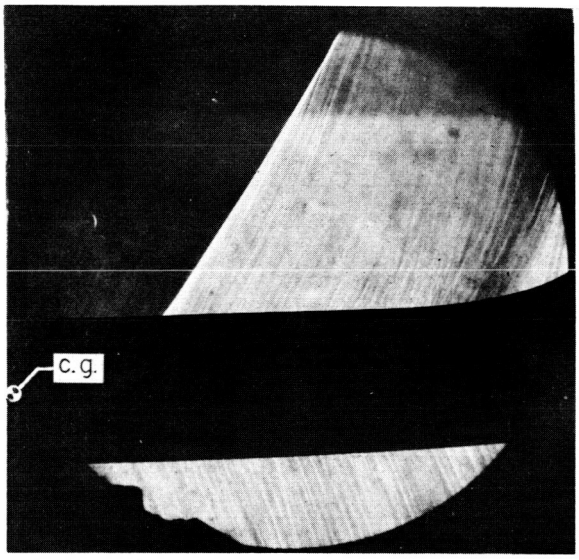

(a) Without wing bodies.

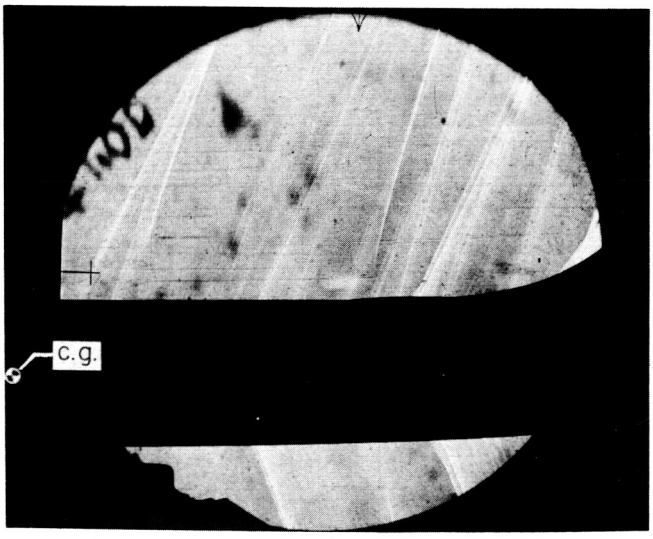

(b) With wing bodies. L-60-5591.1

Figure 17.- Schlieren photographs of shock waves in the flow about transonic-transport basic model. $\Lambda = 45^{\circ}$; $\Gamma = 6^{\circ}$; $M = 1.00$; $C_L \approx 0.2$.

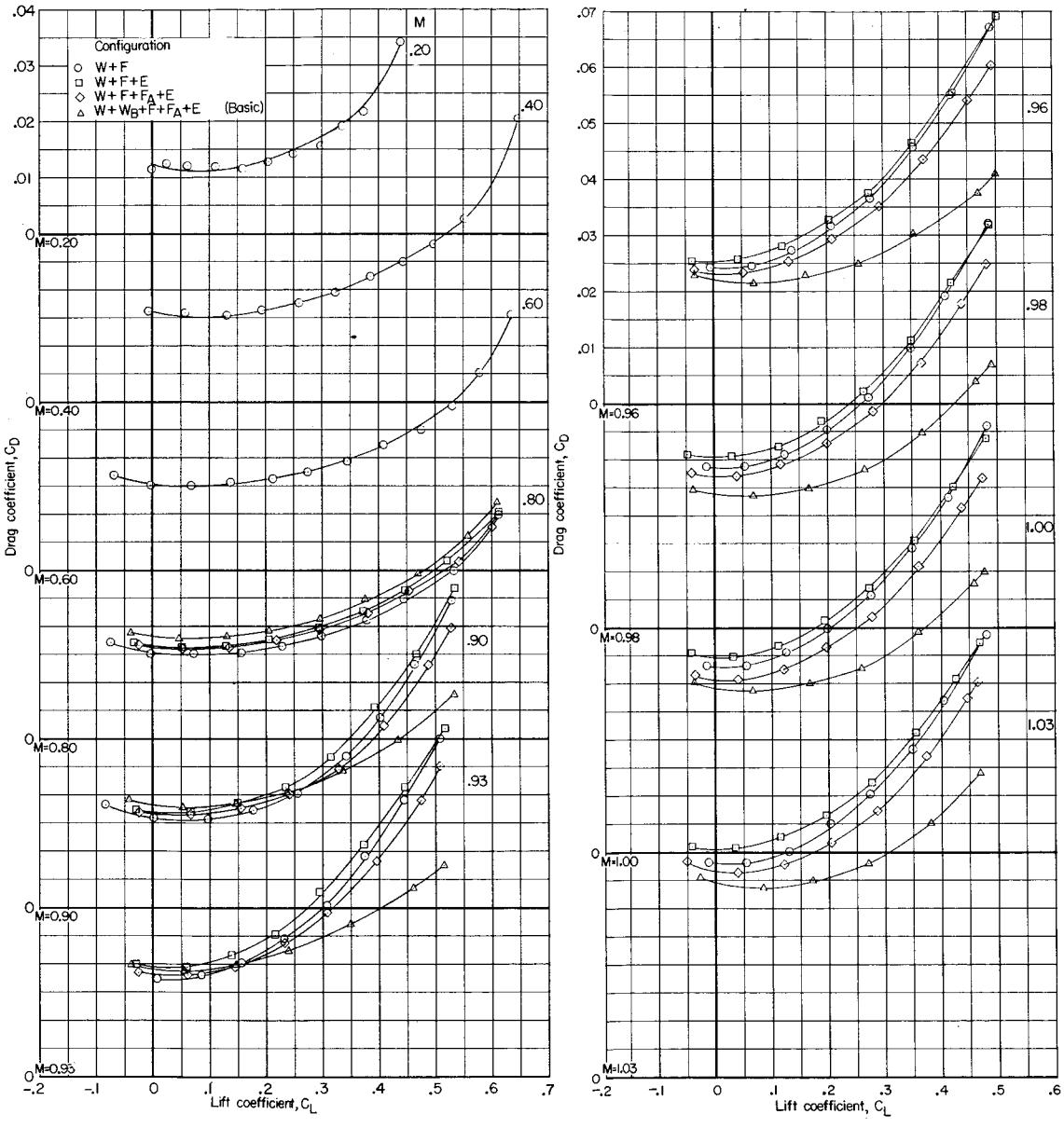

Figure 18.- Effect of various basic components on aerodynamic drag characteristics of basic model. $\Lambda = 45^{\circ}$; $\Gamma = 6^{\circ}$; $\beta = 0^{\circ}$.

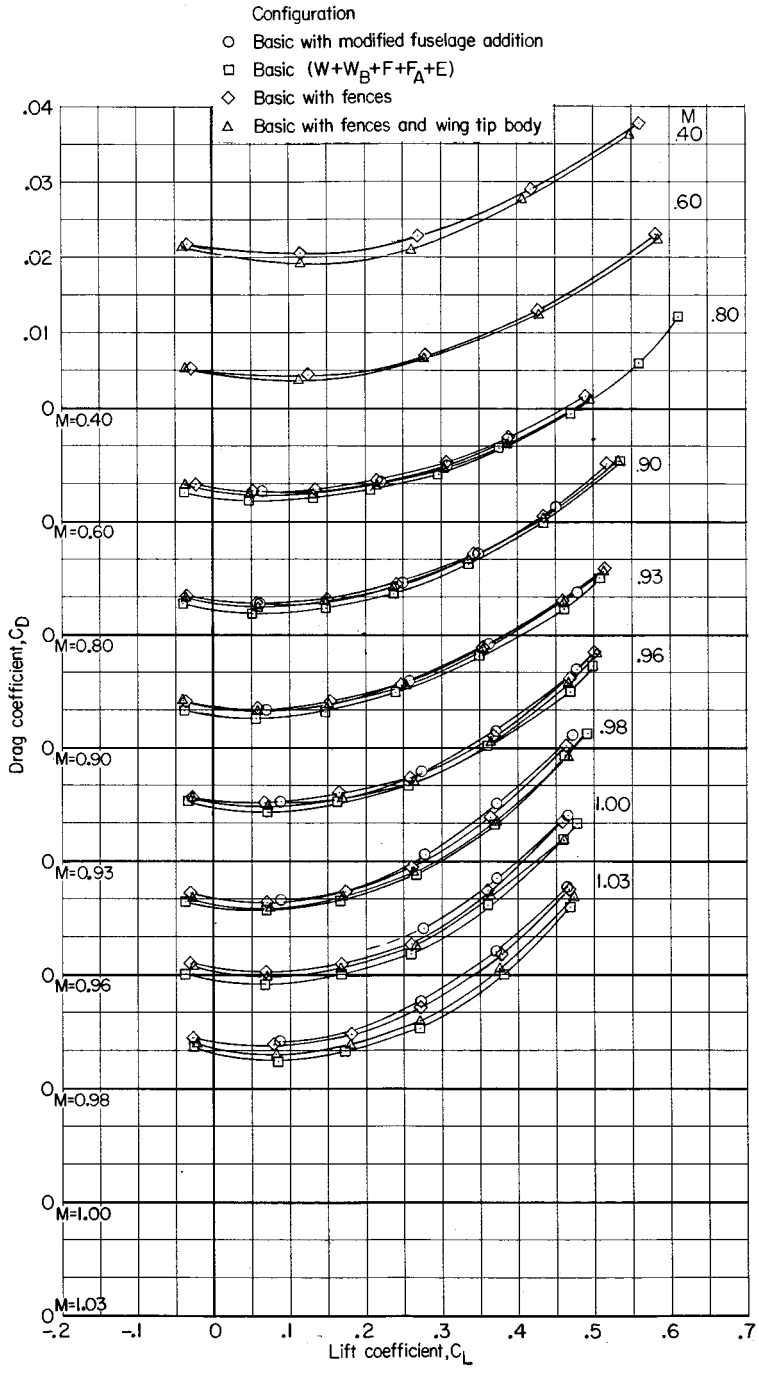

Figure 19.- Effect of modified fuselage addition, fences, and wing-tip bodies on aerodynamic drag characteristics of basic model. $\Lambda = 45^{\circ}$; $\Gamma = 6^{\circ}$; $\beta = 0^{\circ}$. Short dash lines indicate extrapolation of data.

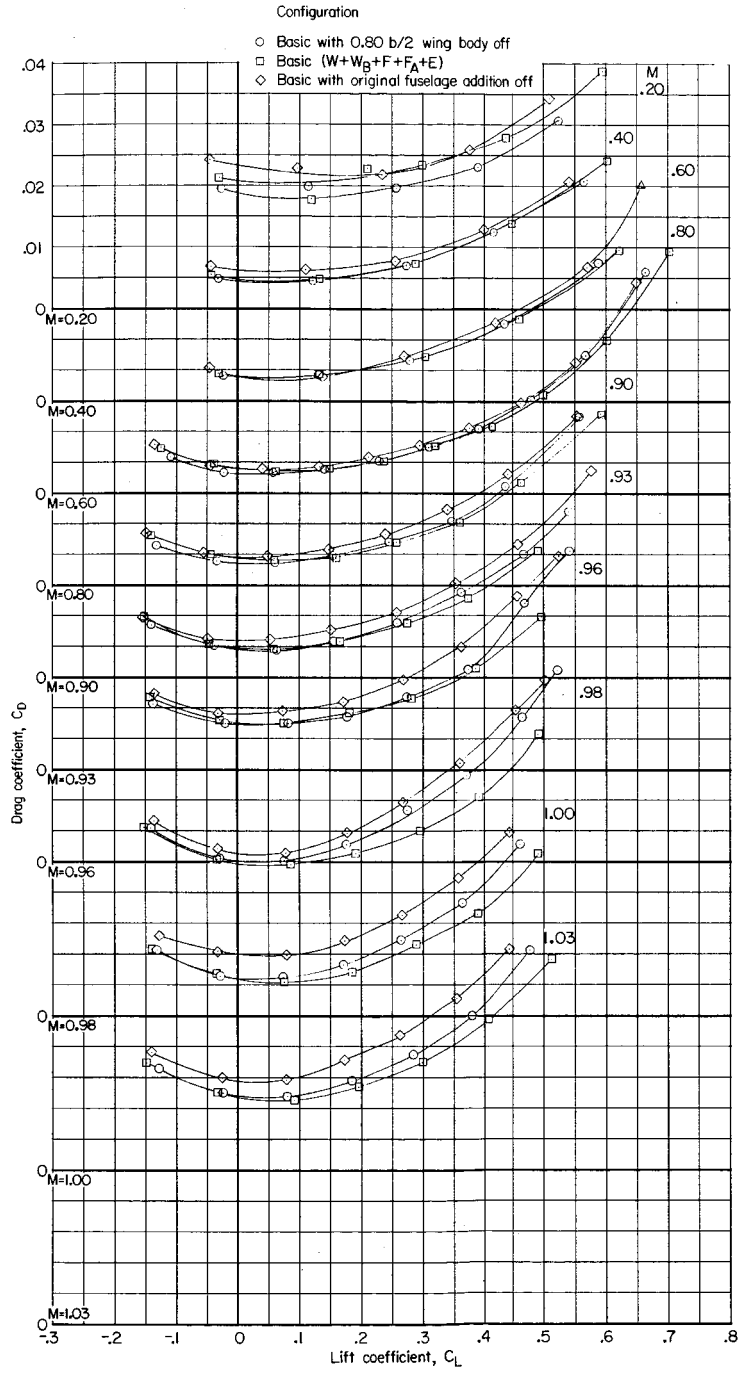

Figure 20.- Effect of 0.80b/2 wing bodies and original fuselage addition on aerodynamic drag characteristics of basic model. $\Lambda = 45^{\circ}$; $\Gamma = 0^{\circ}$; $\beta = 0^{\circ}$.

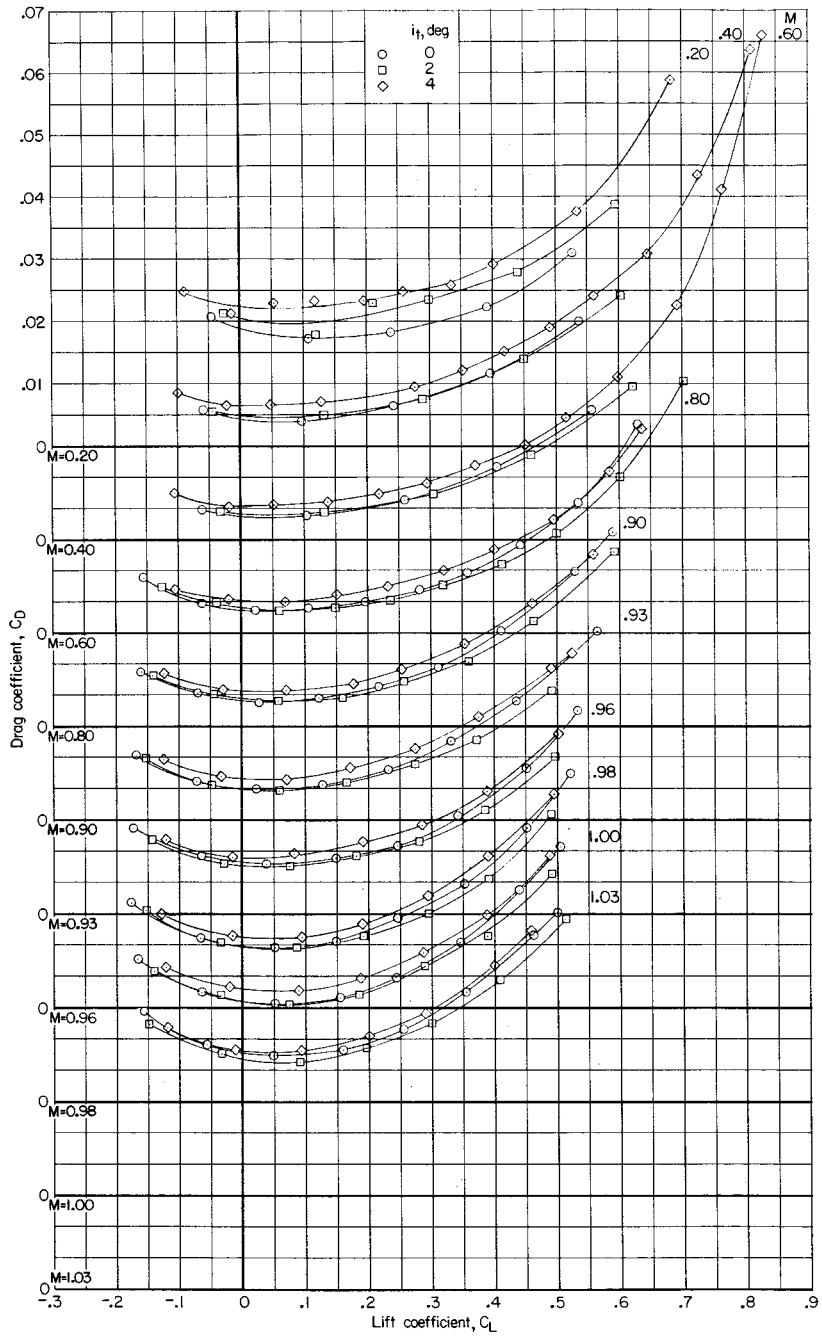

Figure 21.- Effect of various horizontal-tail settings on aerodynamic drag characteristics of basic model $(W + W_B + F + F_A + E)$. $\Lambda = 45^\circ$; $\Gamma = 0^\circ$; $\beta = 0^\circ$.

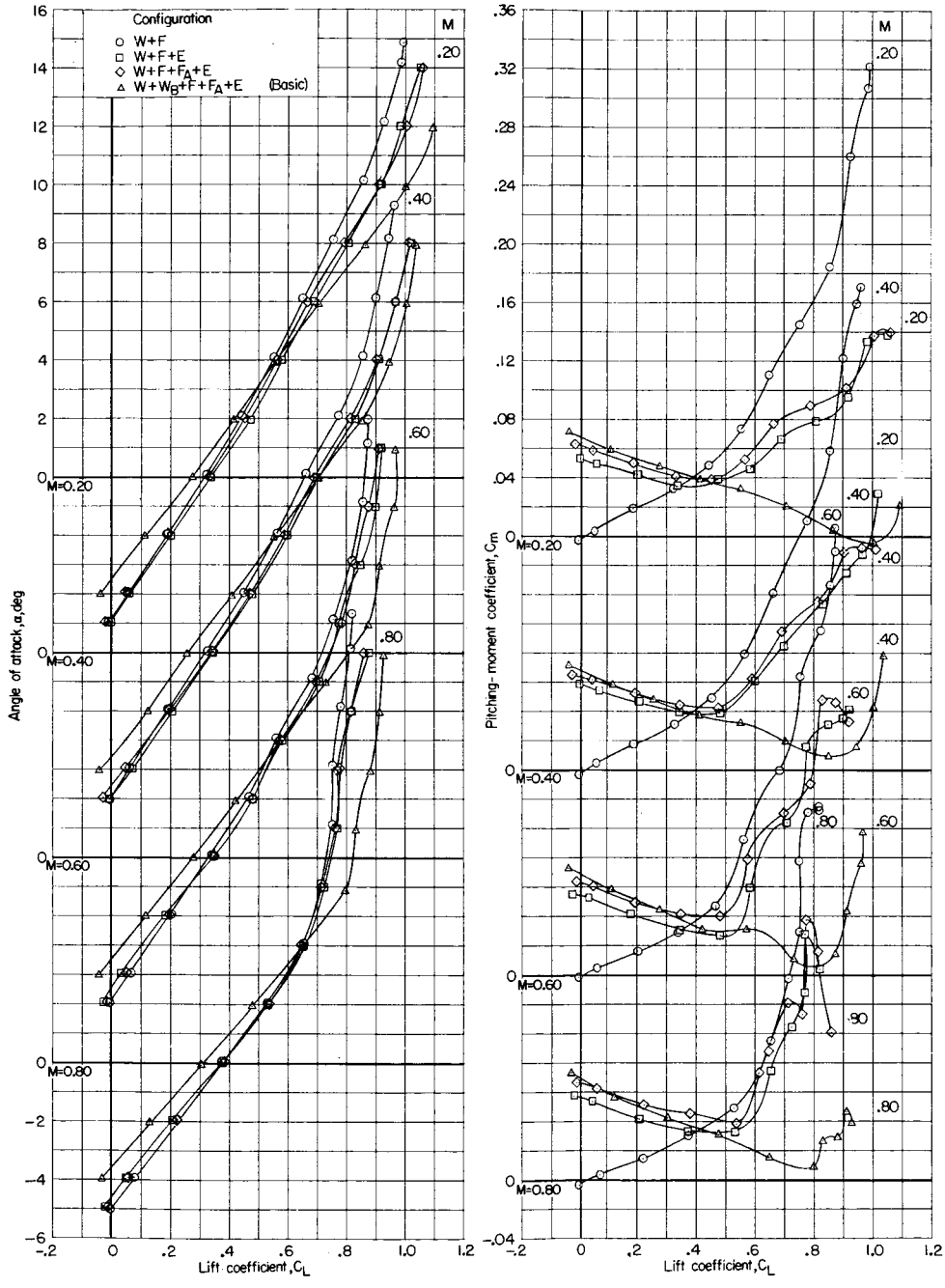

(a) M = 0.20 to 0.80.

Figure 22.- Effect of various basic components on aerodynamic lift and pitching-moment characteristics of basic model. $\Lambda = 45^\circ$; $\Gamma = 6^\circ$; $\beta = 0^\circ$.

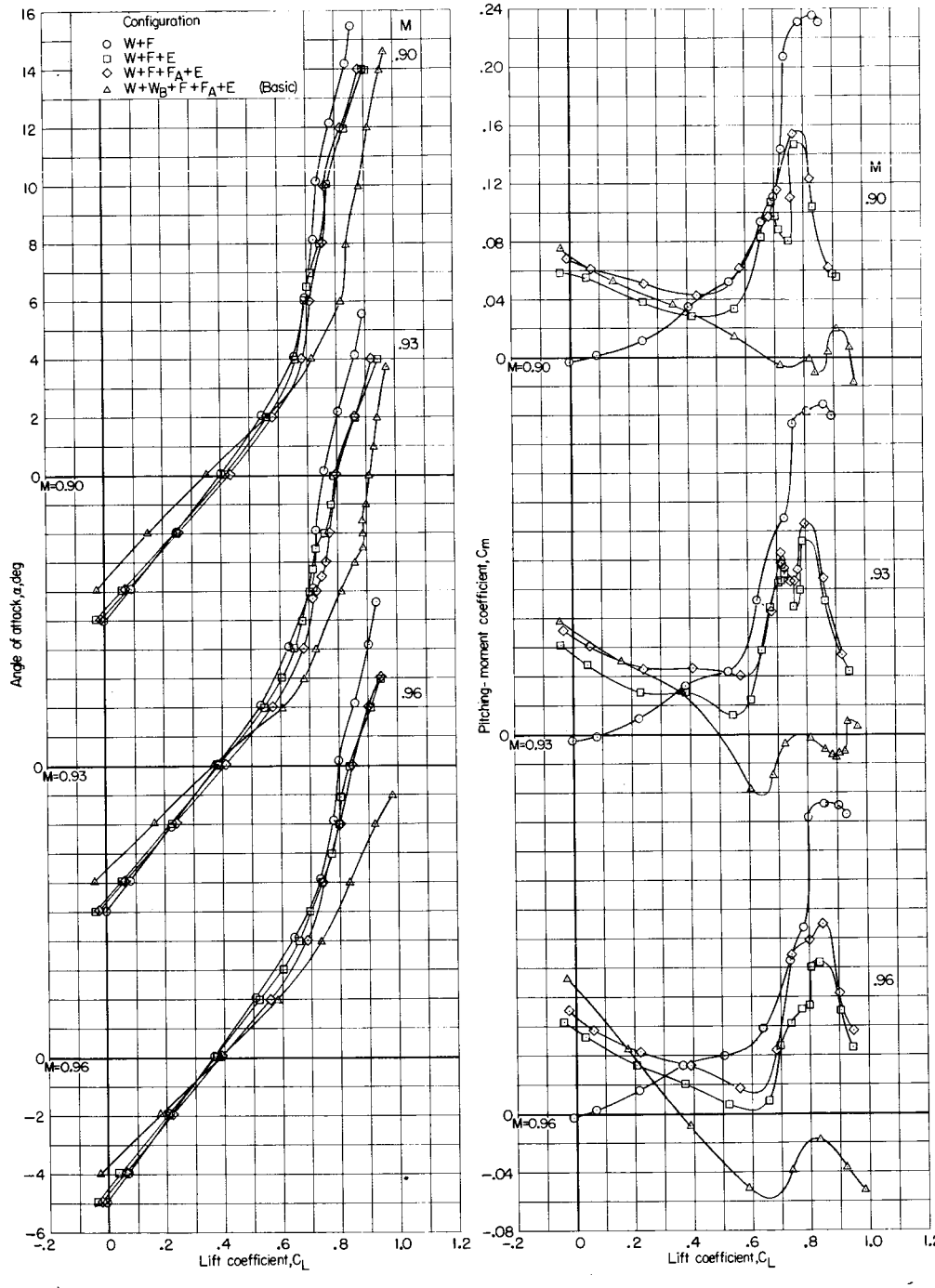

(b) M = 0.90 to 0.96.

Figure 22.- Continued.

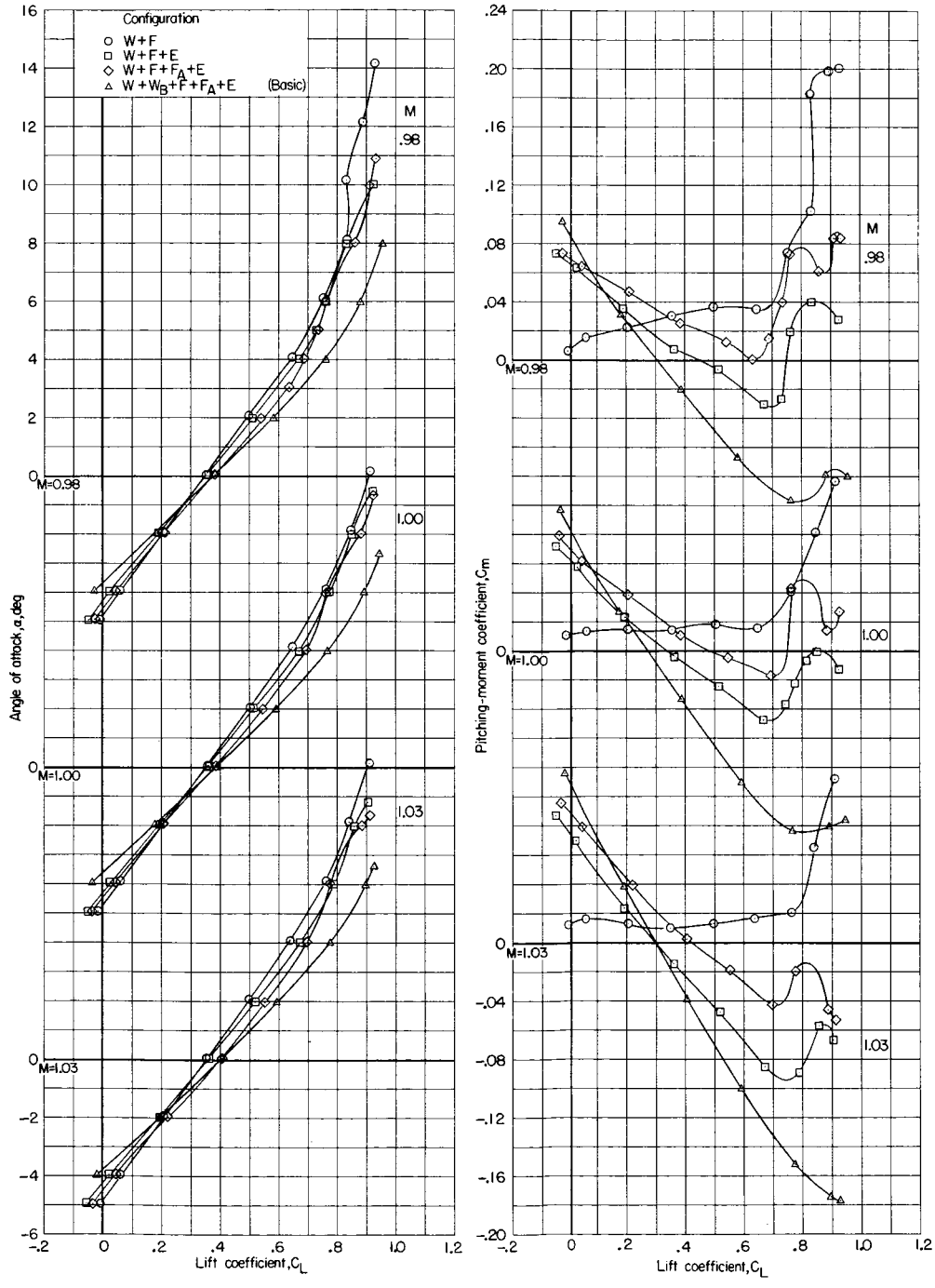

(c) M = 0.98 to 1.03.

Figure 22.- Concluded.

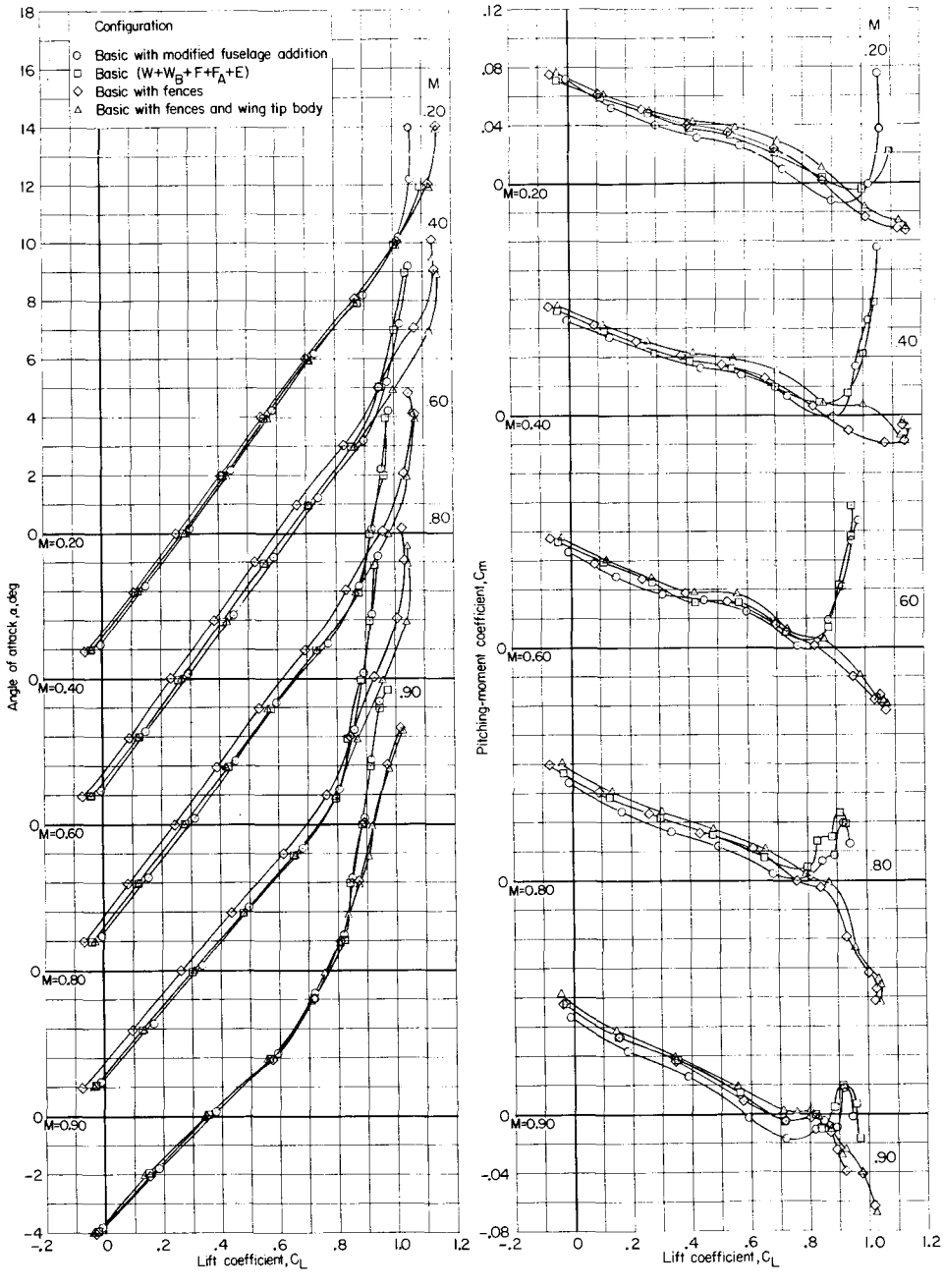

(a) M = 0.20 to 0.90.

Figure 23.- Effect of modified fuselage addition, fences, and wing-tip bodies on aerodynamic lift and pitching-moment characteristics of basic model. $\Lambda = 45^{\circ}$; $\Gamma = 6^{\circ}$; $\beta = 0^{\circ}$.

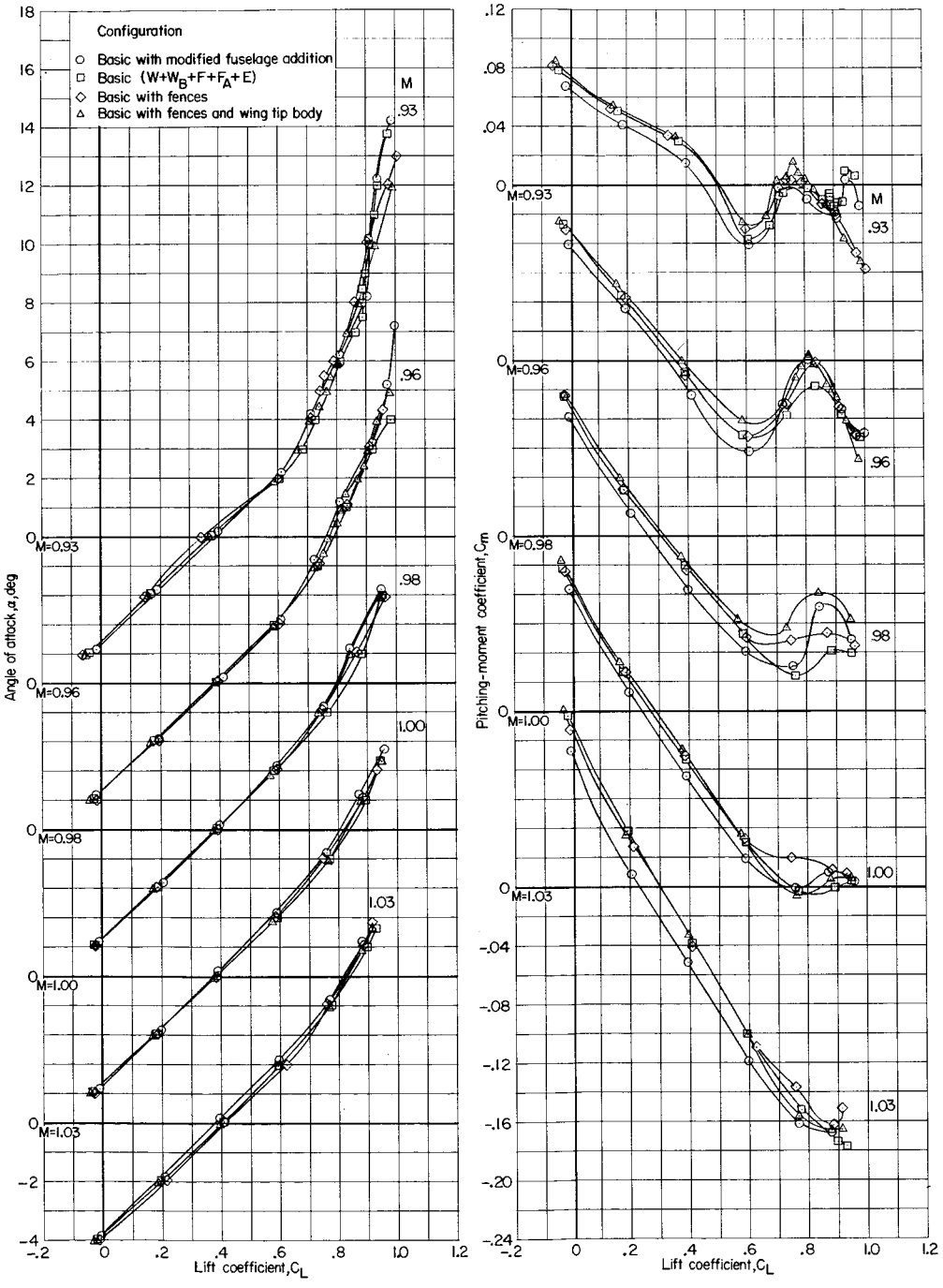

(b) M = 0.93 to 1.03.

Figure 23.- Concluded.

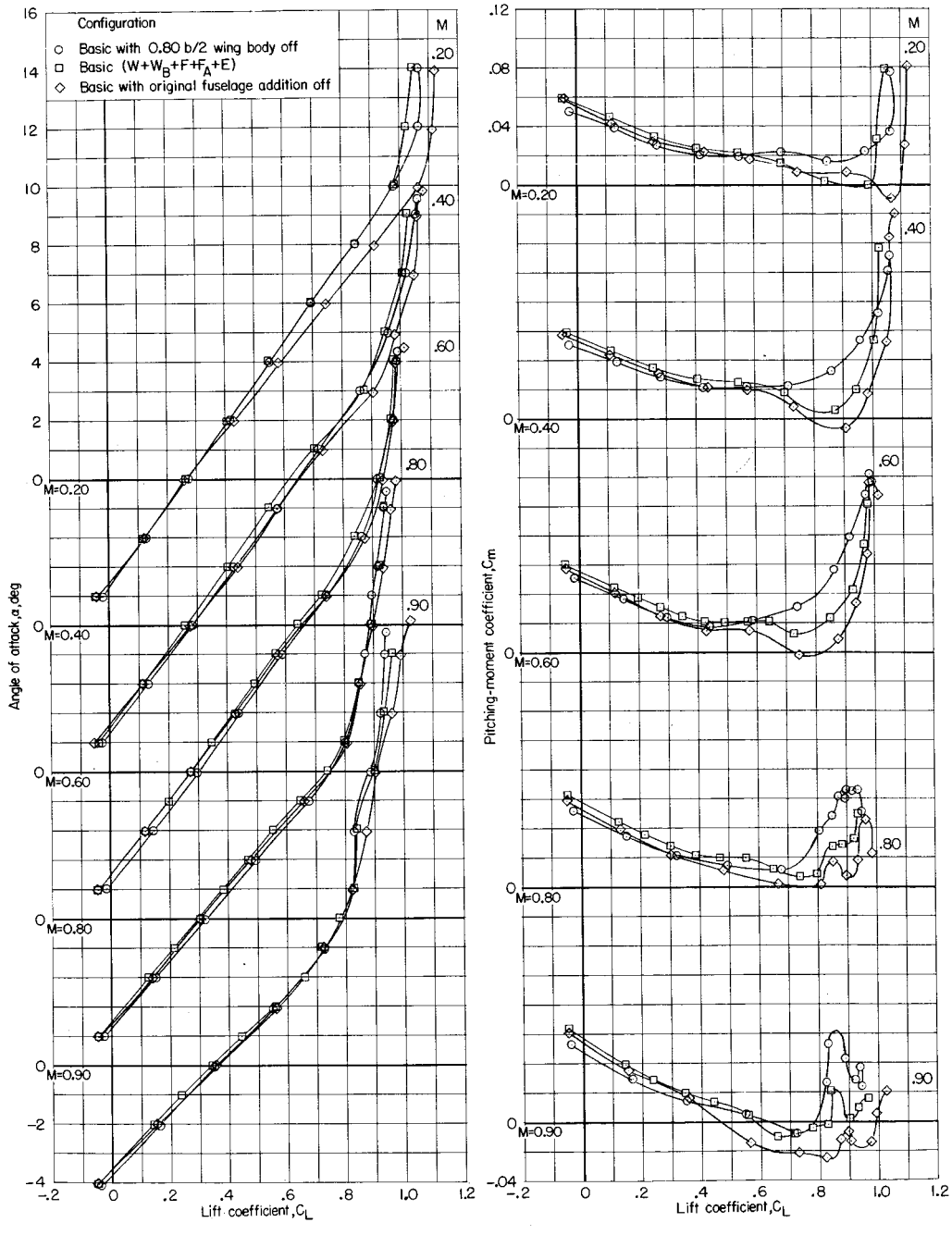

(a) M = 0.20 to 0.90.

Figure 24.- Effect of 0.80b/2 wing bodies and original fuselage addition on aerodynamic lift and pitching-moment characteristics of basic model. $\Lambda = 45^{\circ}$; $\Gamma = 0^{\circ}$; $\beta = 0^{\circ}$.

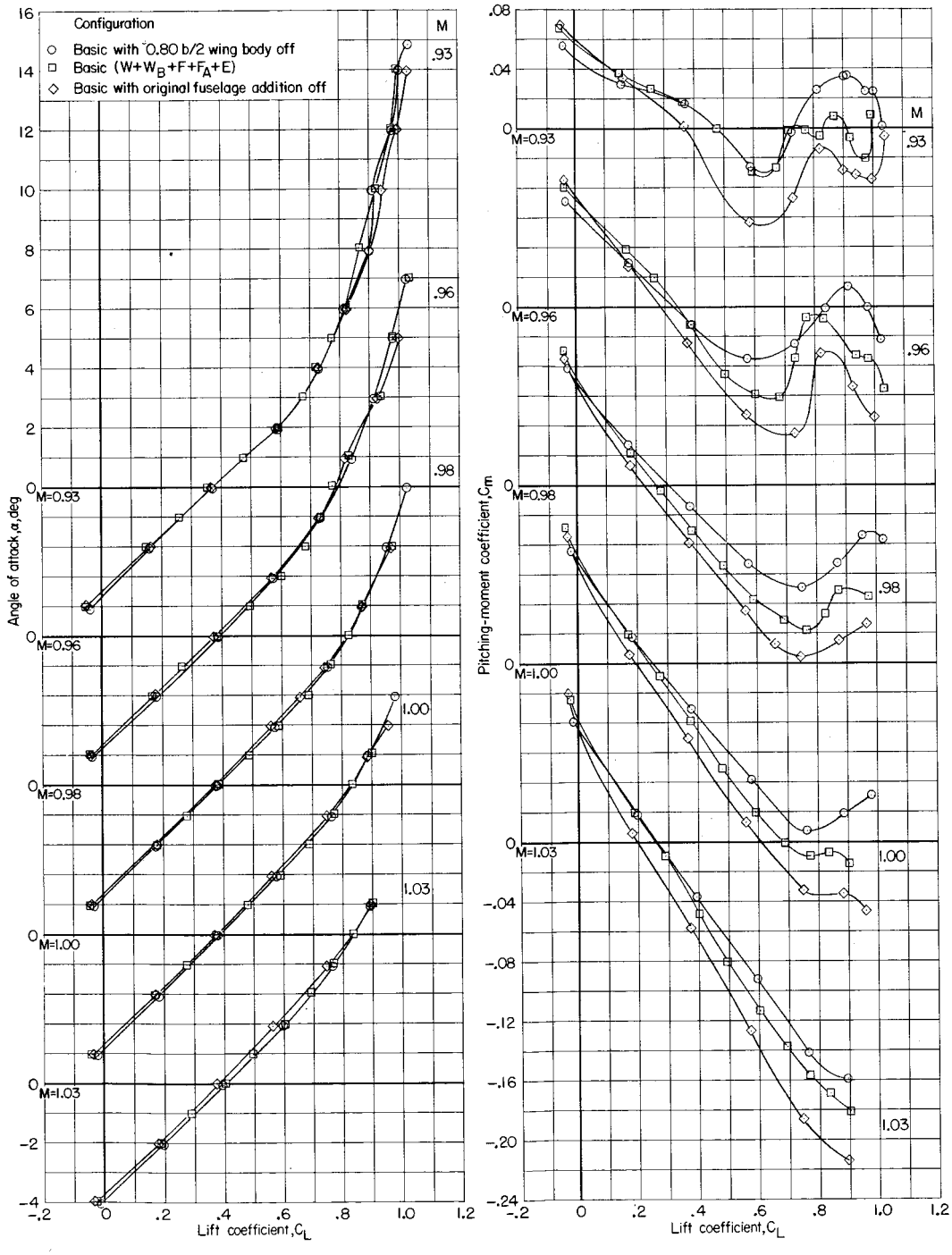

(b) M = 0.93 to 1.03.

Figure 24.- Concluded.

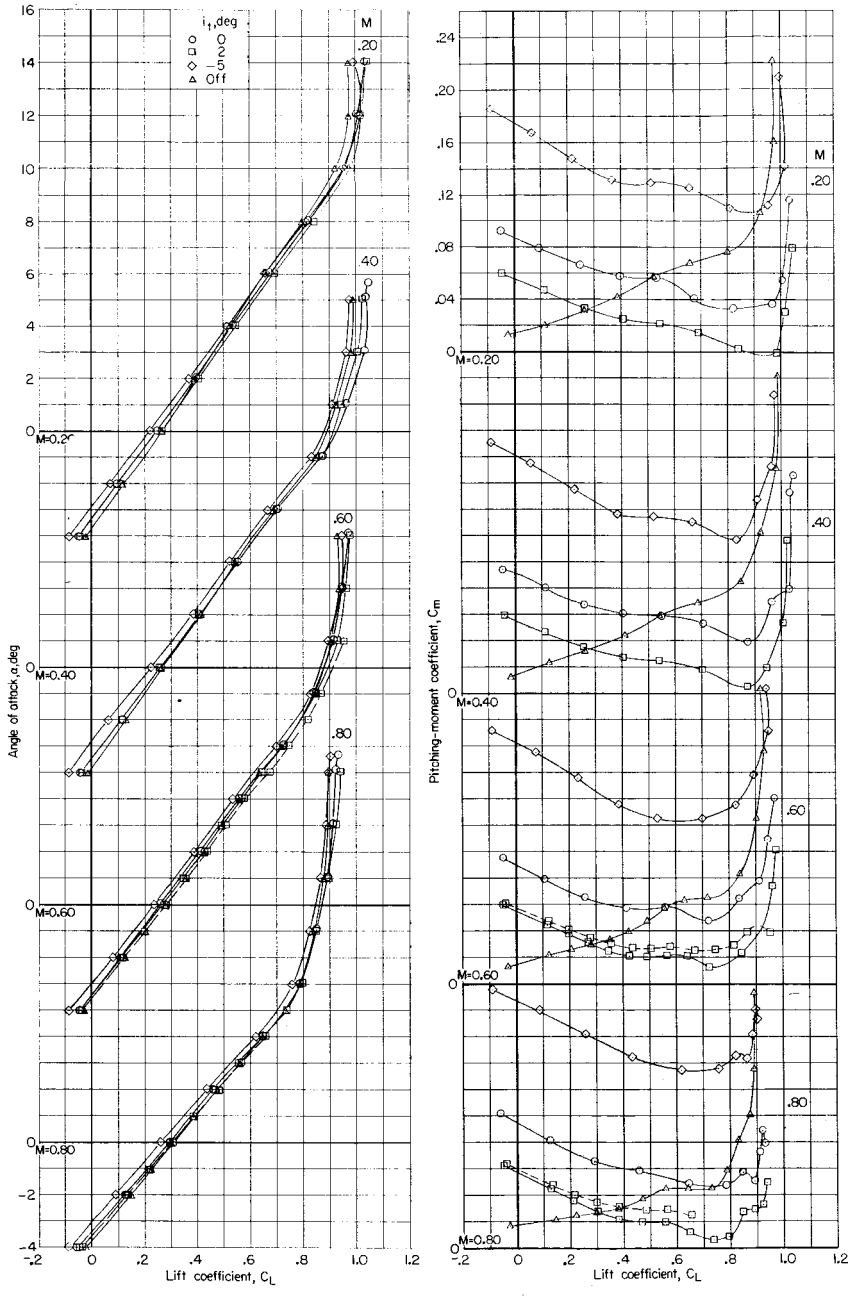

(a) M = 0.20 to 0.80.

Figure 25.- Effect of horizontal tail and various horizontal-tail settings on aerodynamic lift and pitching-moment characteristics of basic model $(W + W_B + F + F_A + E)$. $\Lambda = 45^\circ$; $\Gamma = 0^\circ$; $\beta = 0^\circ$; dashed lines indicate data obtained at performance-phase Reynolds numbers.

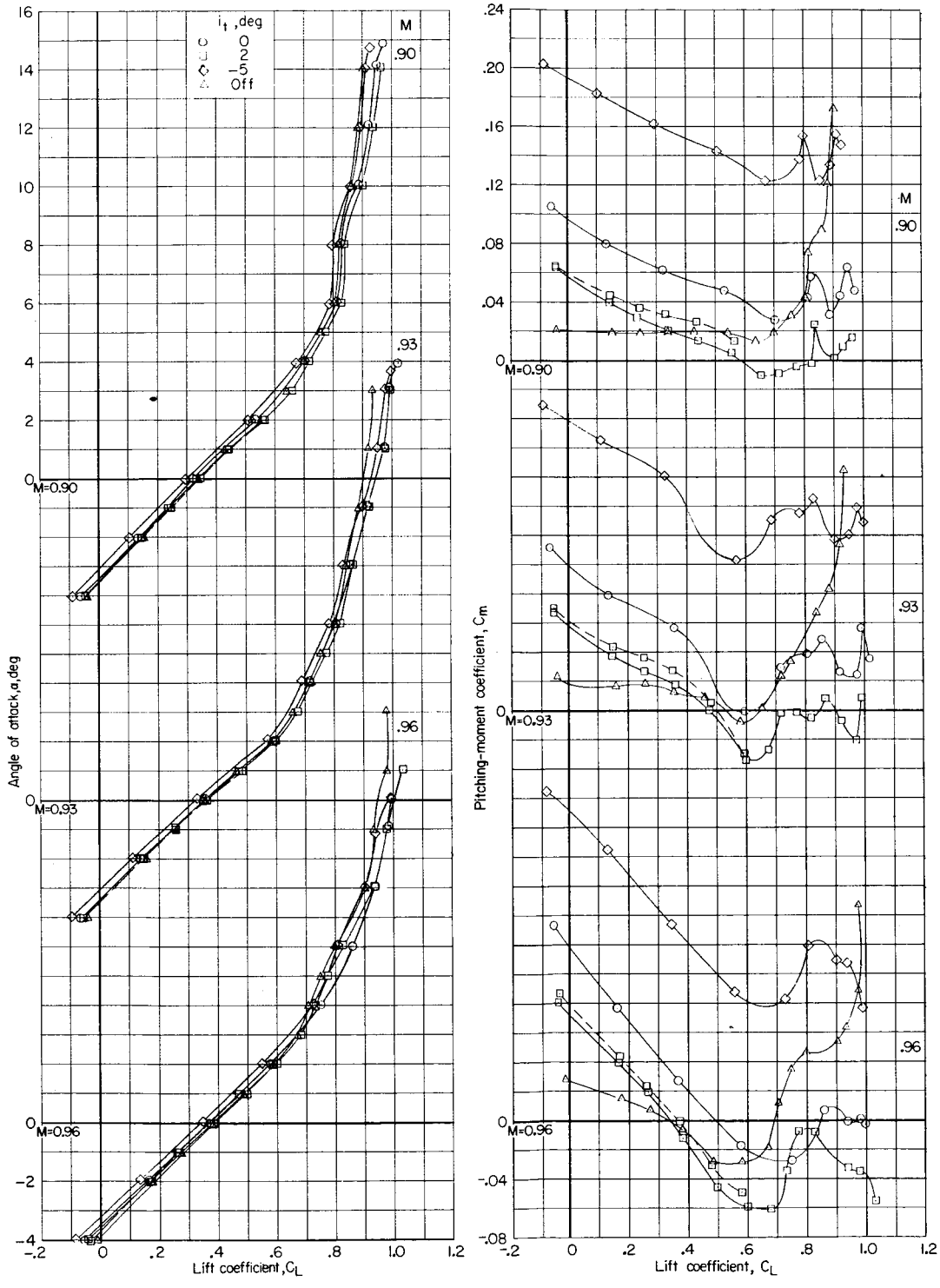

(b) M = 0.90 to 0.96.

Figure 25.- Continued.

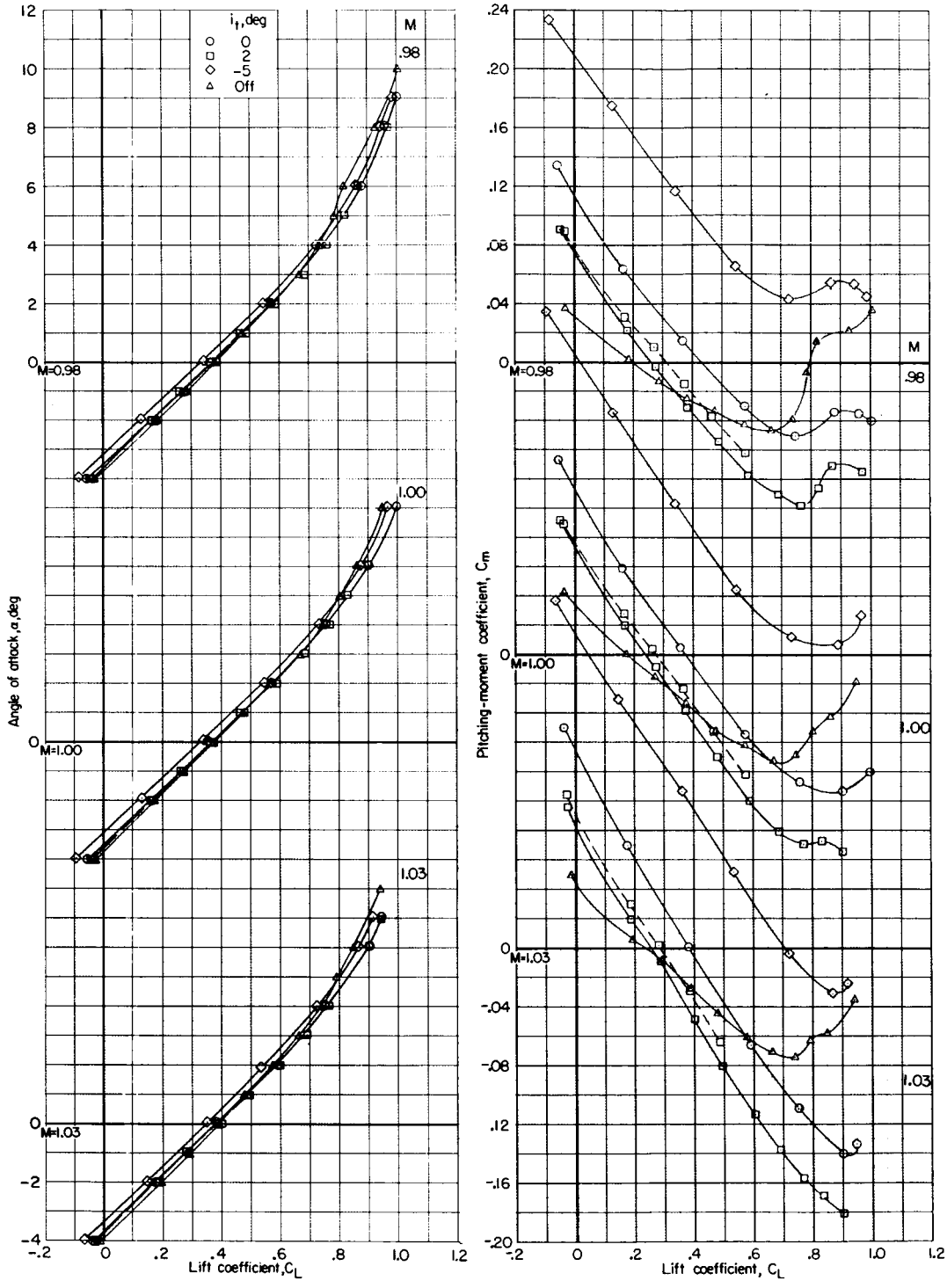

(c) M = 0.98 to 1.03.

Figure 25.- Concluded.

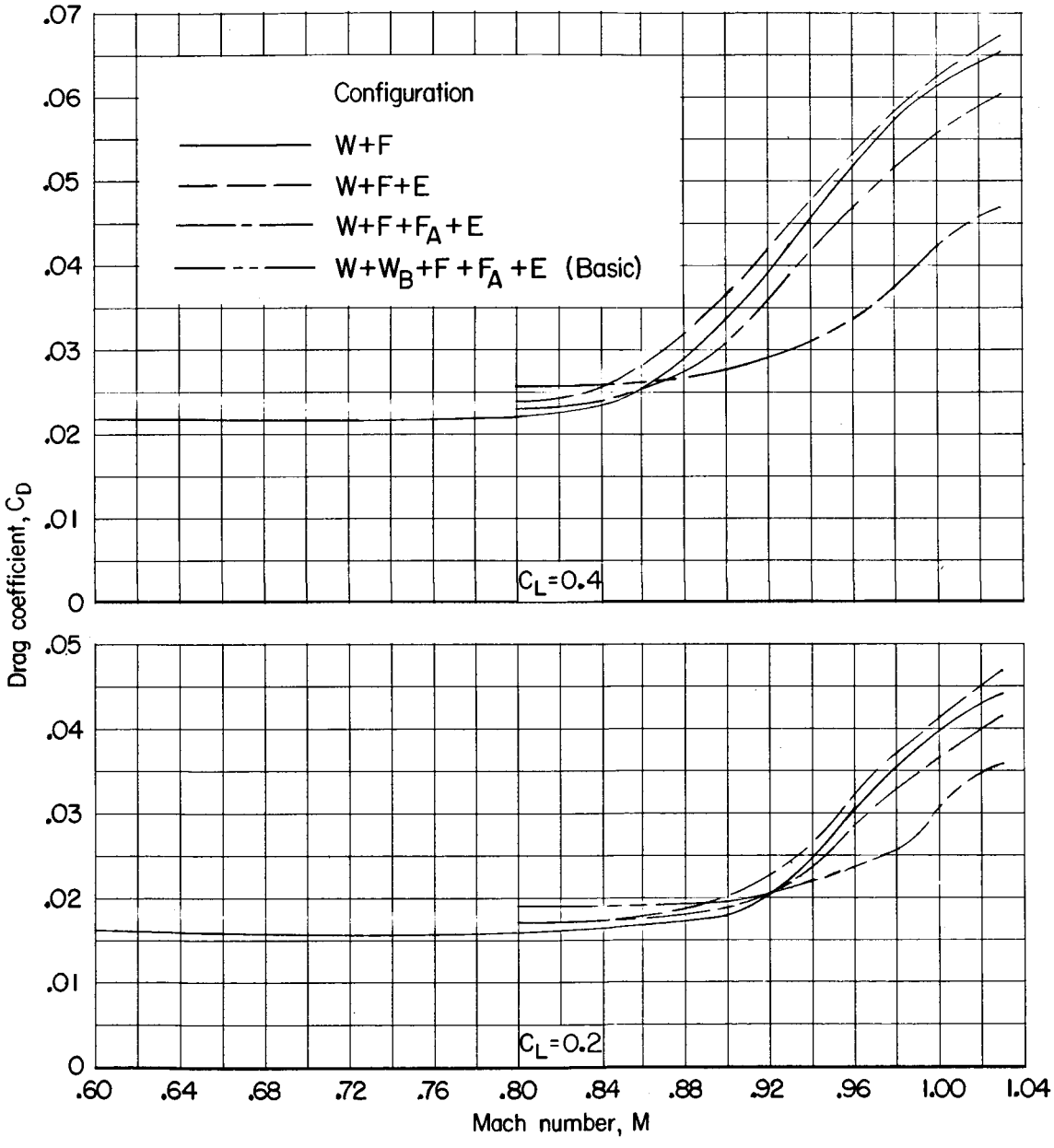

Figure 26.- Drag-coefficient variation with Mach number for various configurations of basic-model components. $\Lambda = 45^{\circ}$; $\Gamma = 6^{\circ}$; $\beta = 0^{\circ}$.

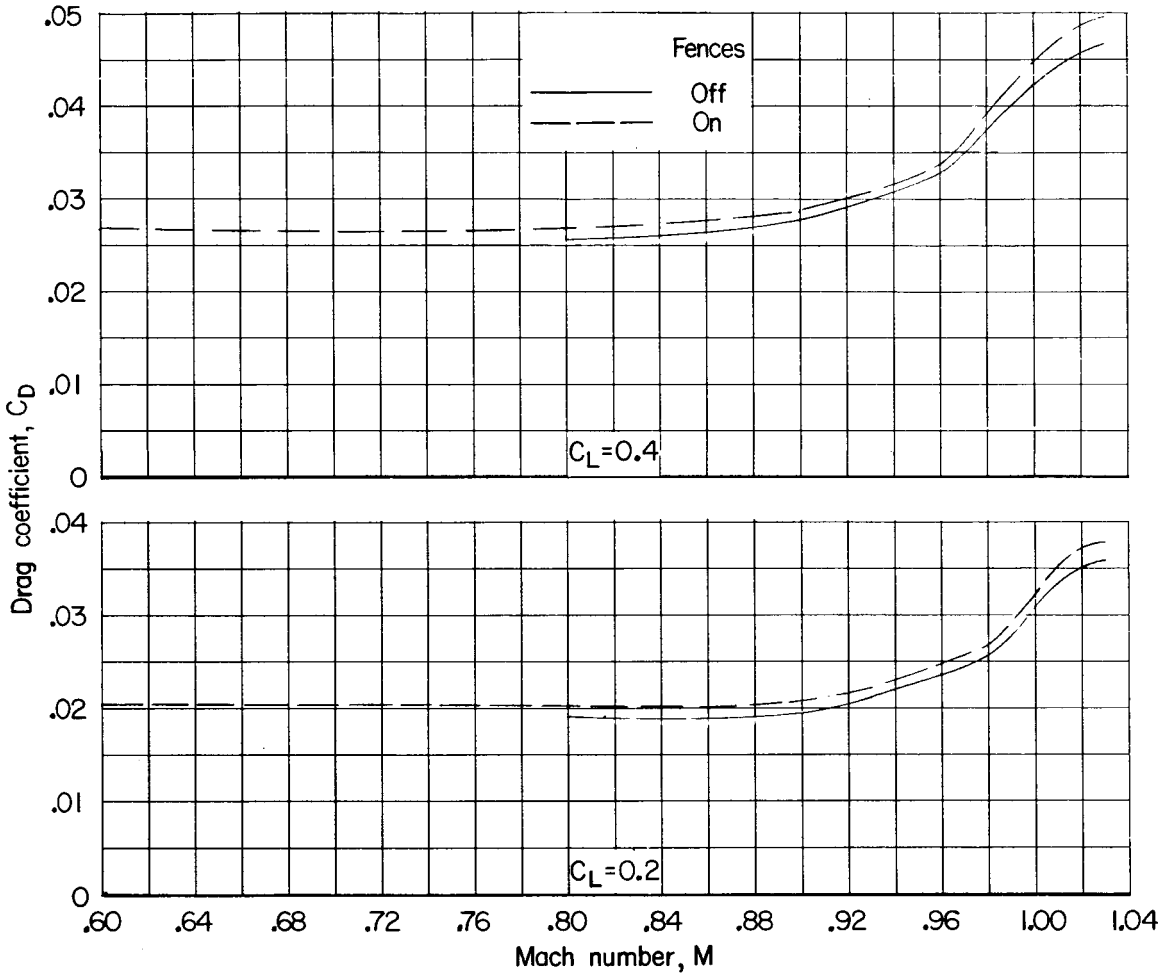

Figure 27.- Drag-coefficient variation with Mach number for basic model $(W + W_B + F + F_A + E)$ without and with fences. $\Lambda = 45^\circ$; $\Gamma = 6^\circ$; $\beta = 0^\circ$.

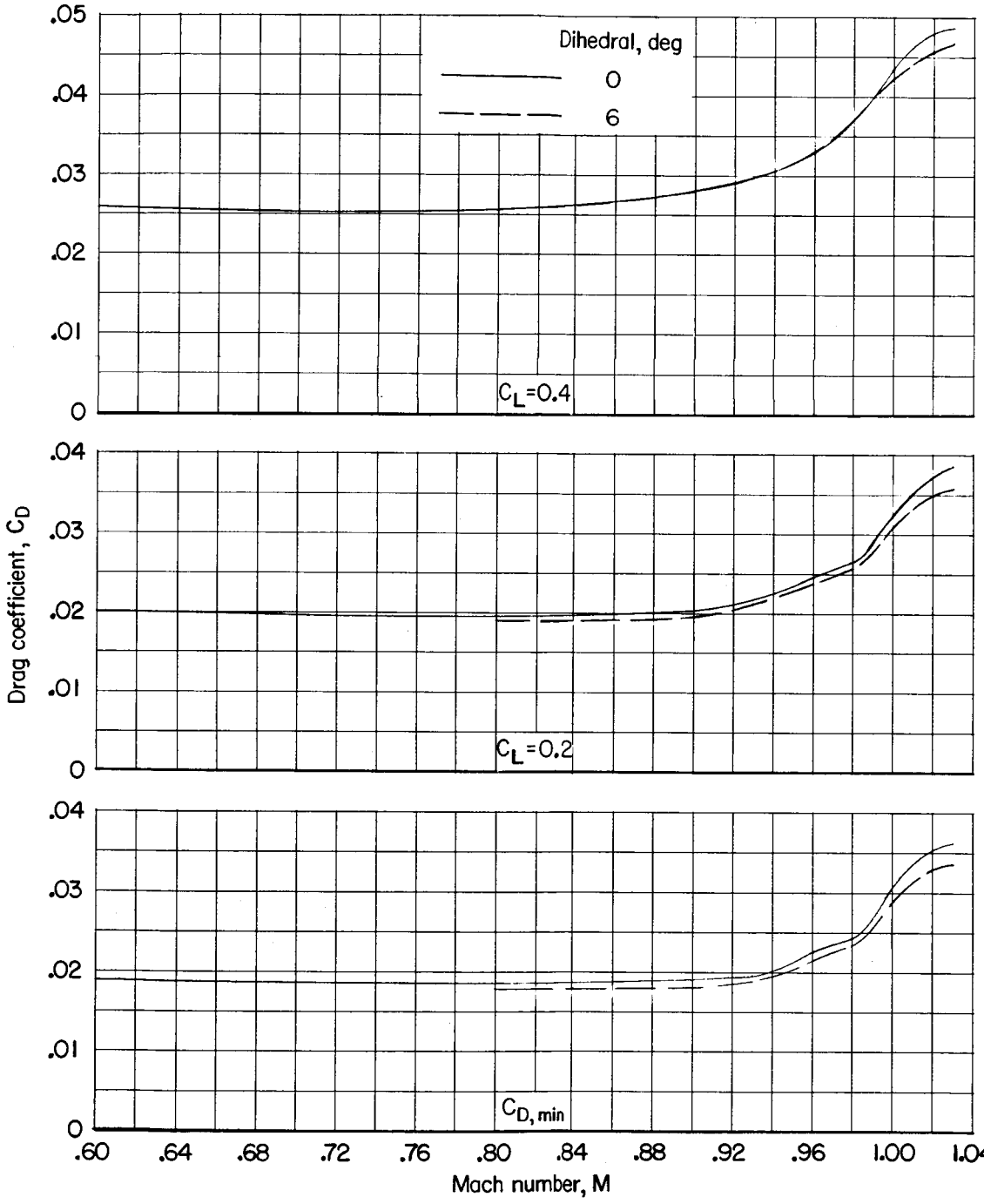

Figure 28.- Drag-coefficient variation with Mach number for basic model $(W + W_B + F + F_A + E)$ with dihedral angles of 0° and 6°. $\Lambda = 45^\circ$; $\beta = 0^\circ$.

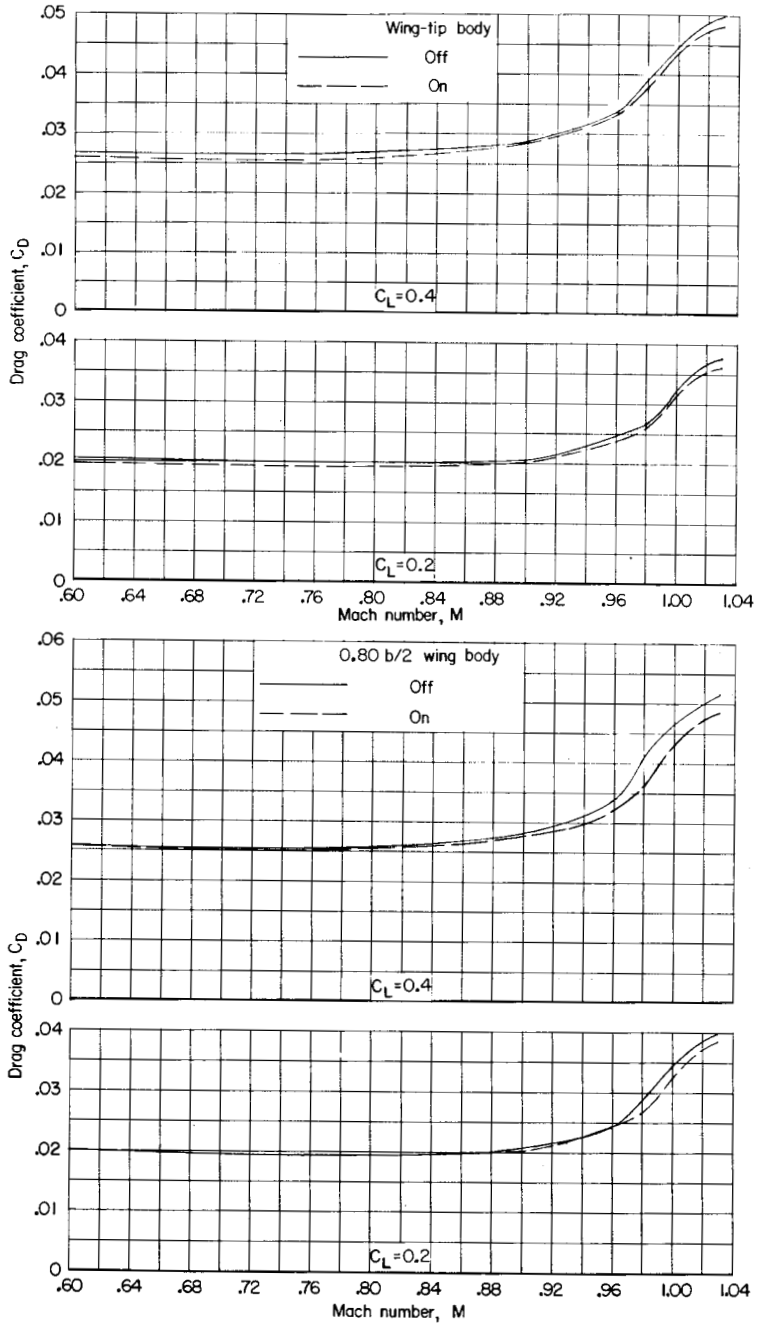

Figure 29.- Drag-coefficient variation with Mach number for basic model $(W + W_B + F + F_A + E)$ without and with 0.80b/2 wing bodies and without and with wing-tip bodies. $\Lambda = 45^\circ$; $\Gamma = 0^\circ$; $\beta = 0^\circ$ for 0.80b/2 wing-body configurations; $\Gamma = 6^\circ$ for wing-tip body configurations.

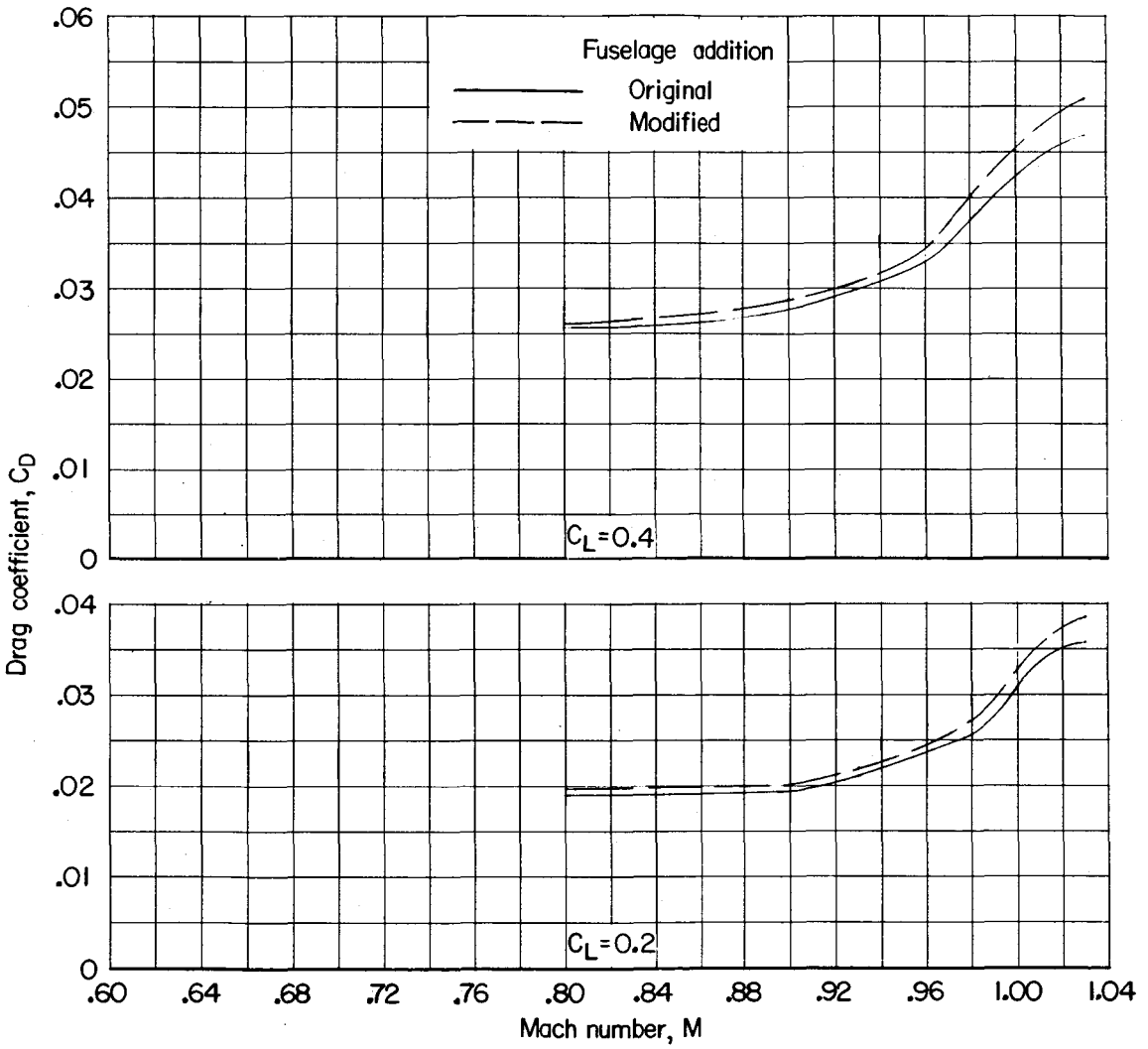

Figure 30.- Drag-coefficient variation with Mach number for basic model $(W + W_B + F + F_A + E)$ with original and modified fuselage additions. $\Lambda = 45^\circ$; $\Gamma = 6^\circ$; $\beta = 0^\circ$.

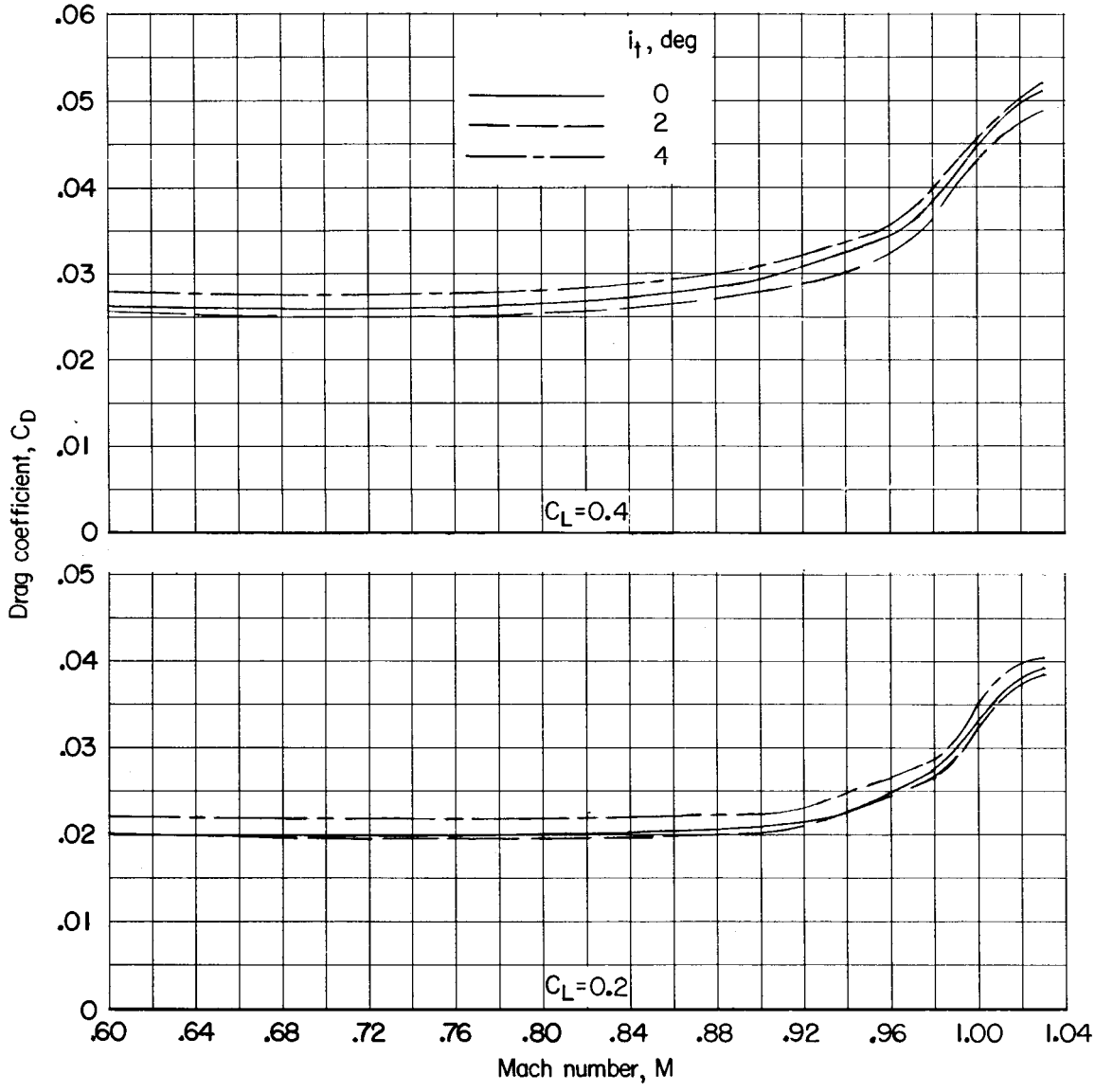

Figure 31.- Drag-coefficient variation with Mach number for basic model $(W + W_B + F + F_A + E)$ with various horizontal-tail settings. $\Lambda = 45^\circ$; $\Gamma = 0^\circ$; $\beta = 0^\circ$.

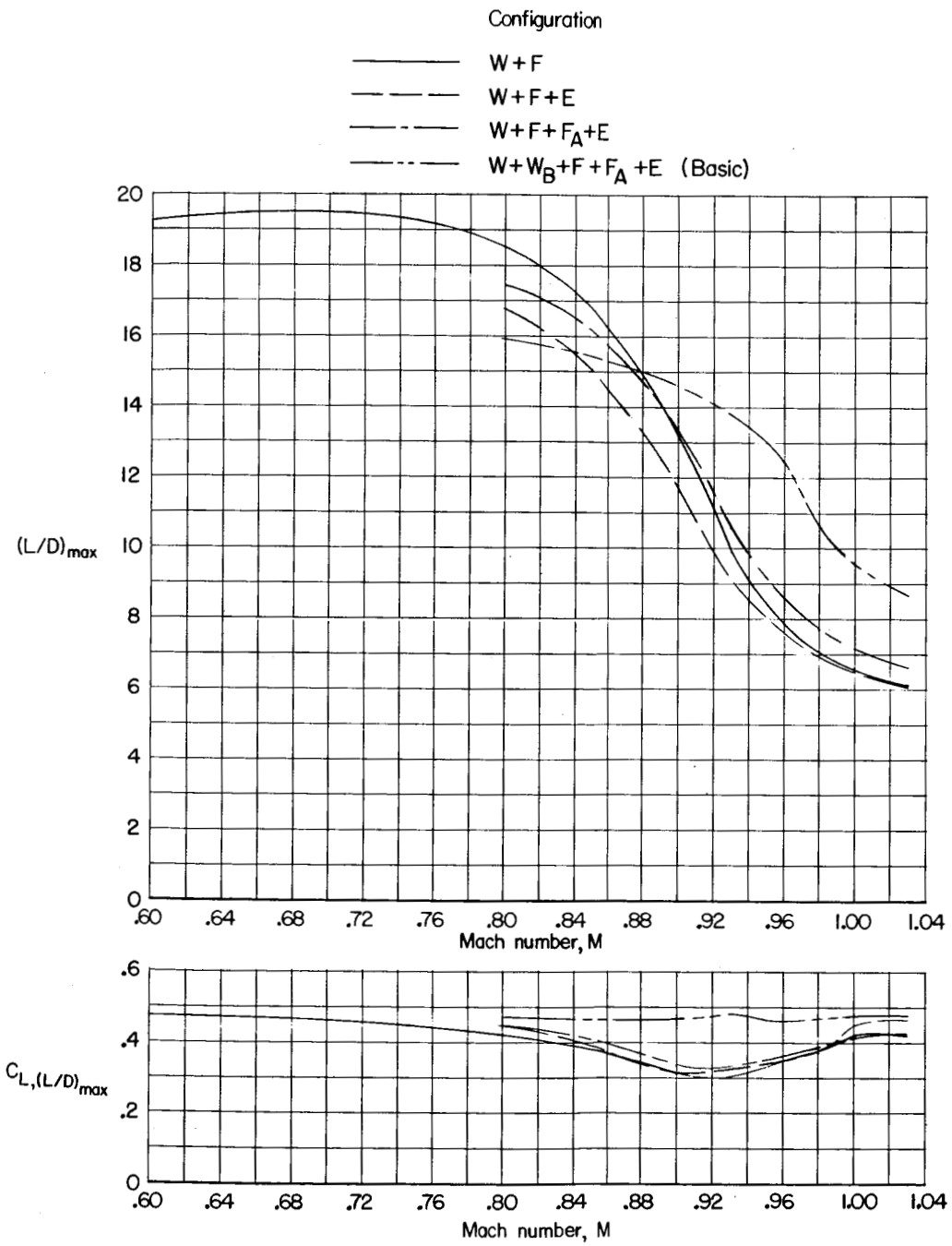

Figure 32.- Maximum untrimmed lift-drag ratio and lift coefficient at maximum untrimmed lift-drag ratio variation with Mach number for various configurations of basic model components. $\Lambda = 45^{\circ}$; $\Gamma = 6^{\circ}$; $\beta = 0^{\circ}$.

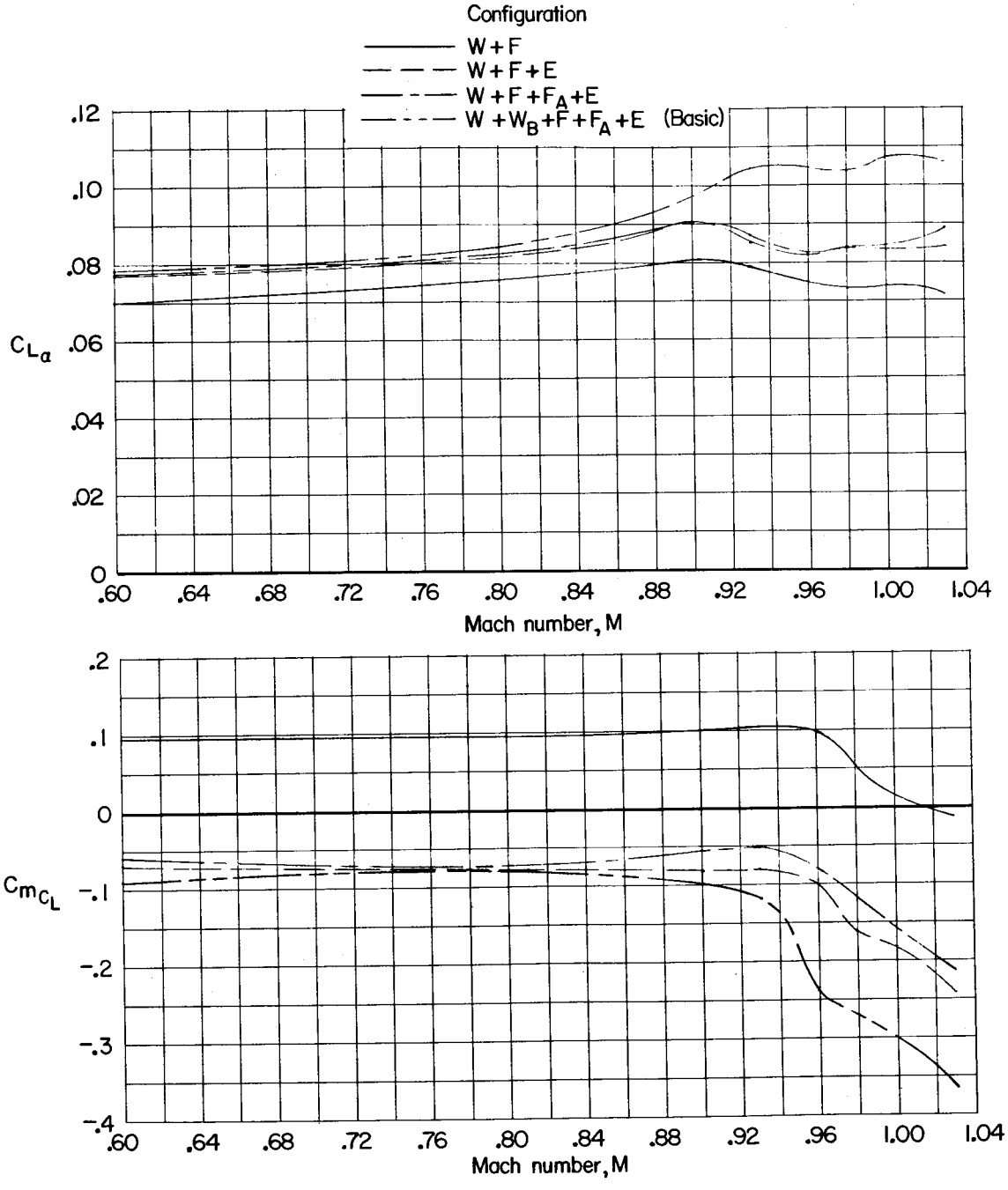

Figure 33.- Lift-curve slope and longitudinal-stability-parameter variation with Mach number for various configurations of basic model components. $\Lambda = 45^{\circ}$; $\Gamma = 6^{\circ}$; $\beta = 0^{\circ}$.

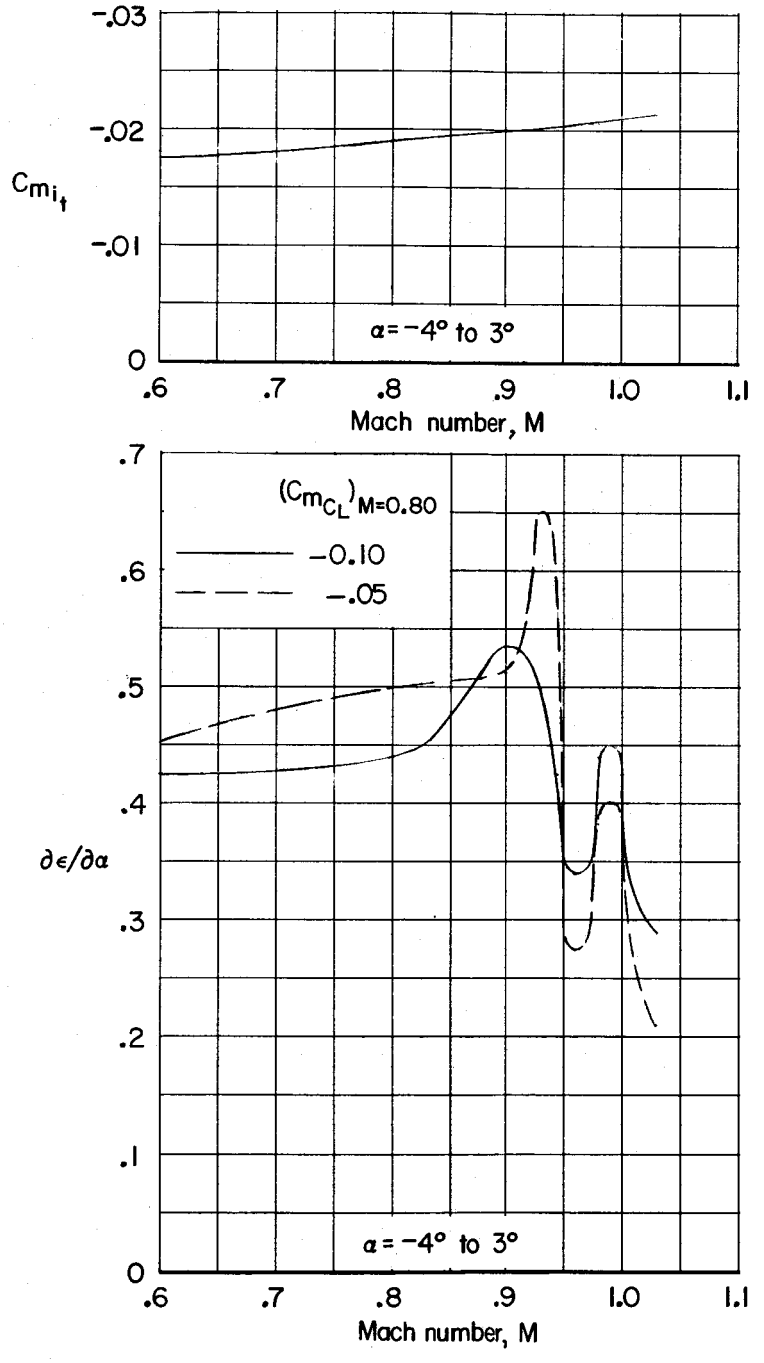

Figure 34.- Horizontal-tail effectiveness and effective downwash variation with Mach number for basic model $(W + W_B + F + F_A + E)$. $\Lambda = 45^\circ$; $\Gamma = 0^\circ$; $\beta = 0^\circ$.

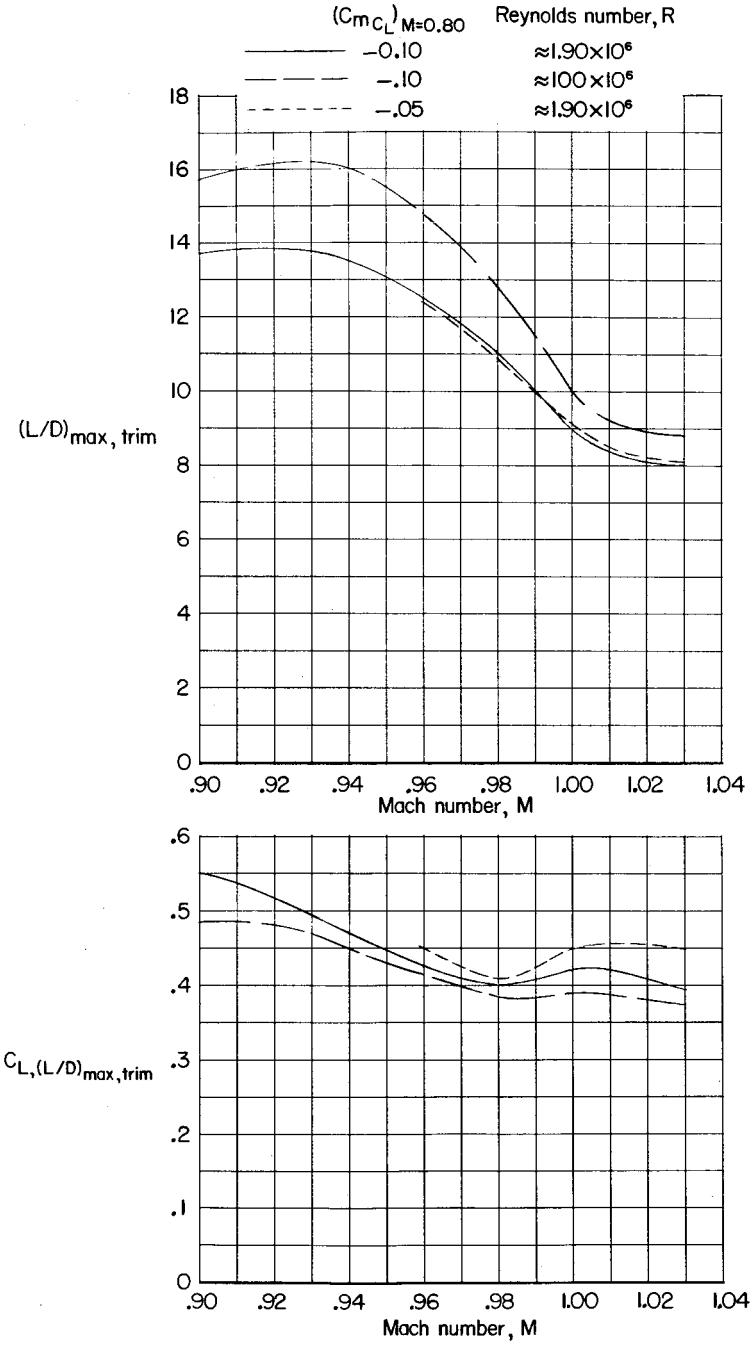

Figure 35.- Maximum trimmed lift-drag ratio and lift coefficient at maximum trimmed lift-drag ratio variation with Mach number for basic model $(W + W_B + F + F_A + E)$. $\Lambda = 45^\circ$; $\Gamma = 0^\circ$; $\beta = 0^\circ$.

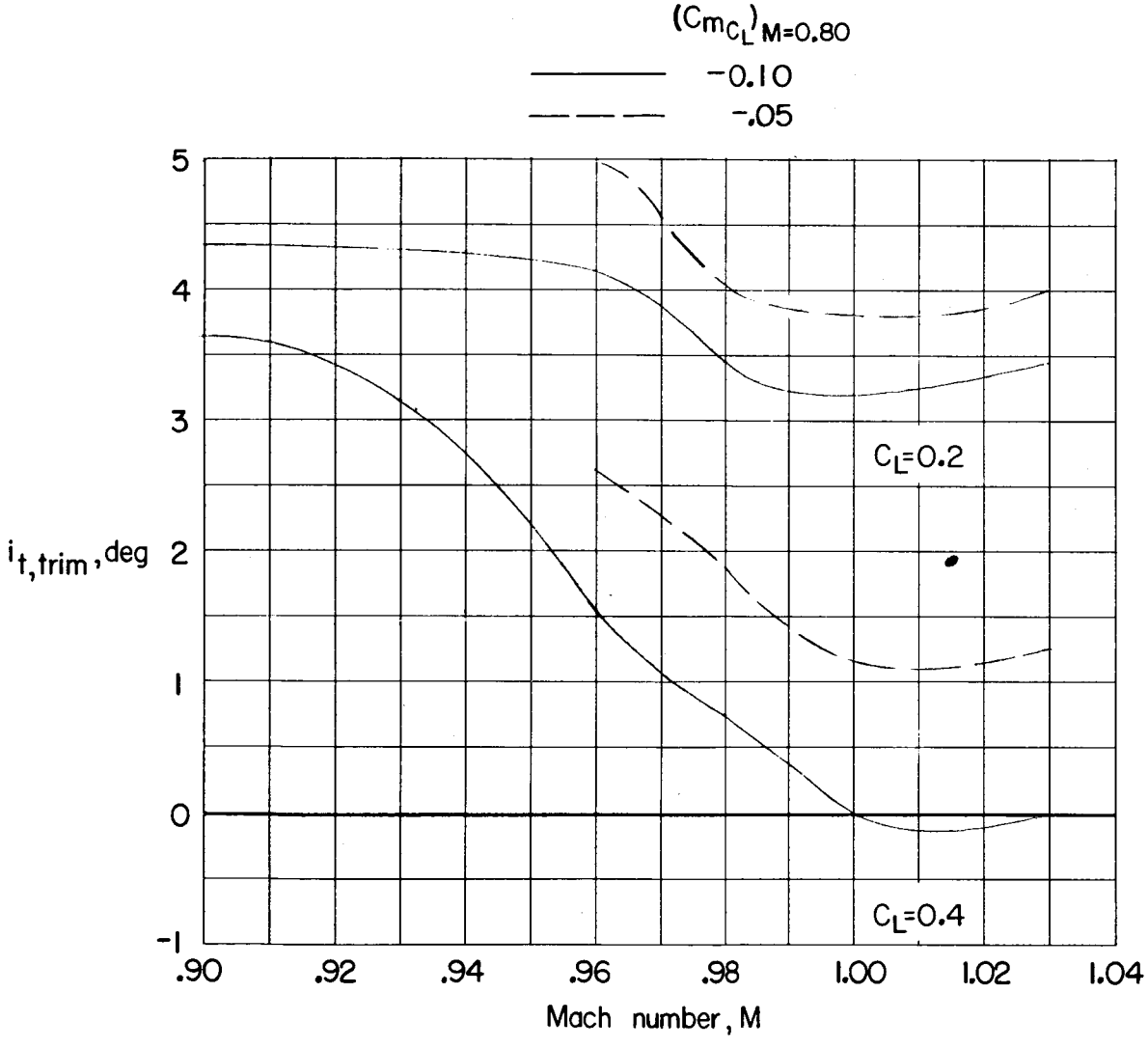

Figure 36.- Horizontal-tail setting for trim variation with Mach number for basic model $(W + W_B + F + F_A + E)$. $A = 45^\circ$; $\Gamma = 0^\circ$; $\beta = 0^\circ$.

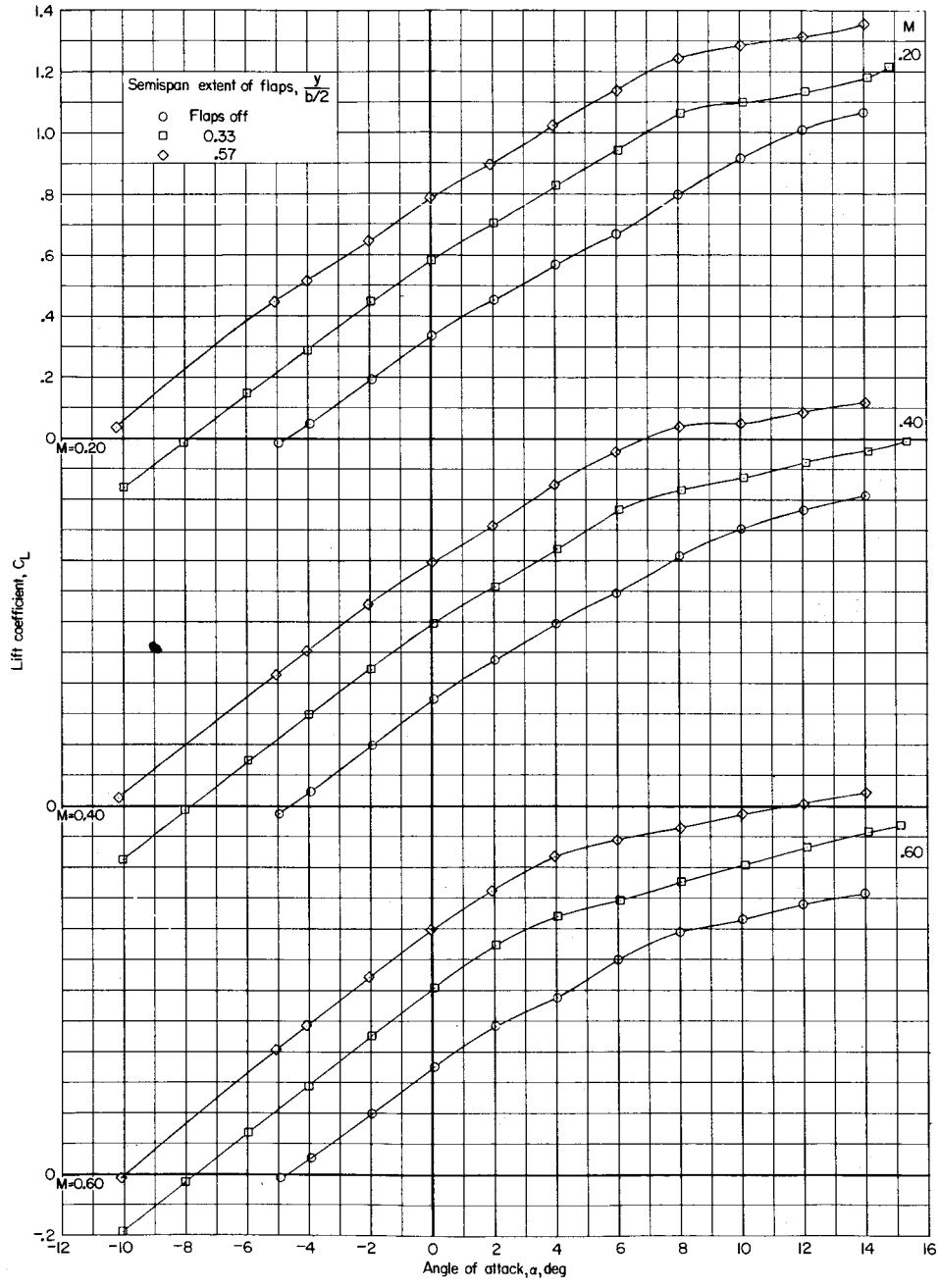

(a) Basic model with wing bodies off $(W + F + F_A + E)$.

Figure 37.- Aerodynamic lift characteristics of various configurations with wing trailing-edge flaps off and on. $\Lambda = 45^\circ$; $\Gamma = 6^\circ$; $\beta = 0^\circ$; $\delta_f = 30^\circ$.

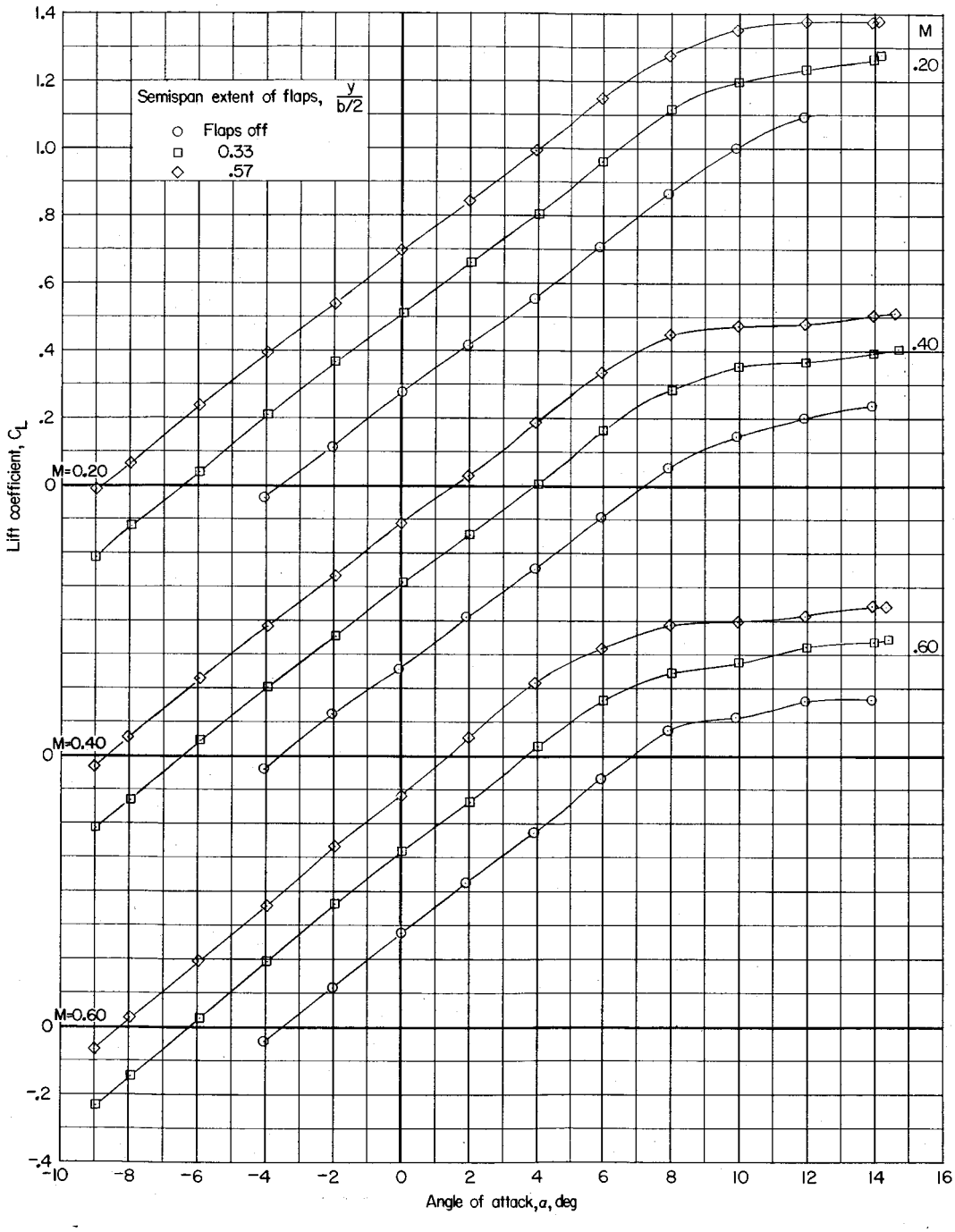

(b) Basic model $(W + W_B + F + F_A + E)$.

Figure 37.- Continued.

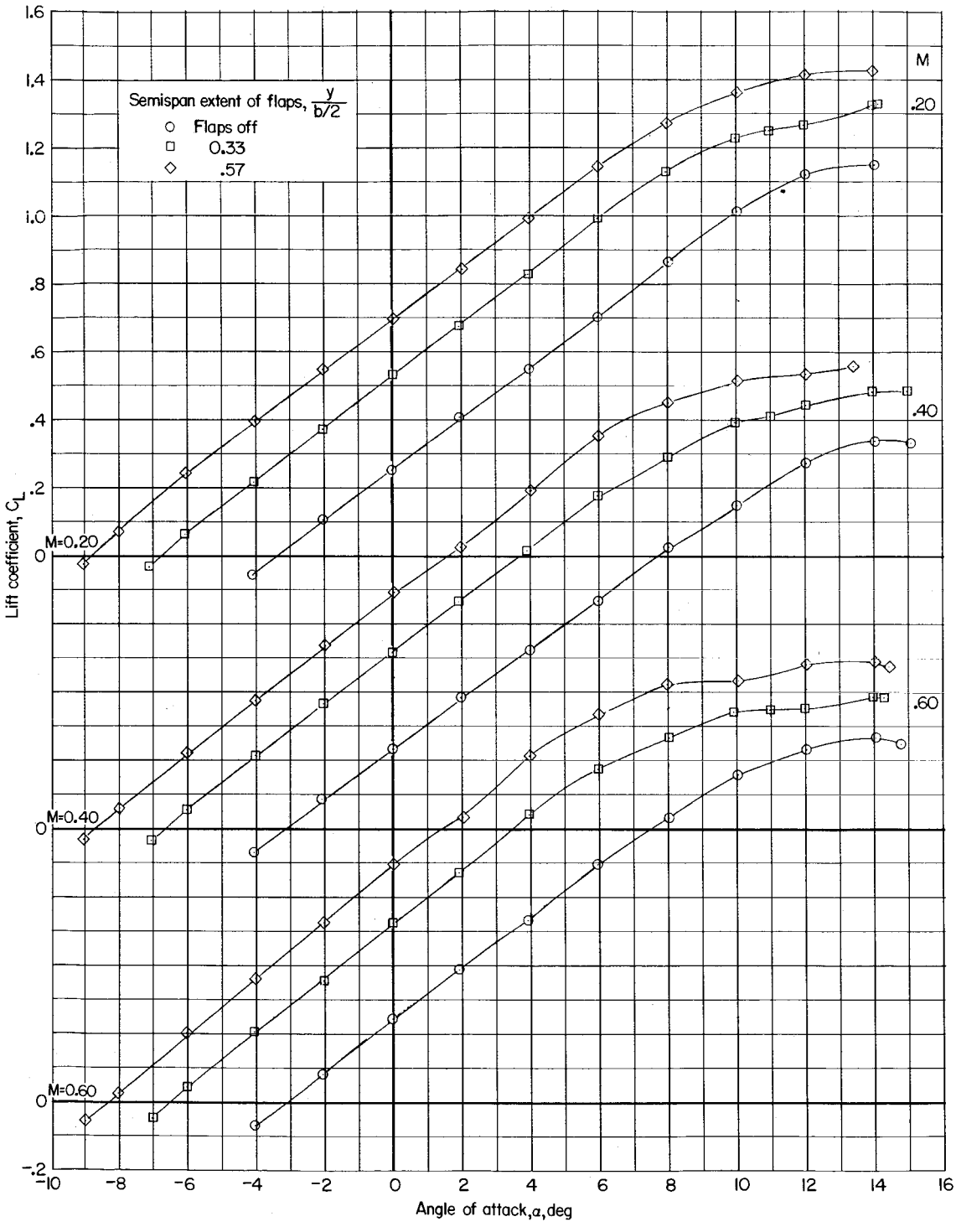

(c) Basic model $(W + W_B + F + F_A + E)$ with fences.

Figure 37.- Concluded.

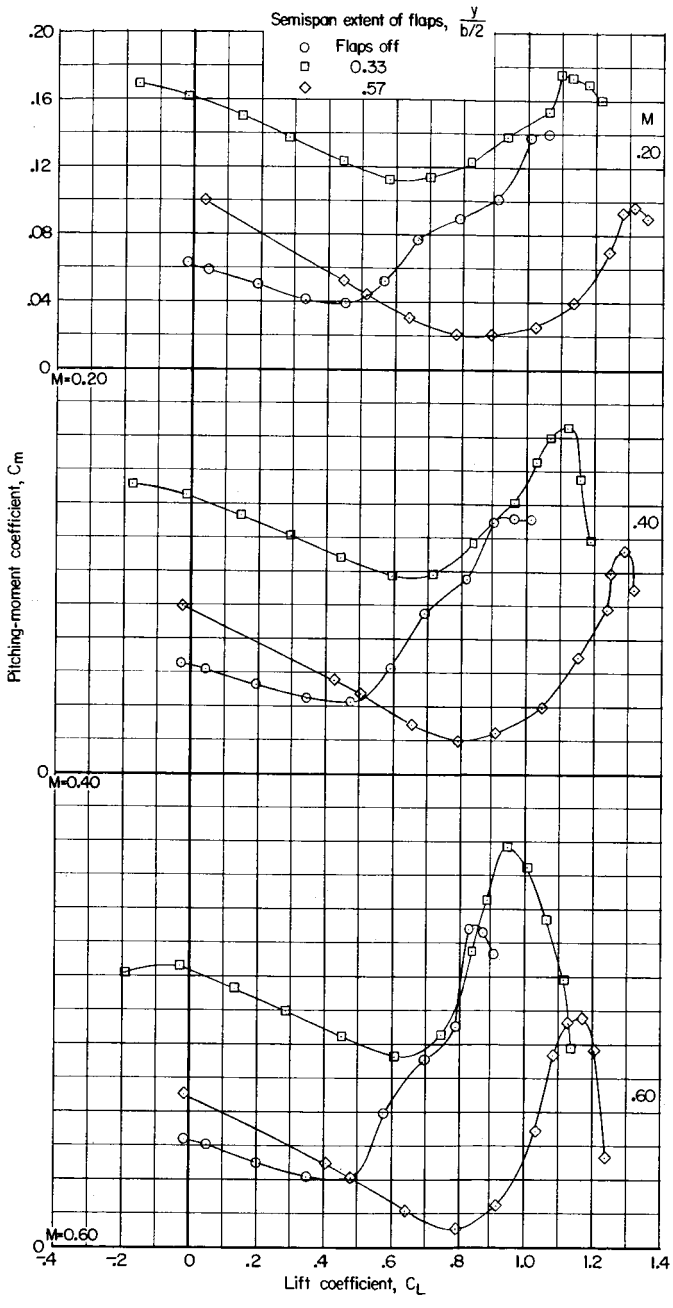

(a) Basic model with wing bodies off $(W + F + F_A + E)$.

Figure 38.- Aerodynamic pitching-moment characteristics of various configurations with trailing-edge flaps off and on. $\Lambda = 45^\circ$; $\Gamma = 6^\circ$; $\beta = 0^\circ$; $\delta_f = 30^\circ$.

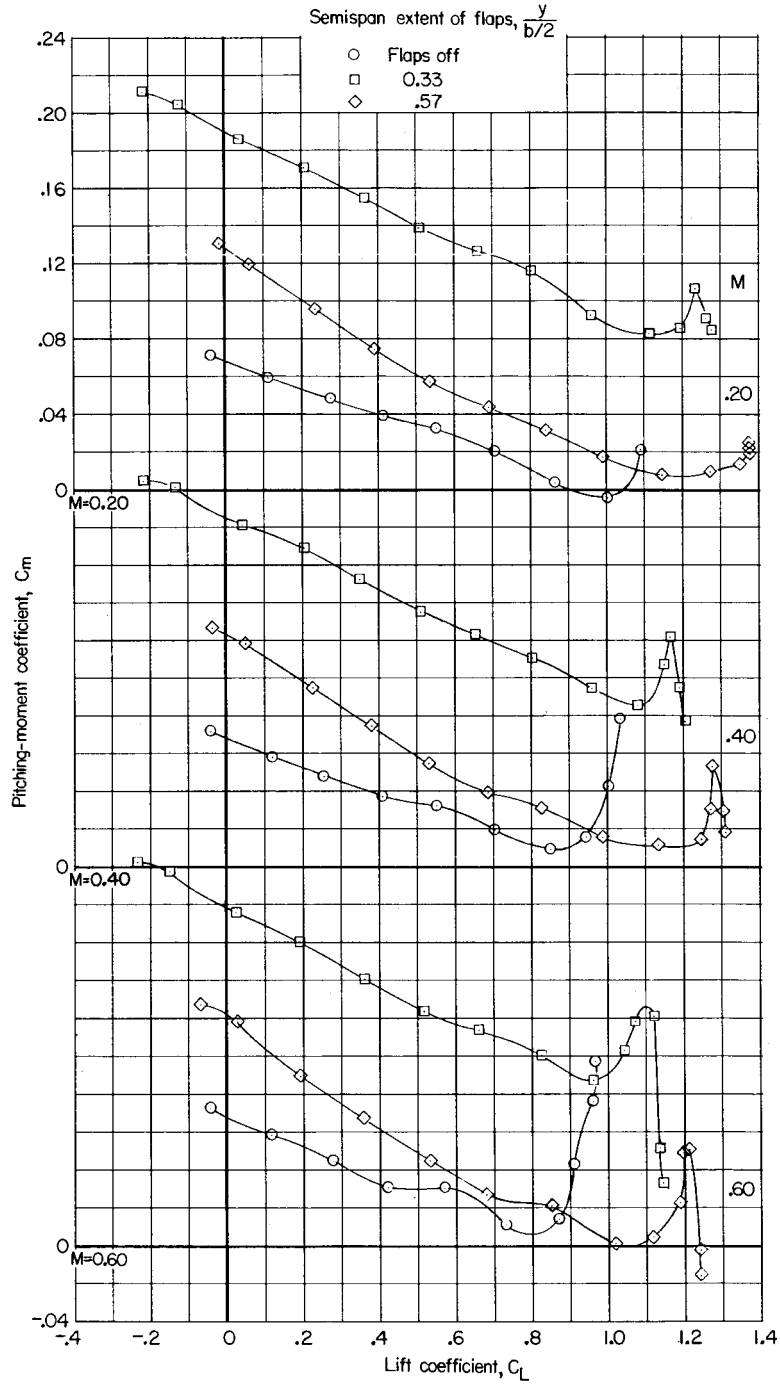

(b) Basic model $(W + W_B + F + F_A + E)$.

Figure 38.- Continued.

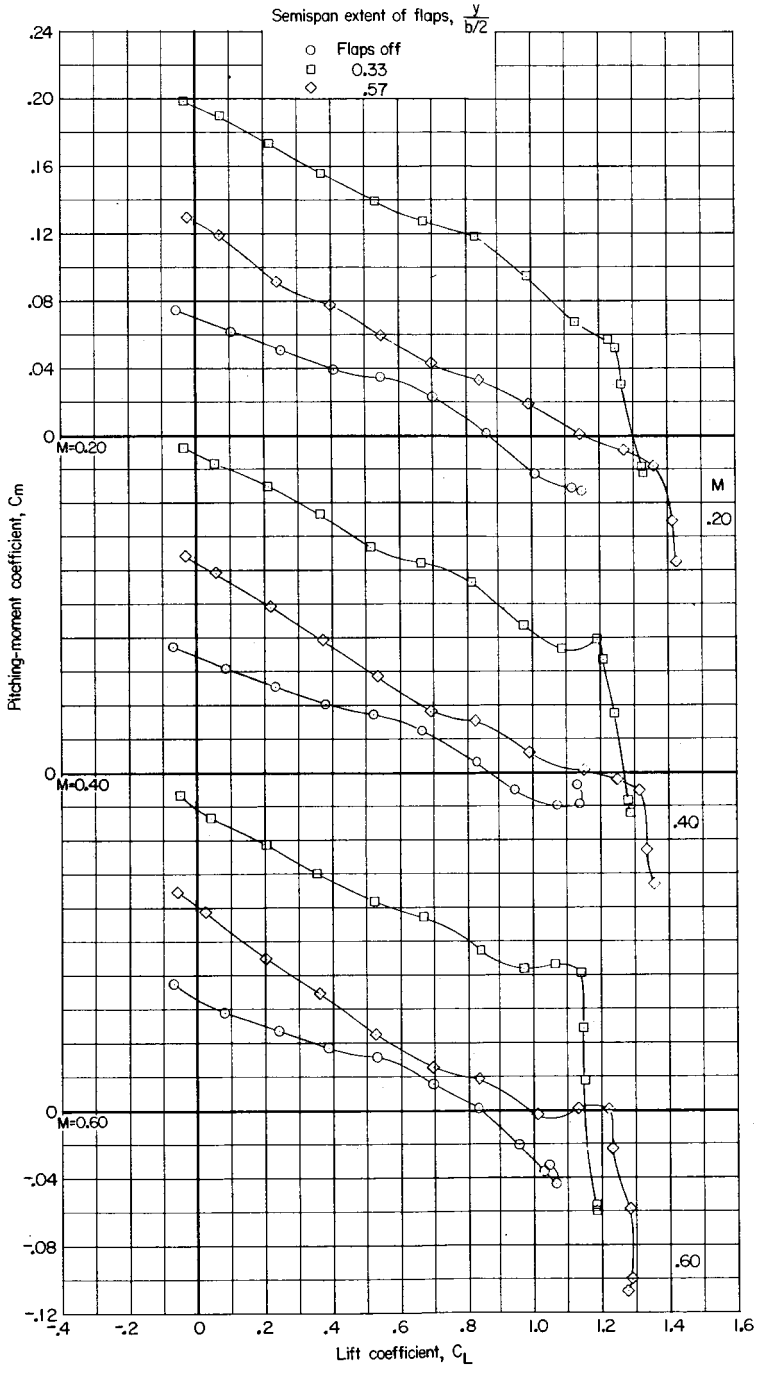

(c) Basic model $(W + W_B + F + F_A + E)$ with fences.

Figure 38.- Concluded.

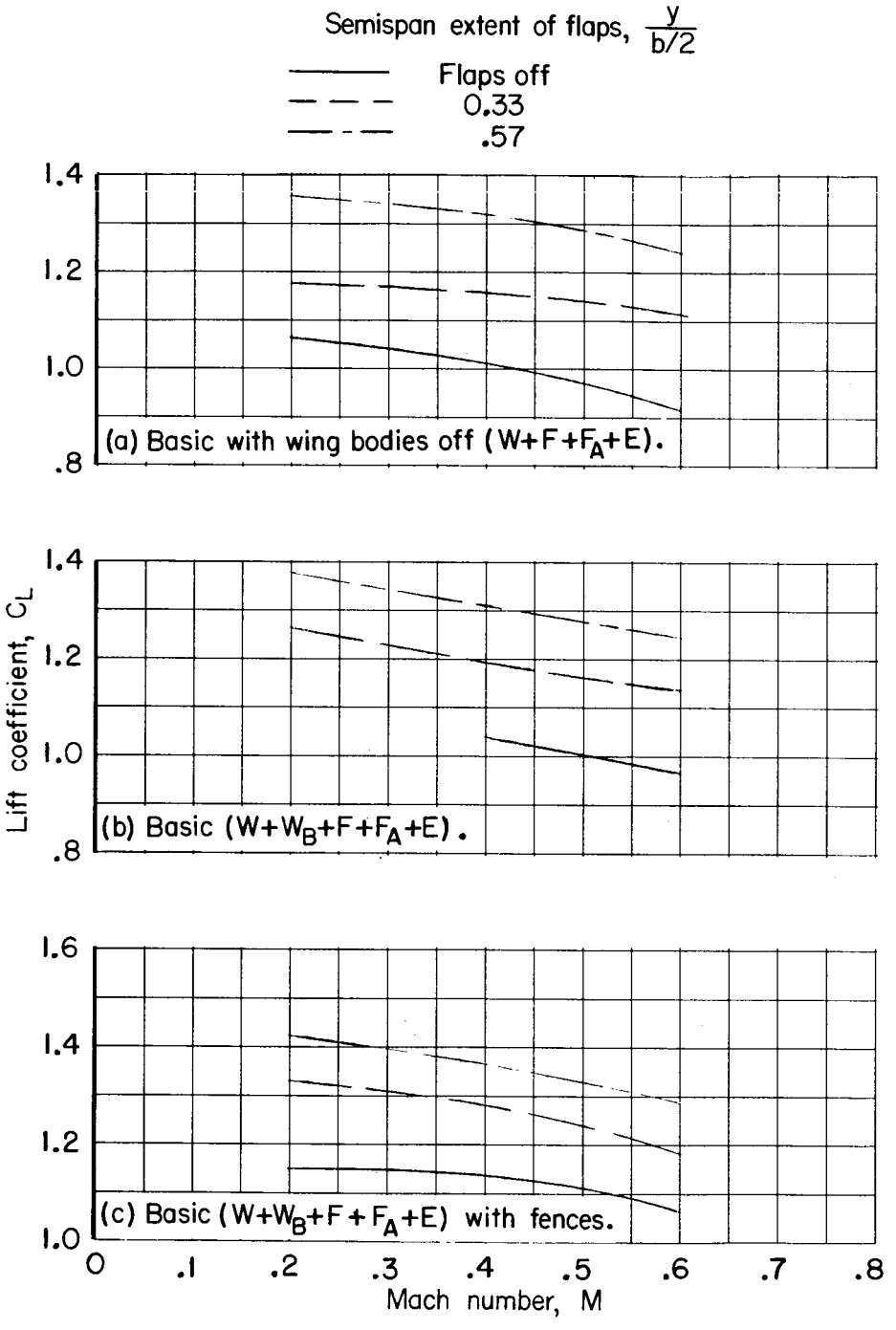

Figure 39.- Variation with Mach number of lift coefficient at an angle of attack of 14° for various configurations with trailing-edge flaps off and on. $\Lambda = 45^{\circ}$; $\Gamma = 6^{\circ}$; $\beta = 0^{\circ}$; $\delta_f = 30^{\circ}$.

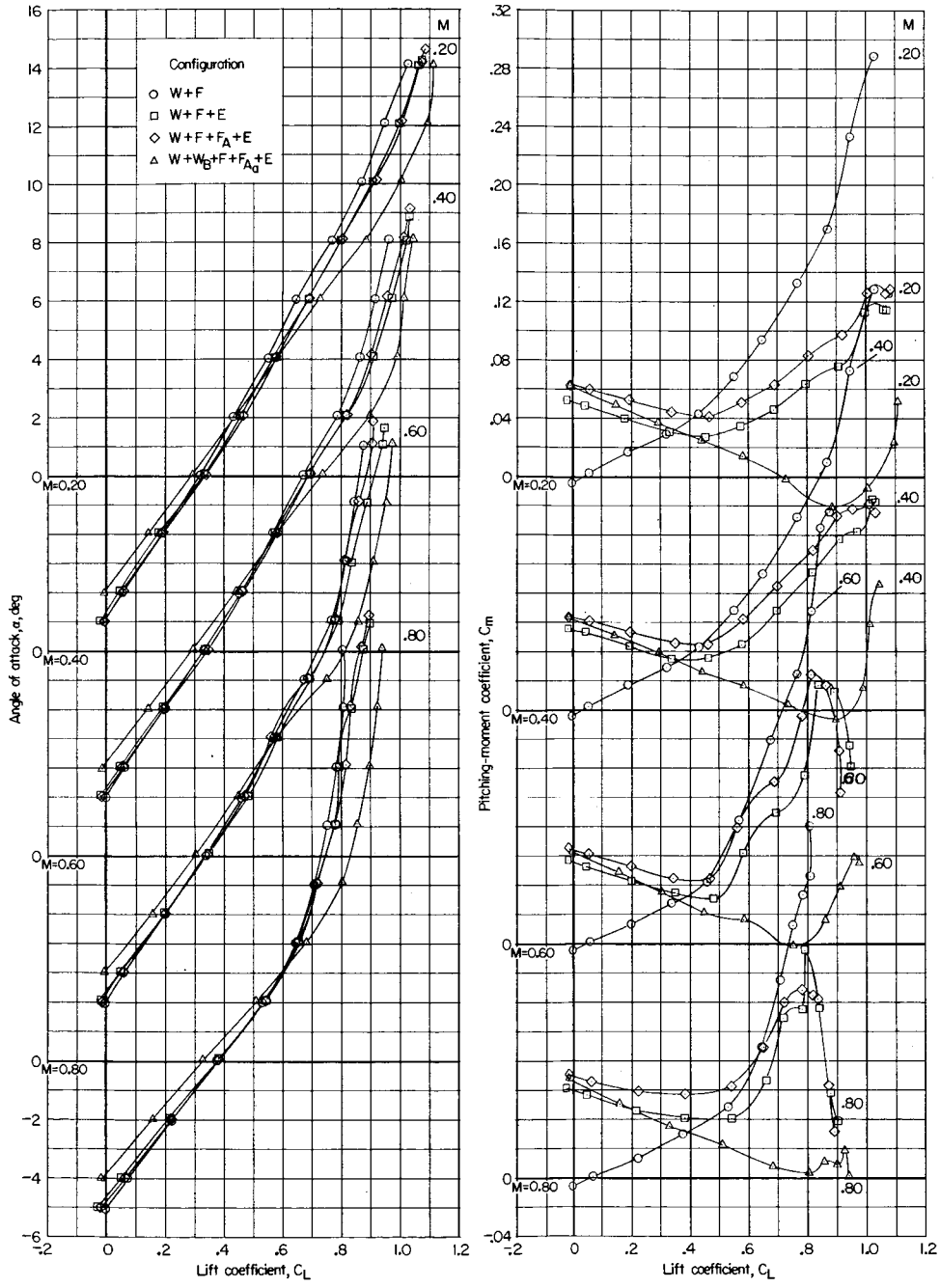

(a) M = 0.20 to 0.80.

Figure 40.- Effect of various components on aerodynamic lift and pitching-moment characteristics of complete model in sideslip. $\Lambda = 45^{\circ}$; $\Gamma = 6^{\circ}$; $\beta = -5^{\circ}$.

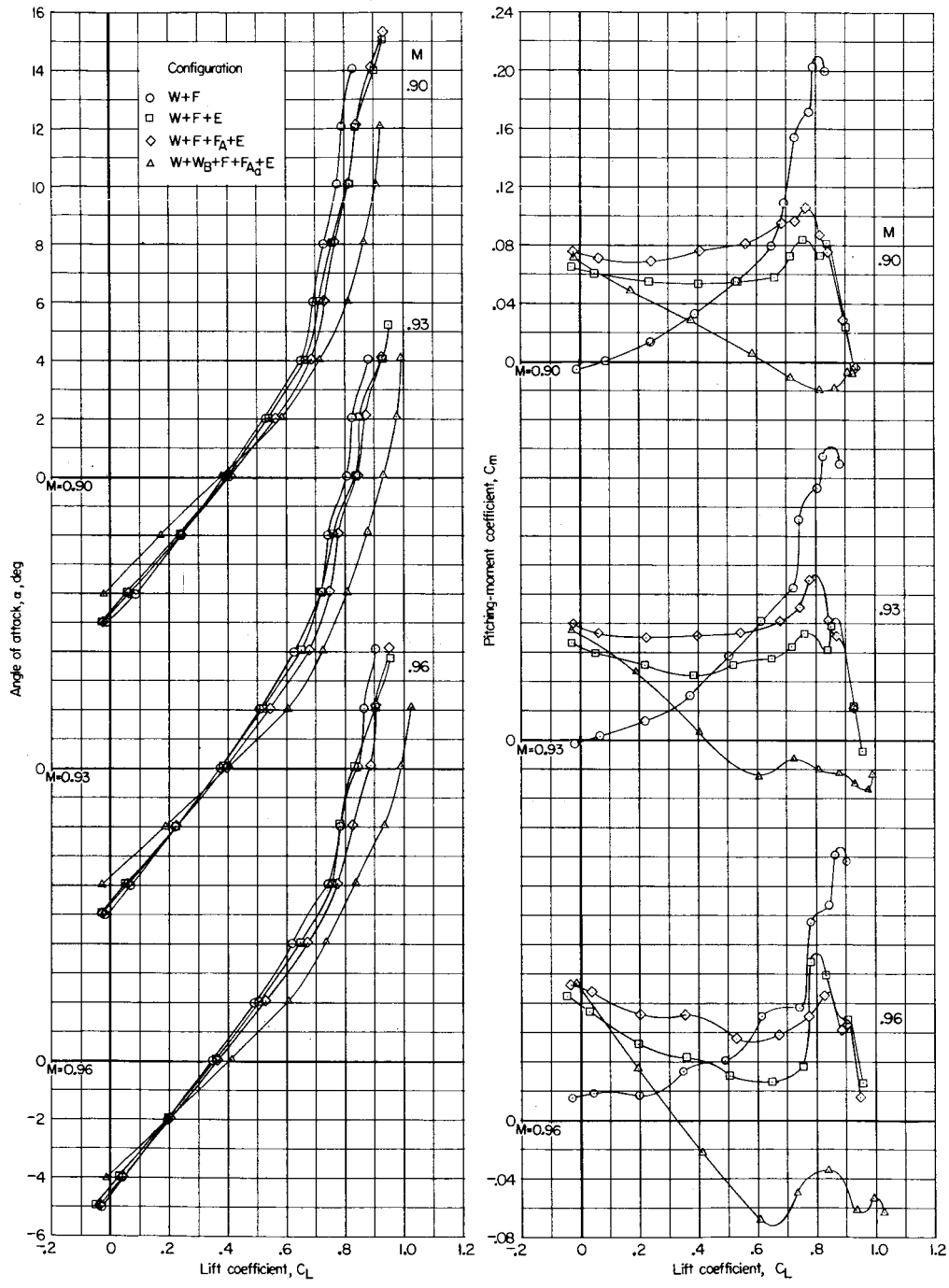

(b) M = 0.90 to 0.96.

Figure 40.- Continued.

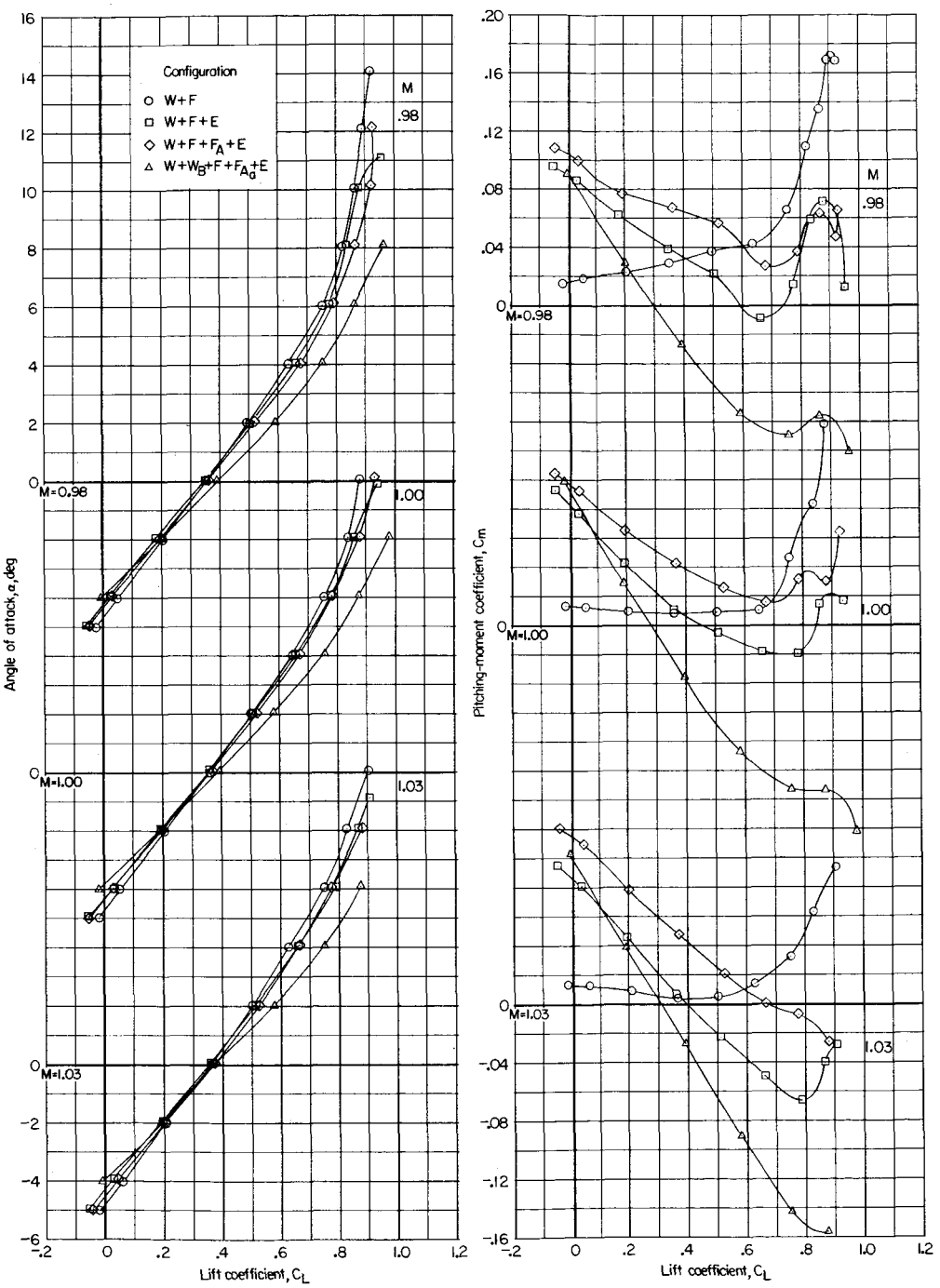

(c) M = 0.98 to 1.03.

Figure 40.- Concluded.

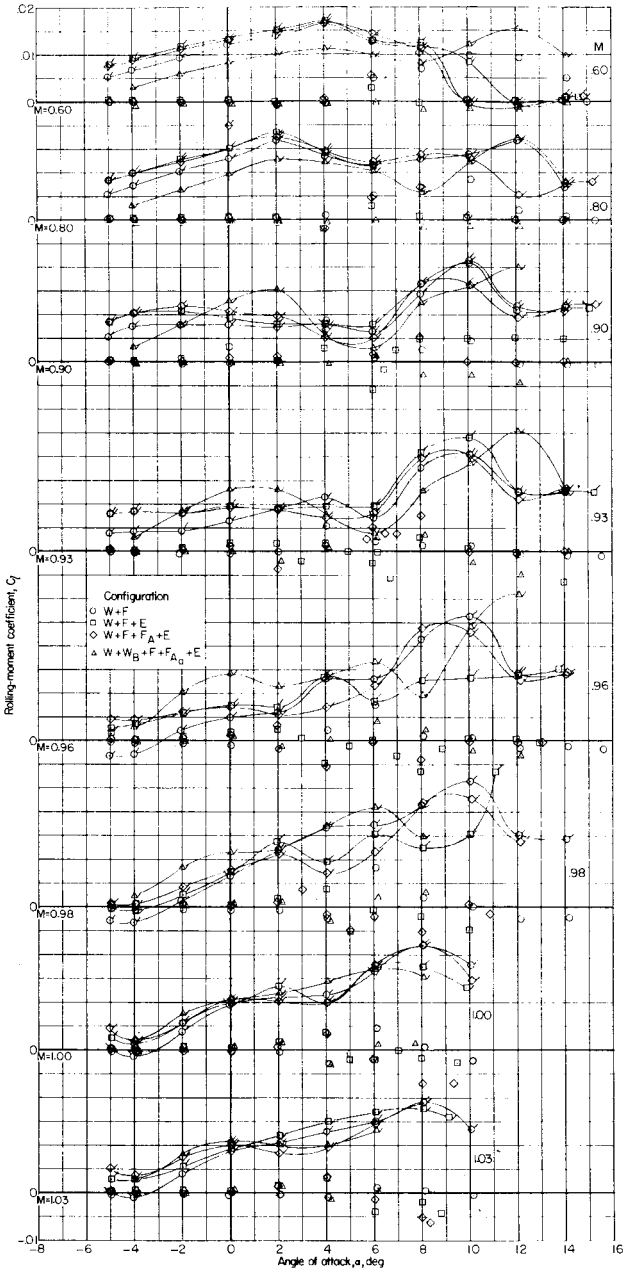

(a) Variation of C_l with α.

Figure 41.- Effect of various components on aerodynamic lateral and directional characteristics of complete model. $\Lambda = 45^\circ$; $\Gamma = 6^\circ$; plain symbols indicate data for $\beta = 0^\circ$; flagged symbols indicate data for $\beta = -5^\circ$.

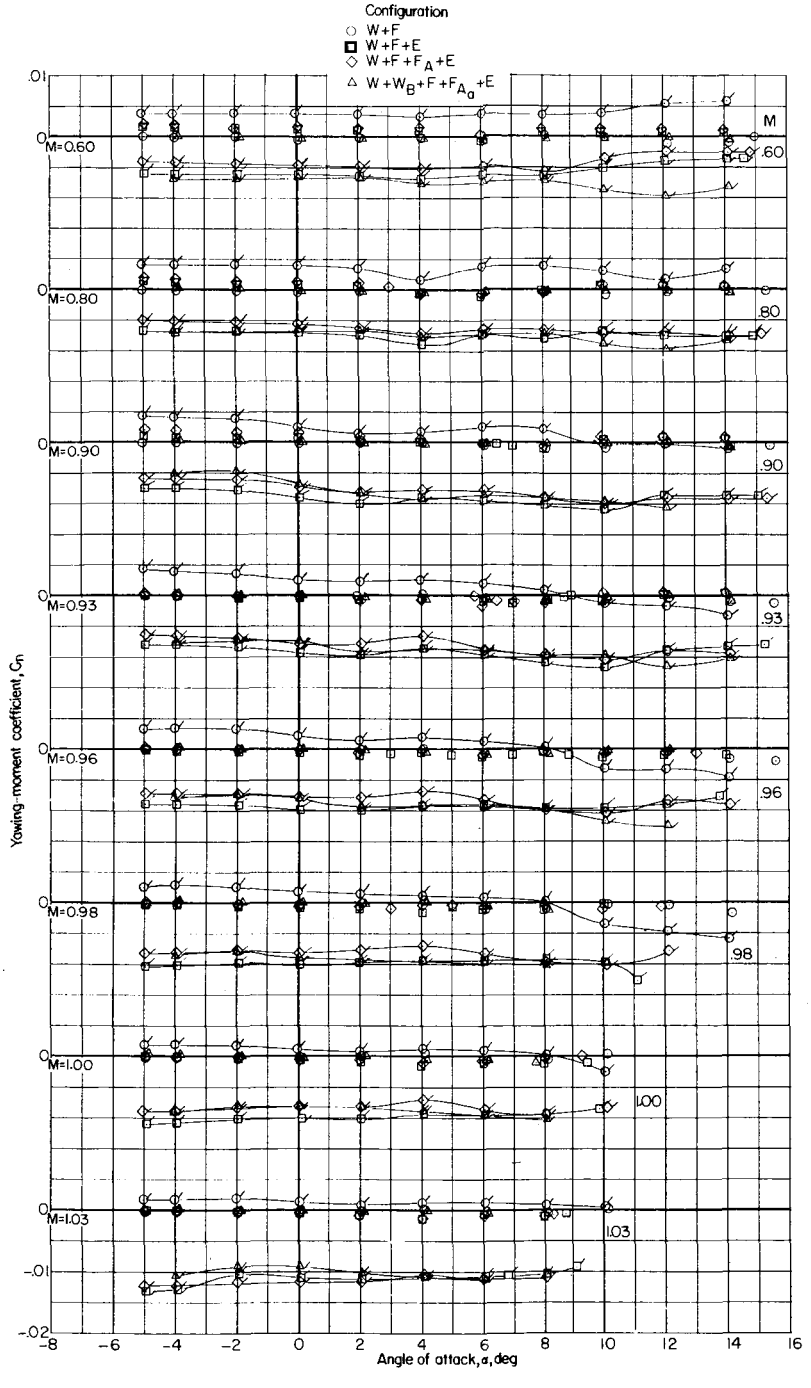

(b) Variation of C_n with α.

Figure 41.- Continued.

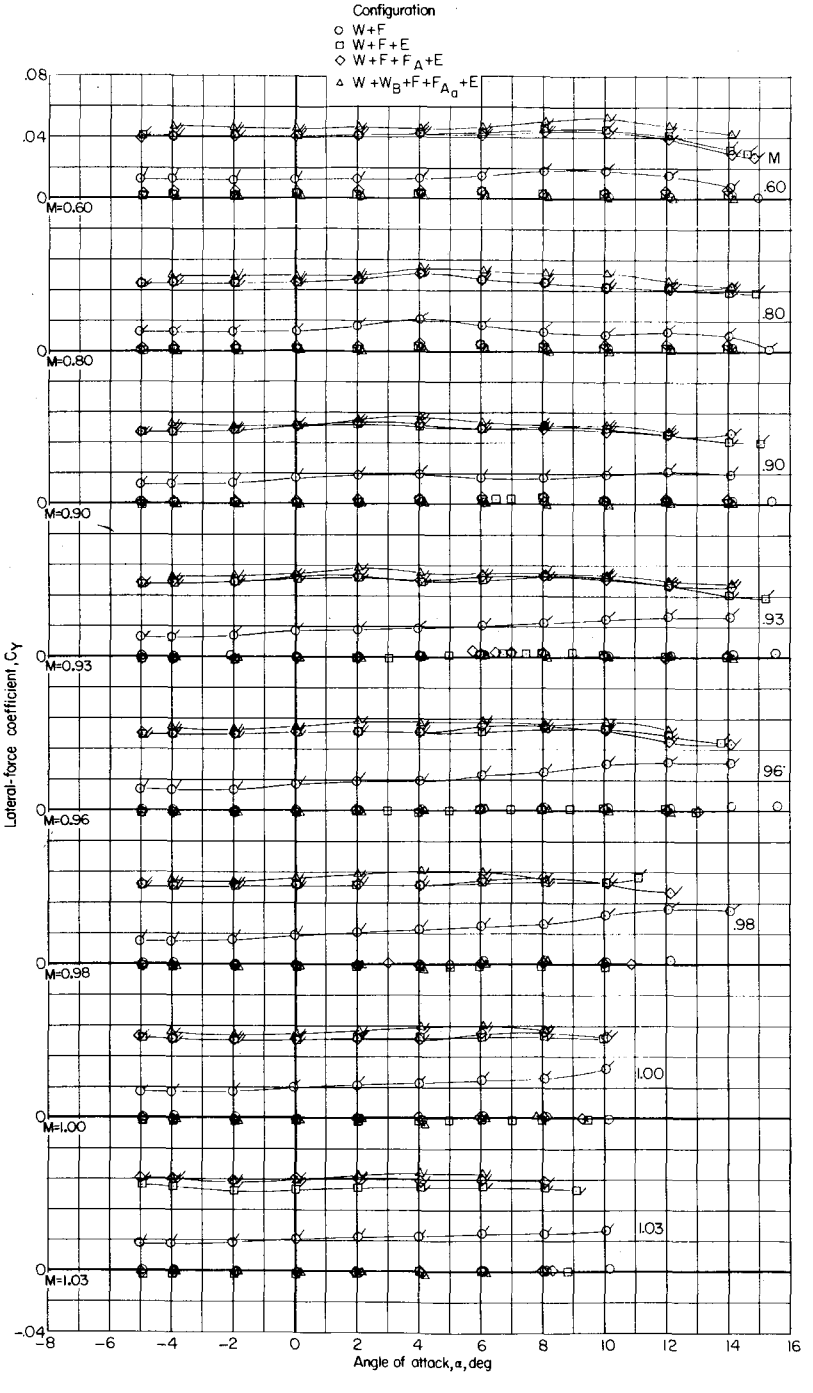

(c) Variation of C_Y with α.

Figure 41.- Concluded.

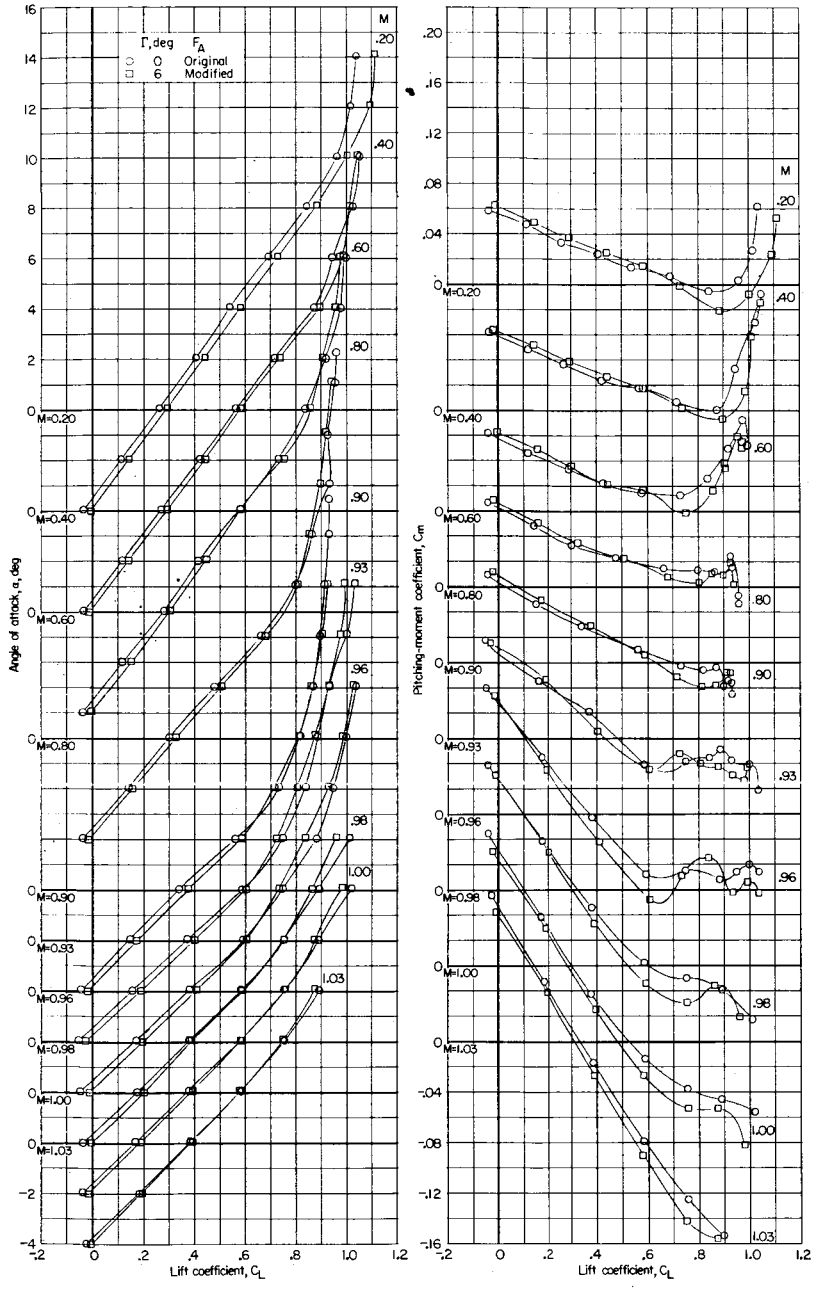

Figure 42.- Effect of dihedral angle on aerodynamic lift and pitching-moment characteristics of complete model in sideslip. $\Lambda = 45^{\circ}$; $\beta = -5^{\circ}$; original fuselage addition on model with $\Gamma = 0^{\circ}$ $(W + W_B + F + F_A + E)$; modified fuselage addition on model with $\Gamma = 6^{\circ}(W + W_B + F + F_{A_a} + E)$.

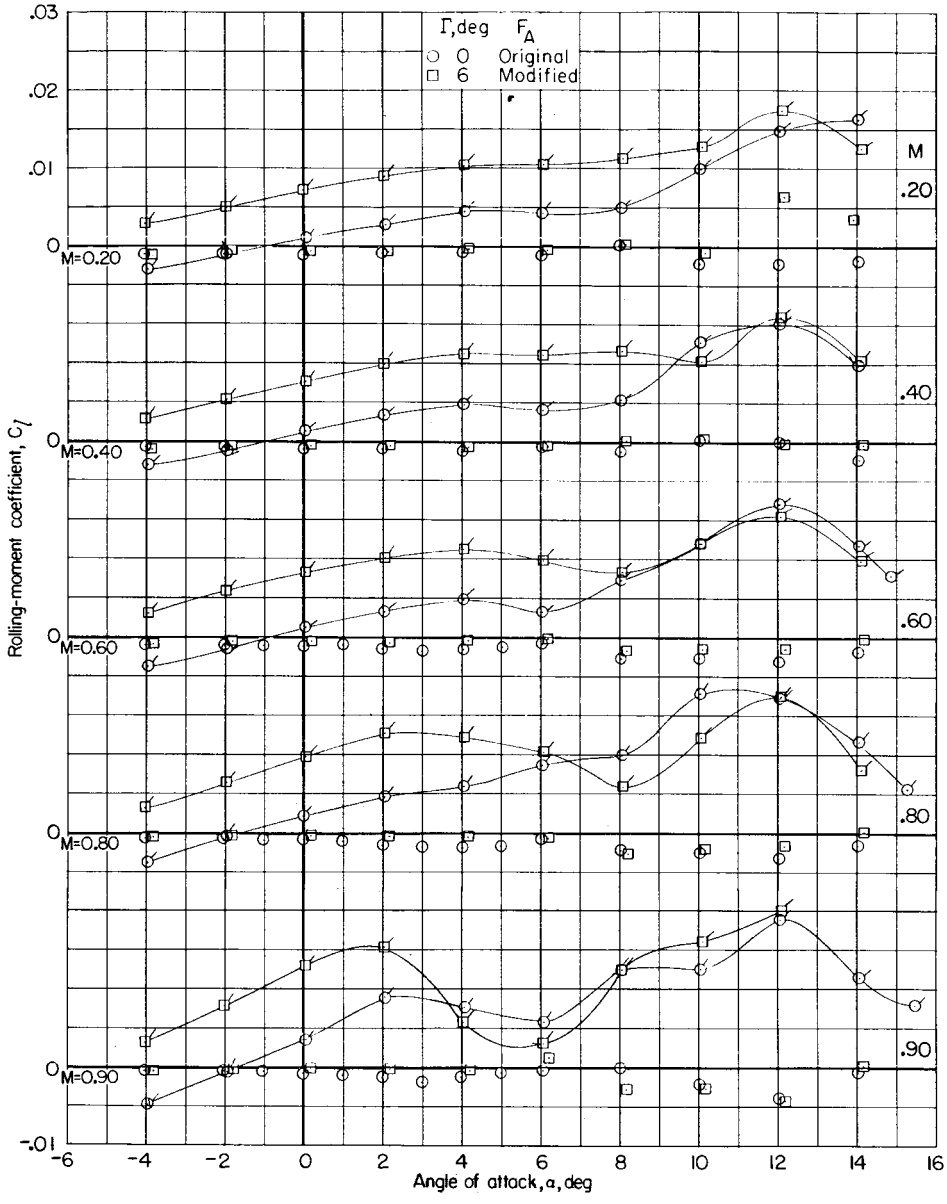

(a) Variation of C_l with α; M = 0.20 to 0.90.

Figure 43.- Effect of dihedral angle on aerodynamic lateral and directional characteristics of complete model in sideslip. $\Lambda = 45^\circ$; original fuselage addition model with $\Gamma = 0^\circ\left(W + W_B + F + F_A + E\right)$; modified fuselage addition on model with $\Gamma = 6^\circ\left(W + W_B + F + F_{A_a} + E\right)$; plain symbols indicate data for $\beta = 0^\circ$; flagged symbols indicate data for $\beta = -5^\circ$.

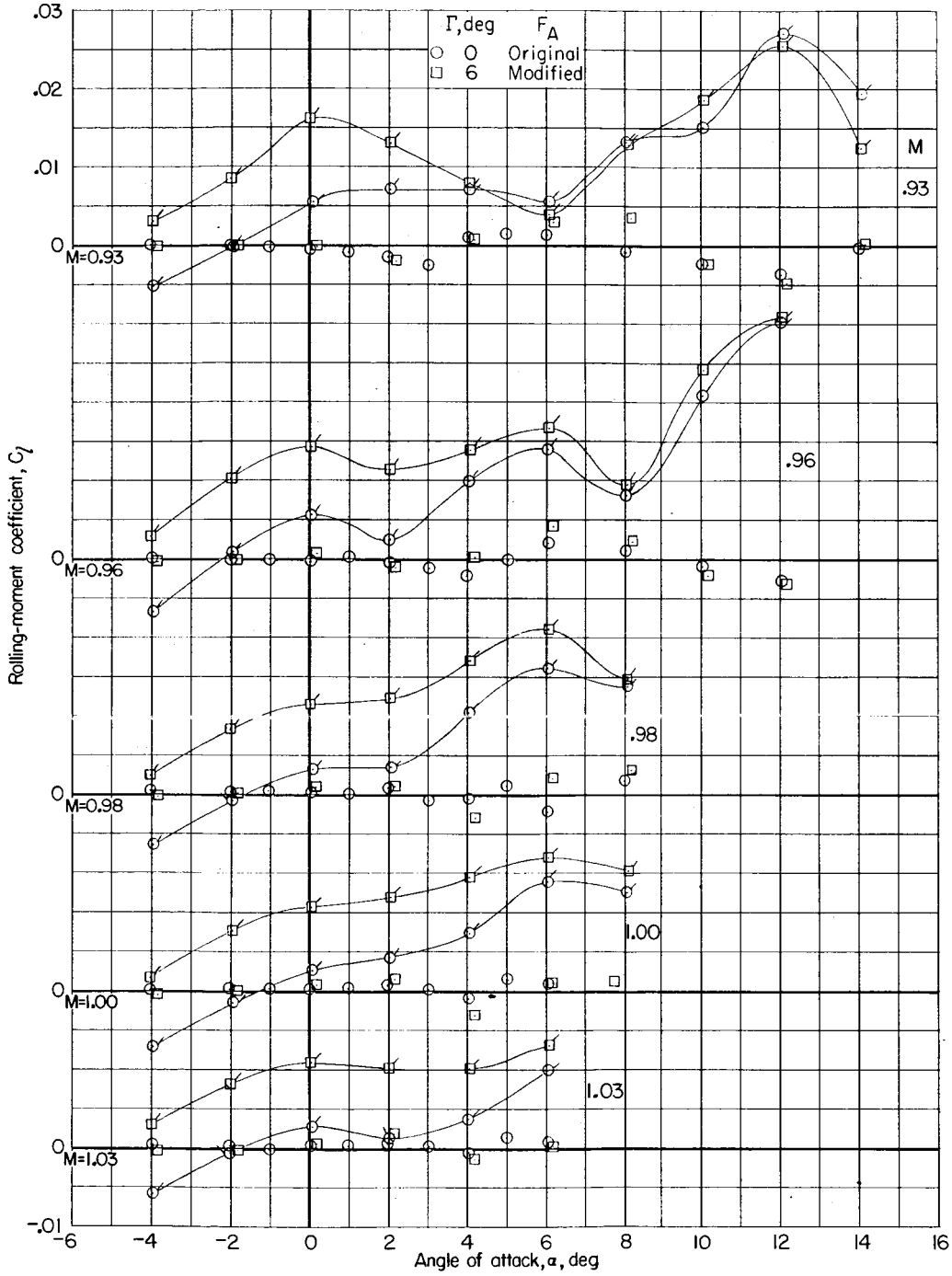

(b) Variation of C_l with α; M = 0.93 to 1.03.

Figure 43.- Continued.

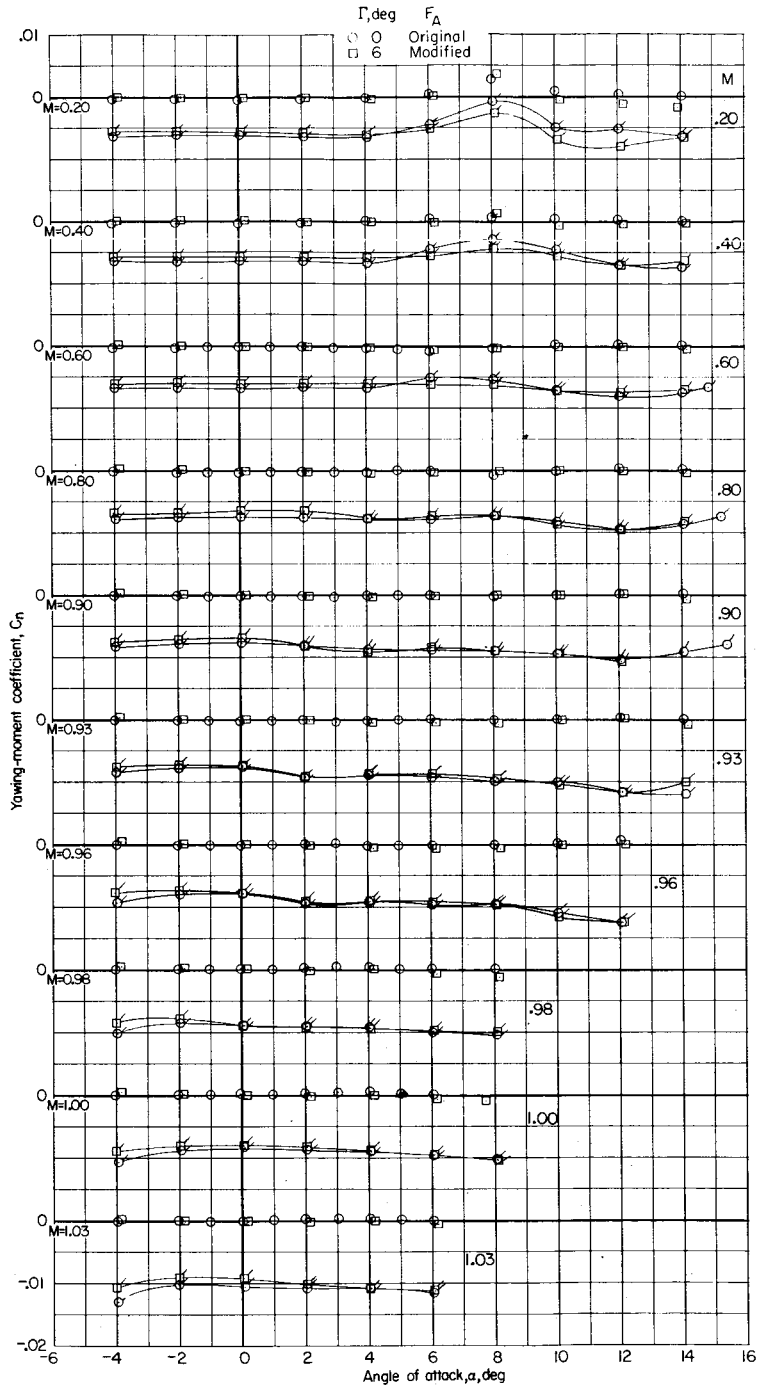

(c) Variation of C_n with α; M = 0.20 to 1.03.

Figure 43.- Continued.

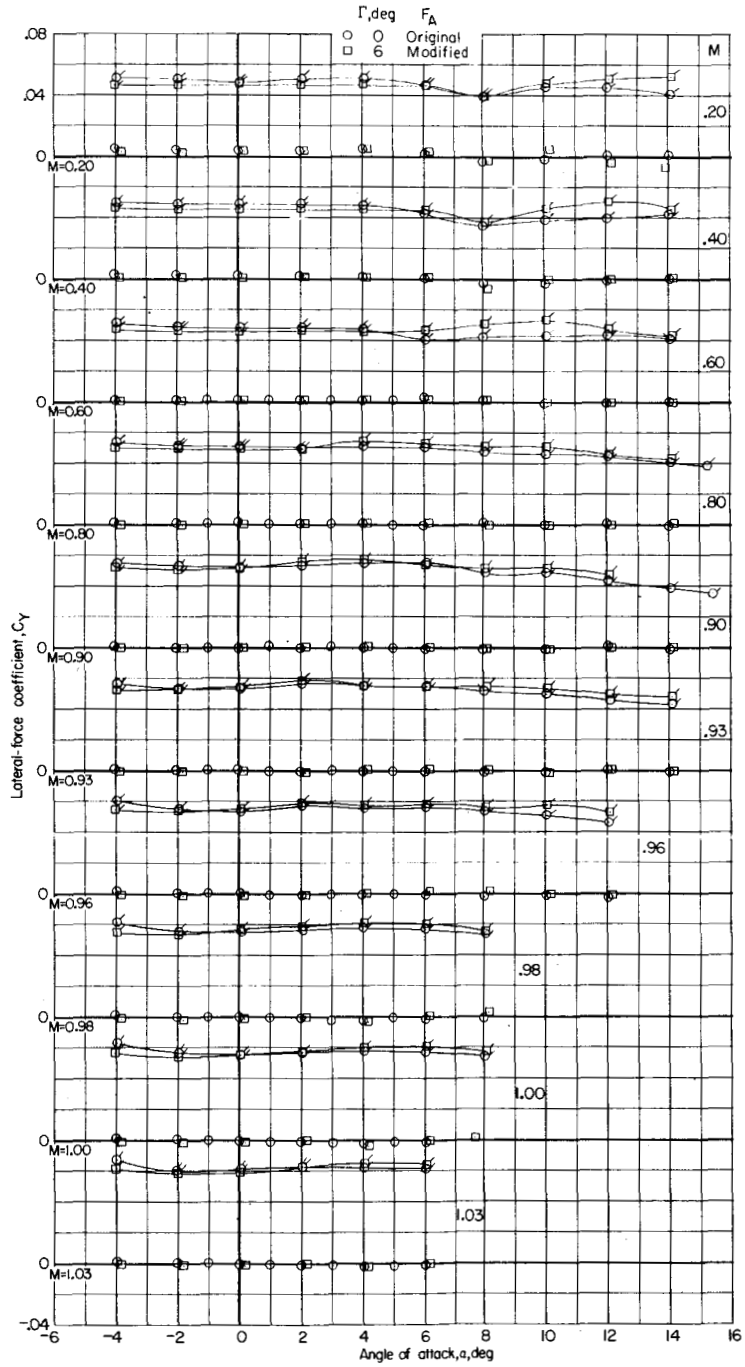

(d) Variation of C_Y with α; M = 0.20 to 1.03.

Figure 43.- Concluded.

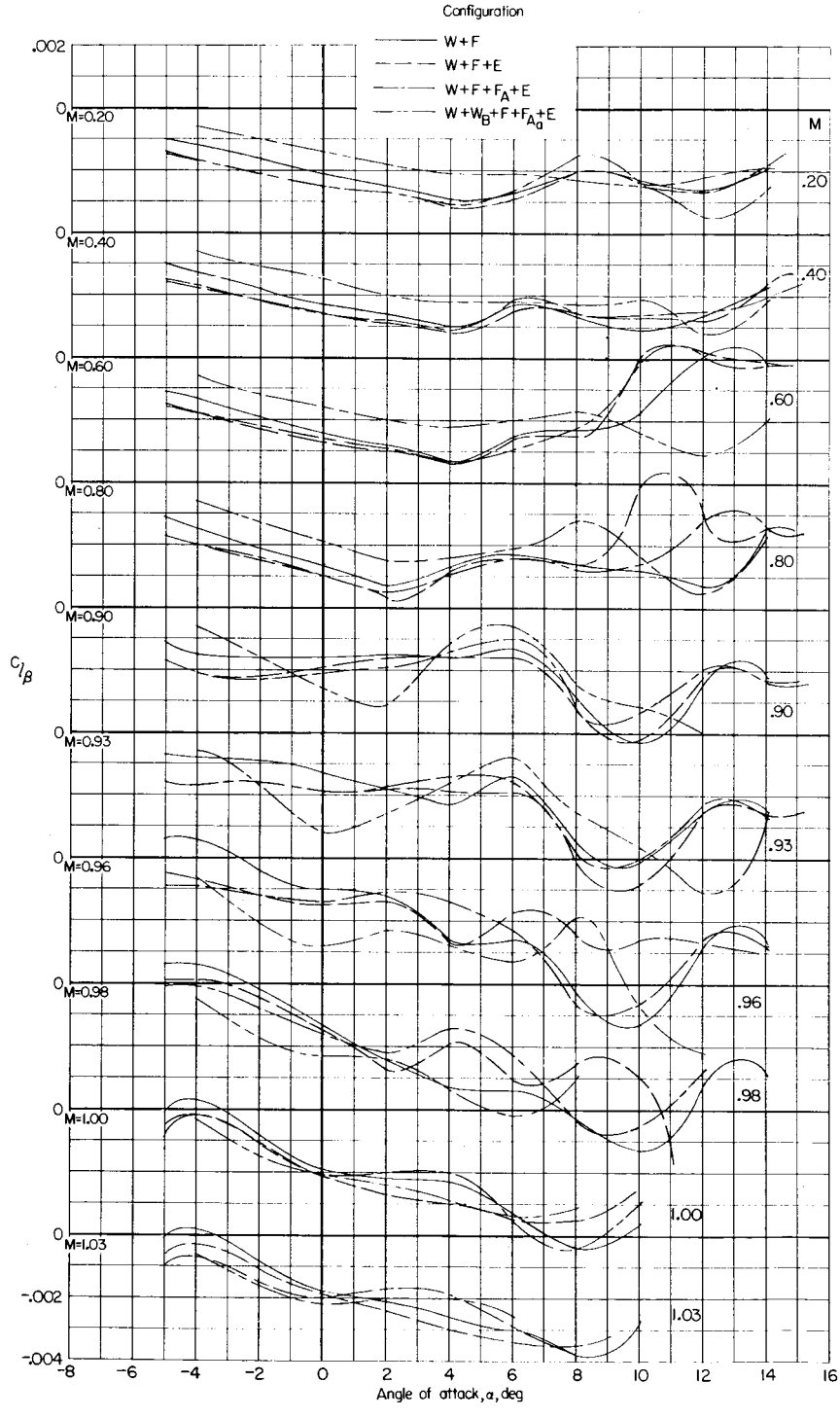

(a) Effective-dihedral derivative.

Figure 44.- Variation with angle of attack of lateral-stability derivatives for various configurations of complete model components. $\Lambda = 45^{\circ}$; $\Gamma = 6^{\circ}$.

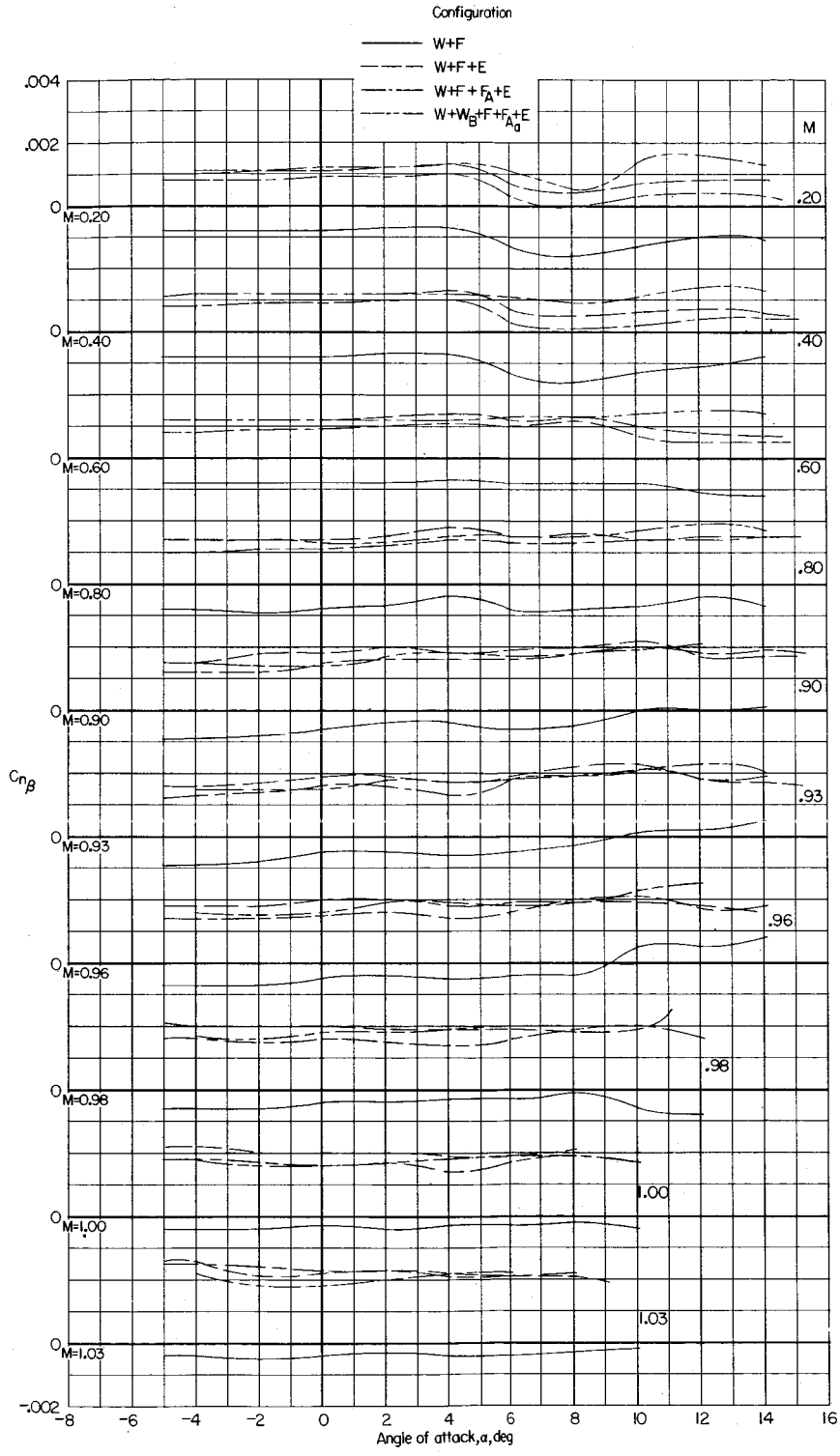

(b) Directional-stability derivative.

Figure 44.- Continued.

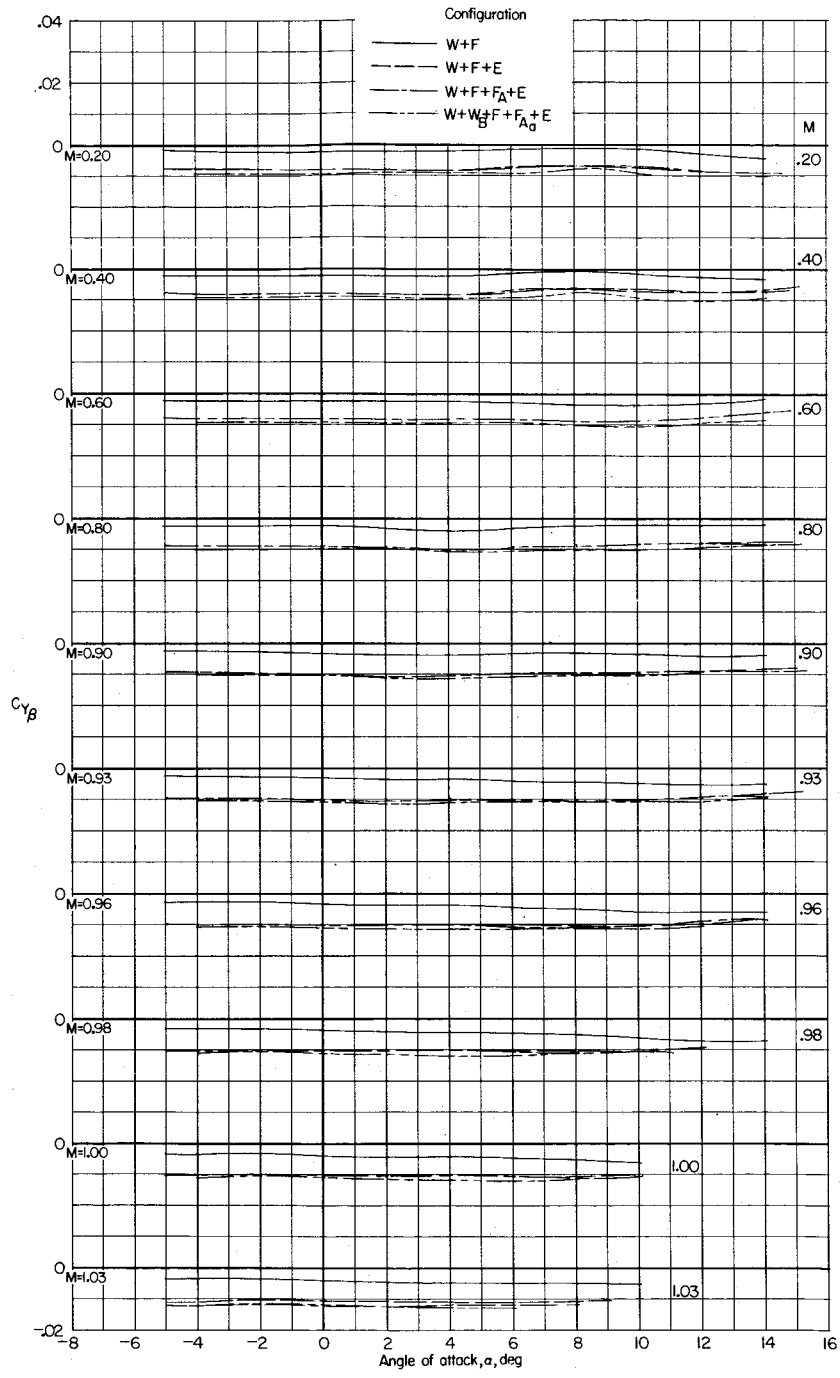

(c) Lateral-force derivative.

Figure 44.- Concluded.

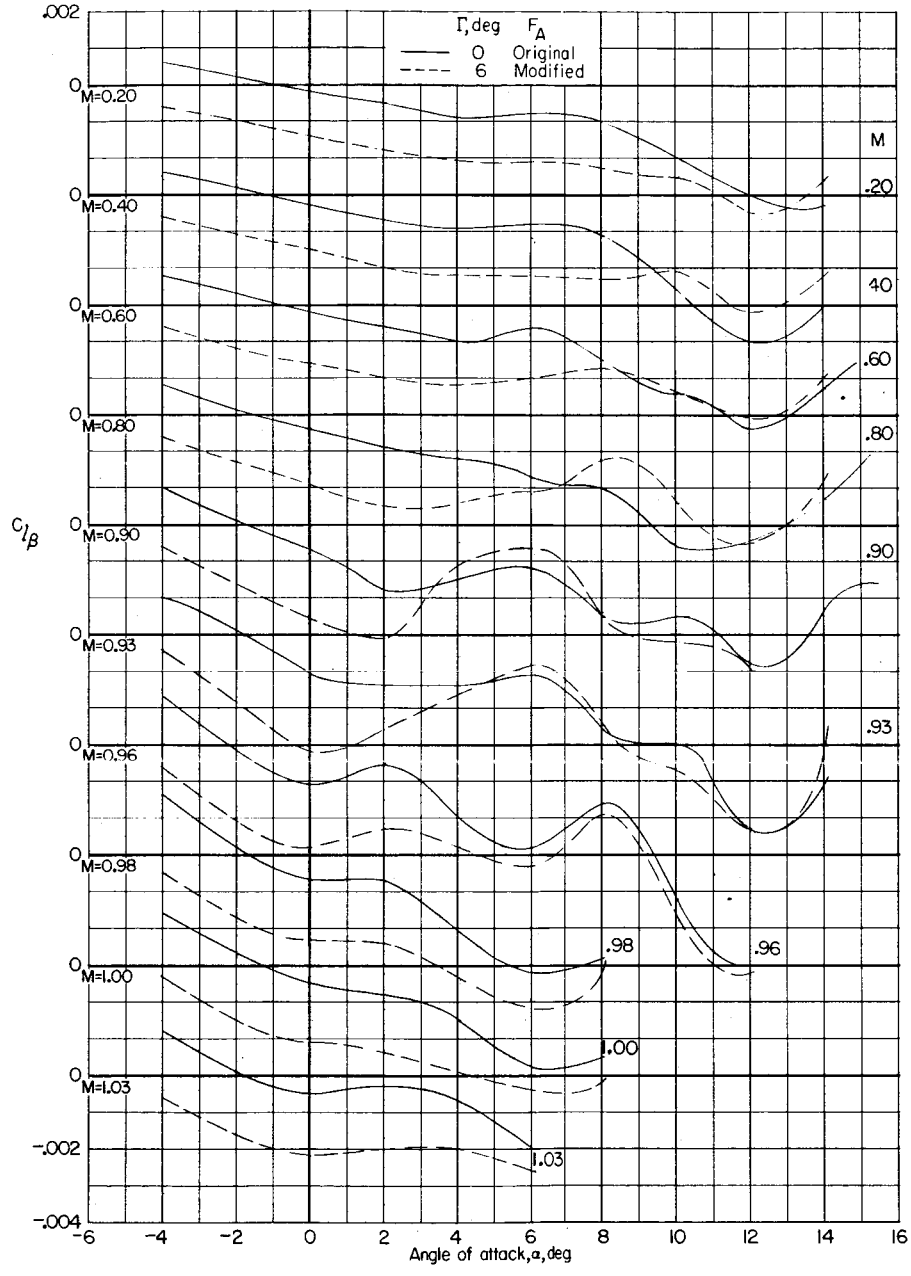

(a) Effective-dihedral derivative.

Figure 45.- Variation with angle of attack of lateral-stability derivatives of complete model with dihedral angle of 0° and 6°. $\Lambda = 45°$; original fuselage addition on model with $\Gamma = 0°\left(W + W_B + F + F_A + E\right)$; modified fuselage addition on model with $\Gamma = 6°\left(W + W_B + F + F_{A_a} + E\right)$.

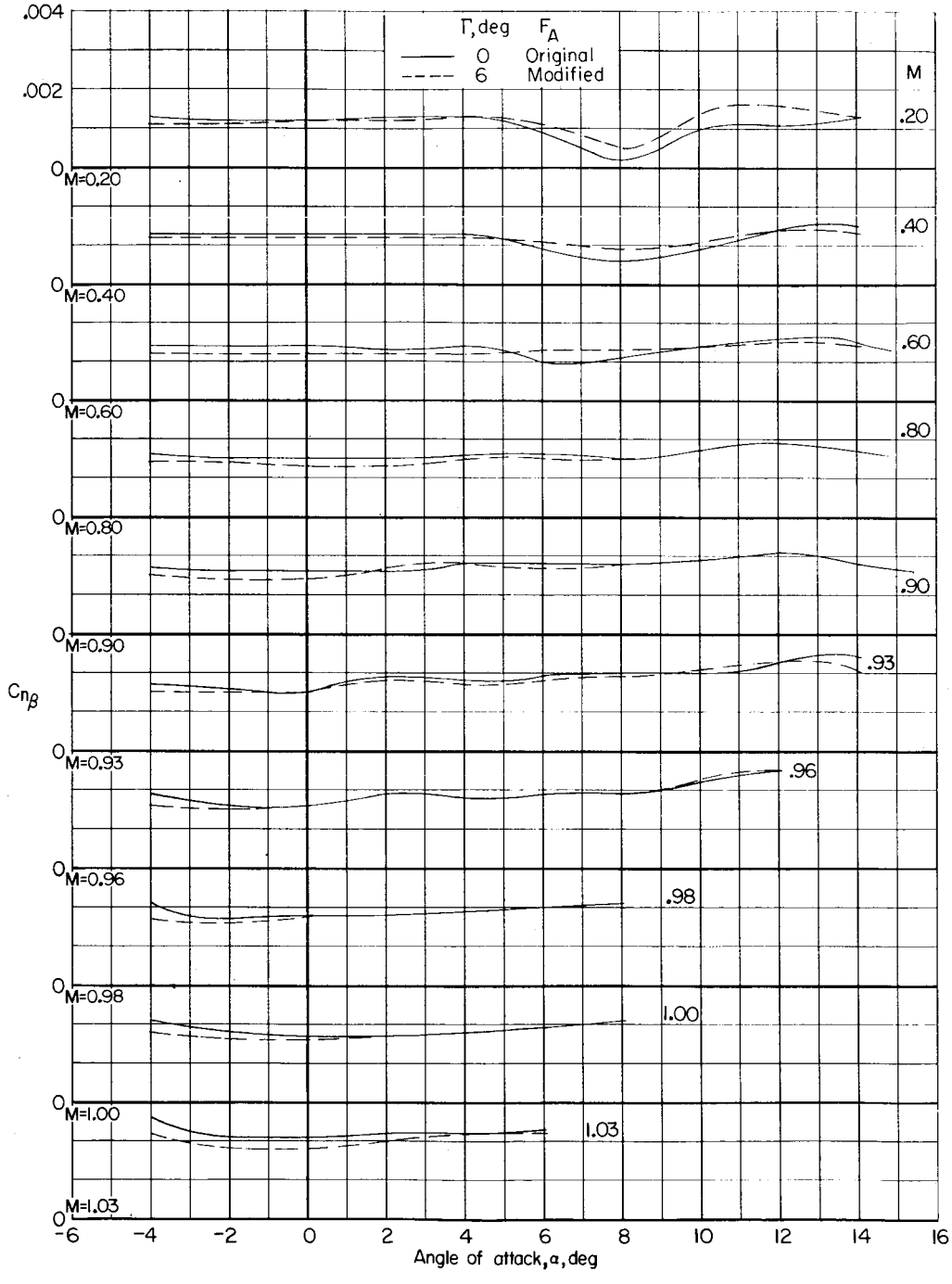

(b) Directional-stability derivative.

Figure 45.- Continued.

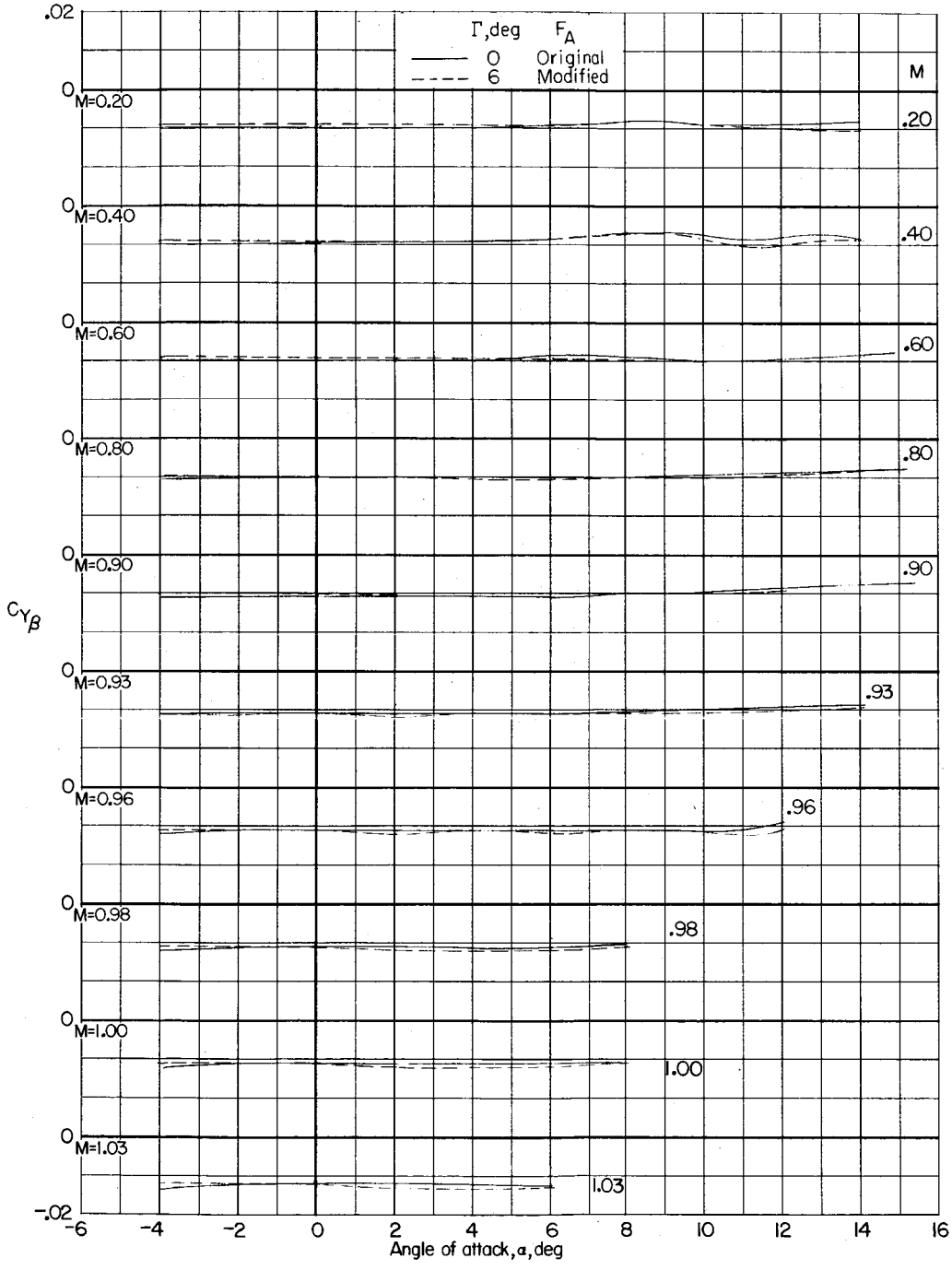

(c) Lateral-force derivative.

Figure 45.- Concluded.

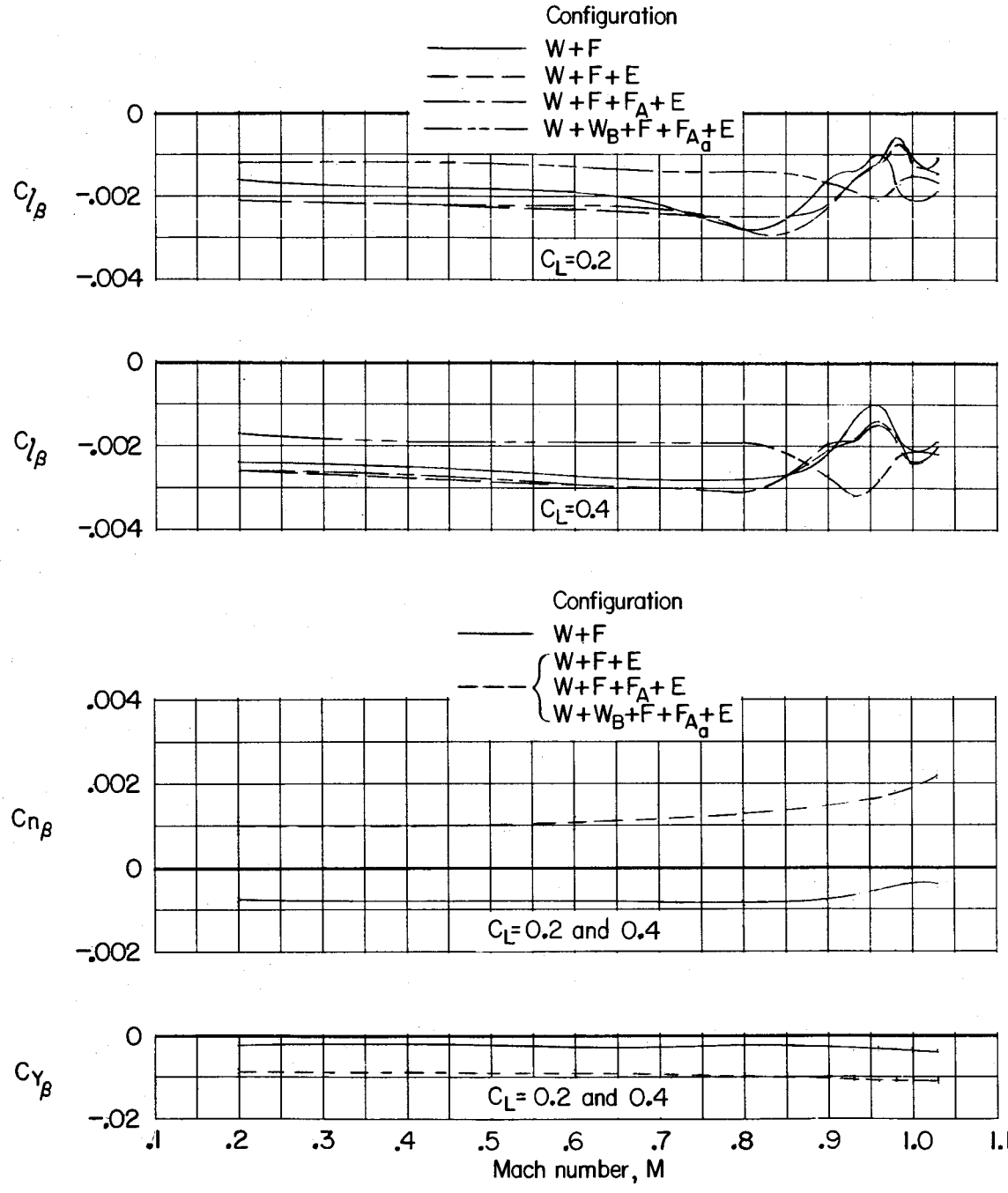

Figure 46.- Variation with Mach number of lateral-stability derivatives for various configurations of complete model components. $\Lambda = 45^\circ$; $\Gamma = 6^\circ$.

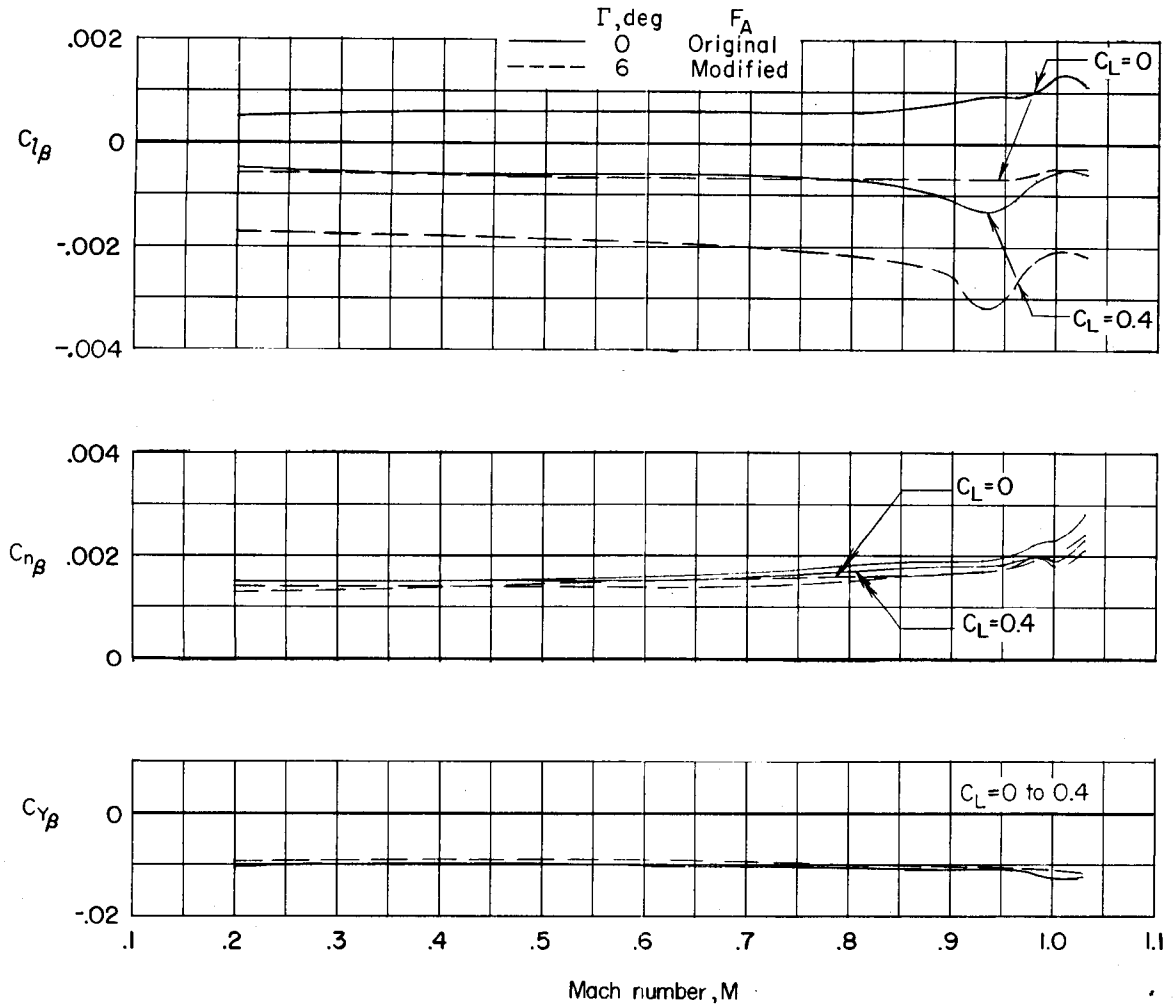

Figure 47.- Variation with Mach number of lateral-stability derivatives of complete model for dihedral angles of 0° and 6°. $\Lambda = 45°$; original fuselage addition on model with $\Gamma = 0°$ $(W + W_B + F + F_A + E)$; modified fuselage addition on model with $\Gamma = 6°(W + W_B + F + F_{A_a} + E)$.

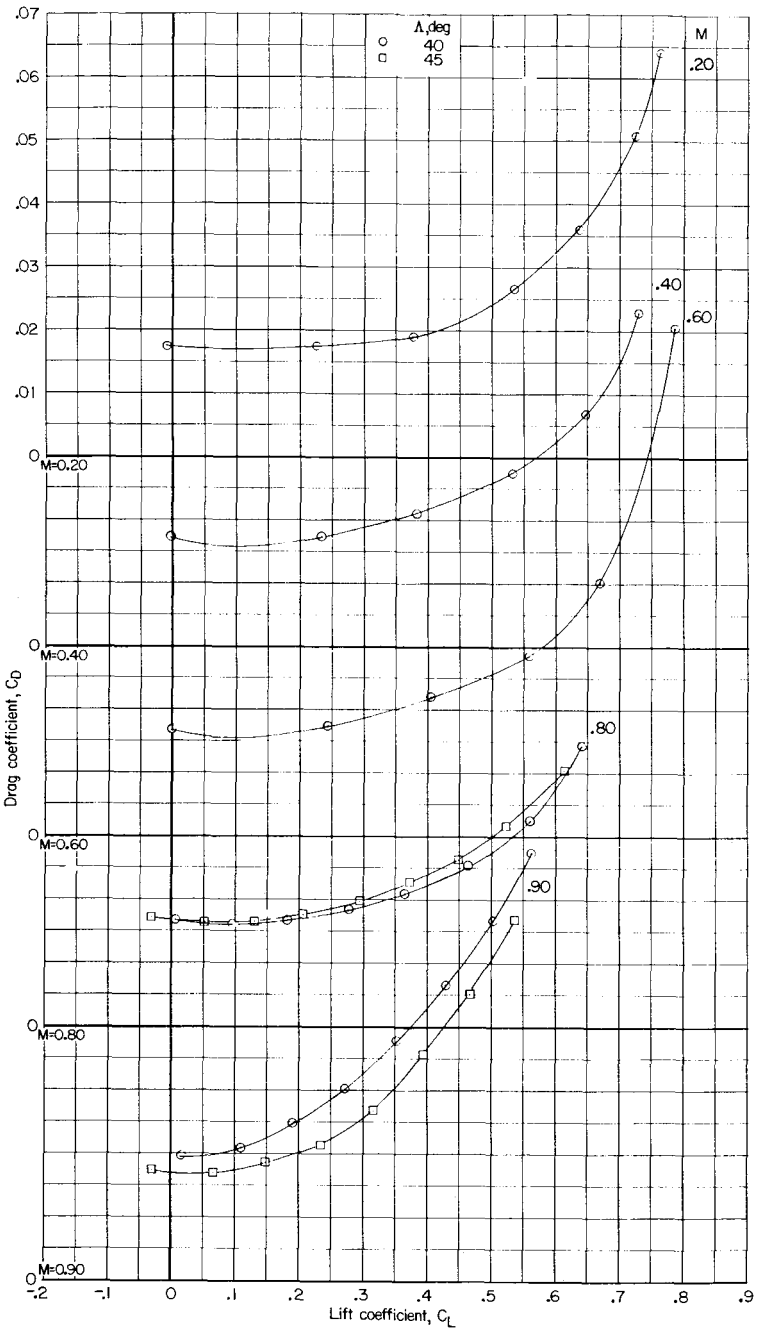

(a) M = 0.20 to 0.90.

Figure 48.- Effect of sweepback angle on aerodynamic drag characteristics of basic model without basic additions (W + F + E). $\Gamma = 6^{\circ}$; $\beta = 0^{\circ}$.

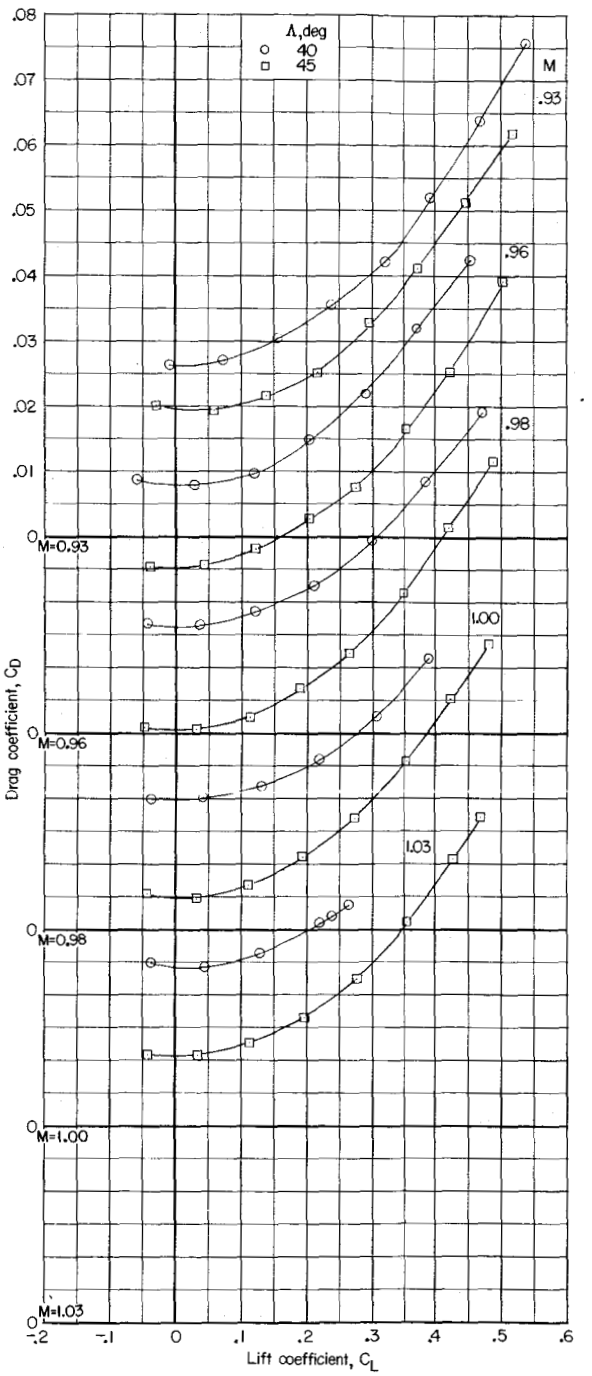

(b) M = 0.93 to 1.03.

Figure 48.- Concluded.

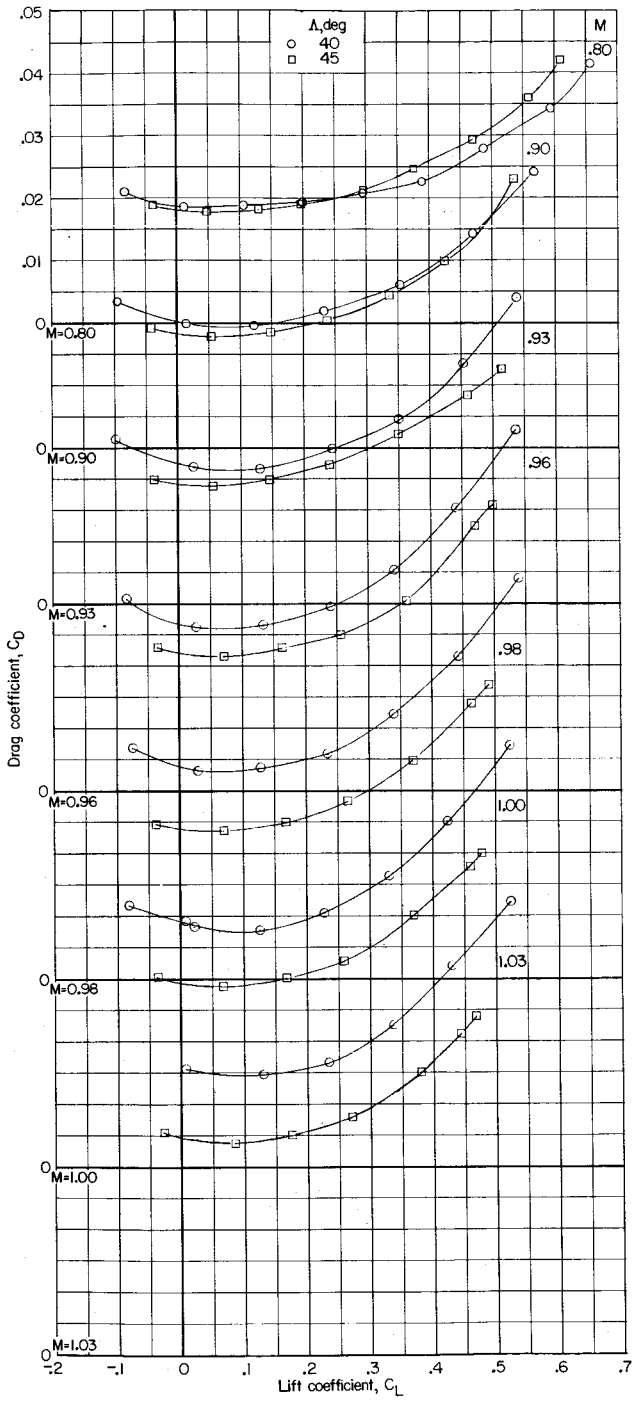

Figure 49.- Effect of sweepback angle on aerodynamic drag characteristics of basic model $(W + W_B + F + F_A + E)$. $\Gamma = 6^\circ$; $\beta = 0^\circ$.

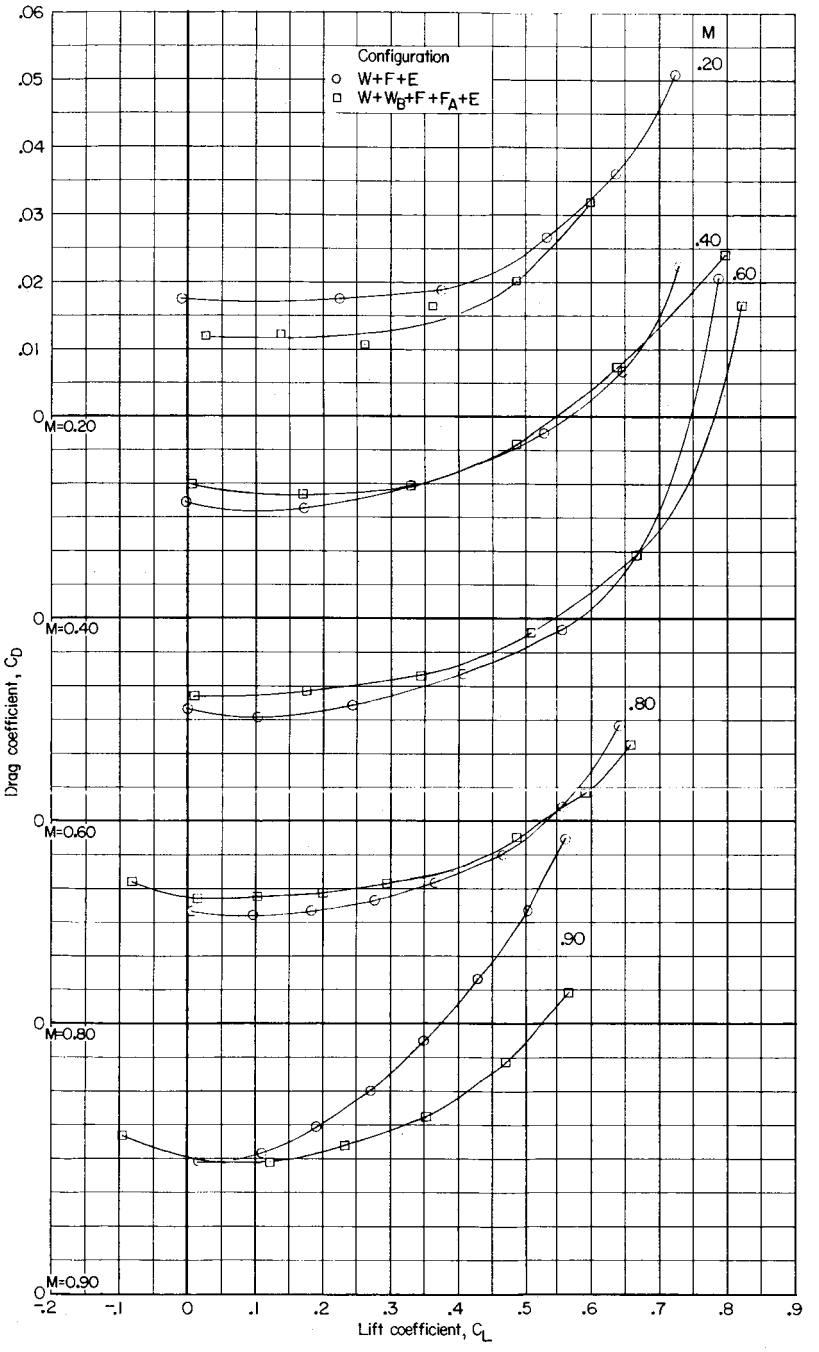

(a) M = 0.20 to 0.90.

Figure 50.- Effect of basic additions on aerodynamic drag characteristics of basic model. $\Lambda = 40^{\circ}$; $\Gamma = 6^{\circ}$; $\beta = 0^{\circ}$.

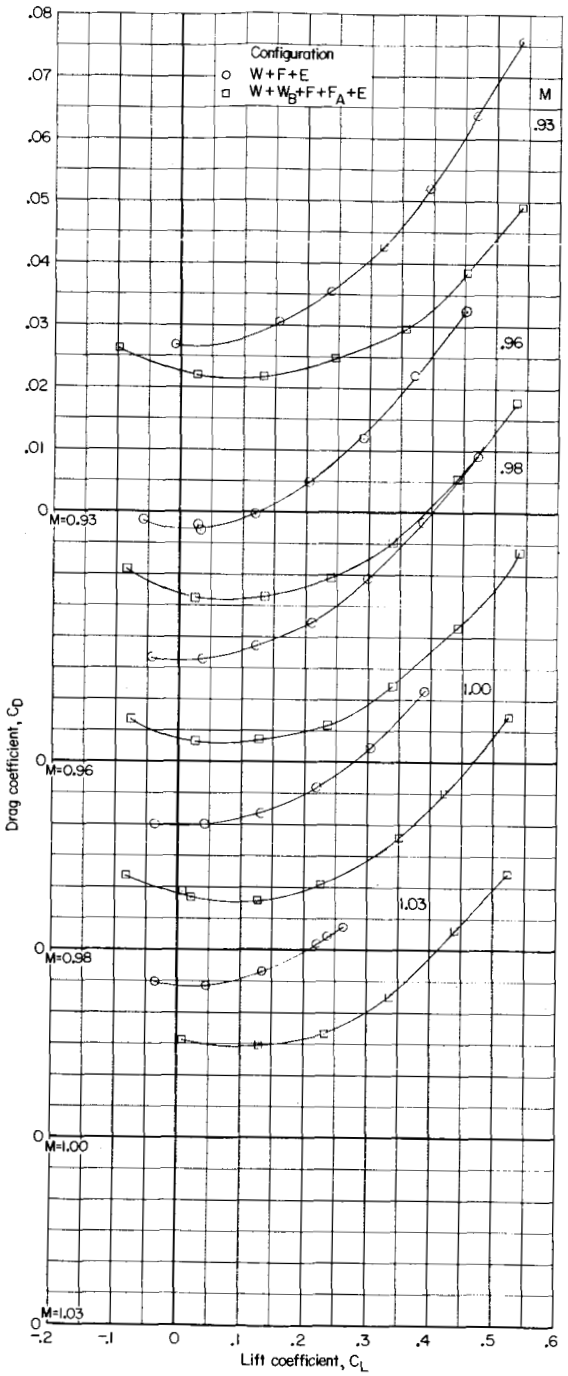

(b) M = 0.93 to 1.03.

Figure 50.- Concluded.

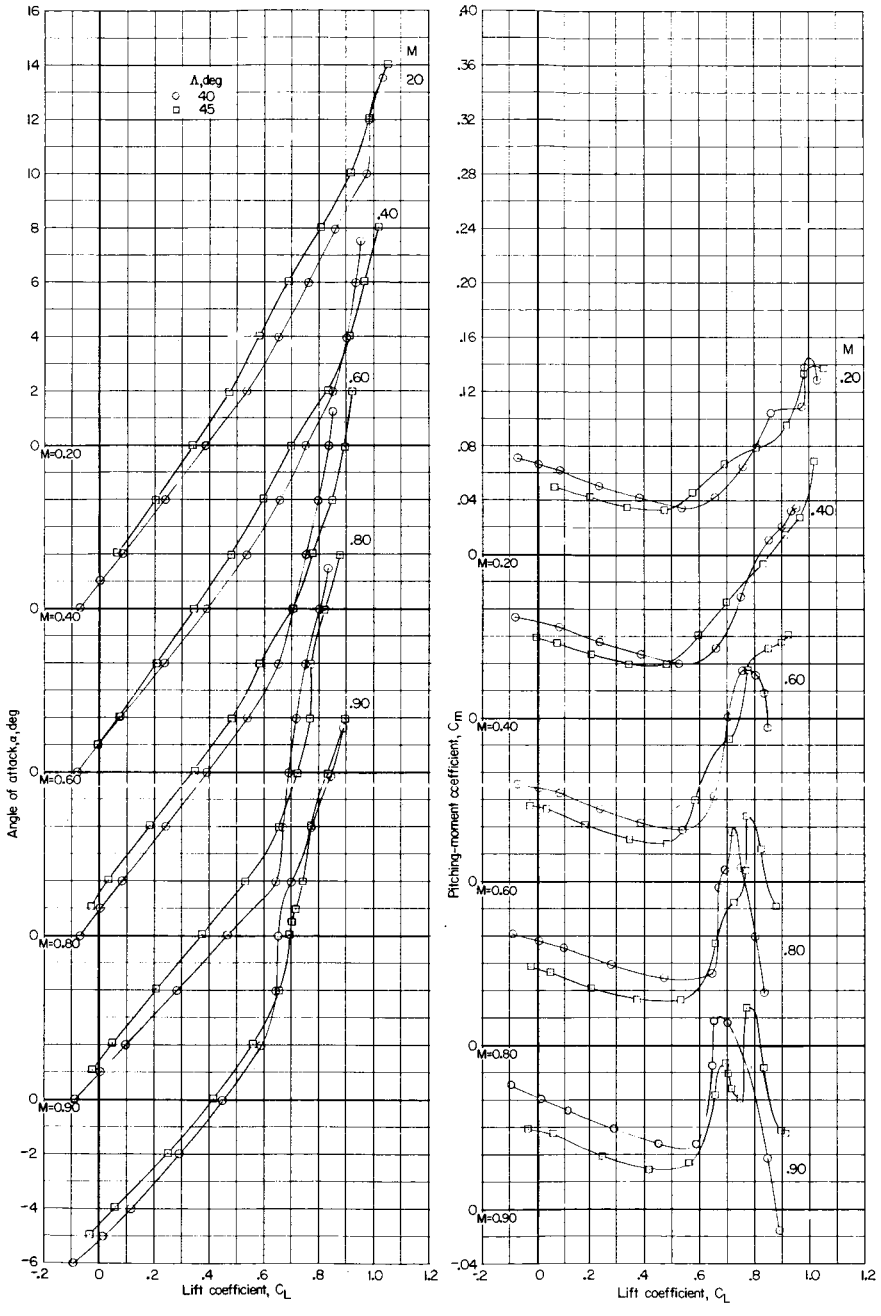

(a) M = 0.20 to 0.90.

Figure 51.- Effect of sweepback angle on aerodynamic lift and pitching-moment characteristics of basic model without basic additions (W + F + E). $\Gamma = 6^{\circ}$; $\beta = 0^{\circ}$.

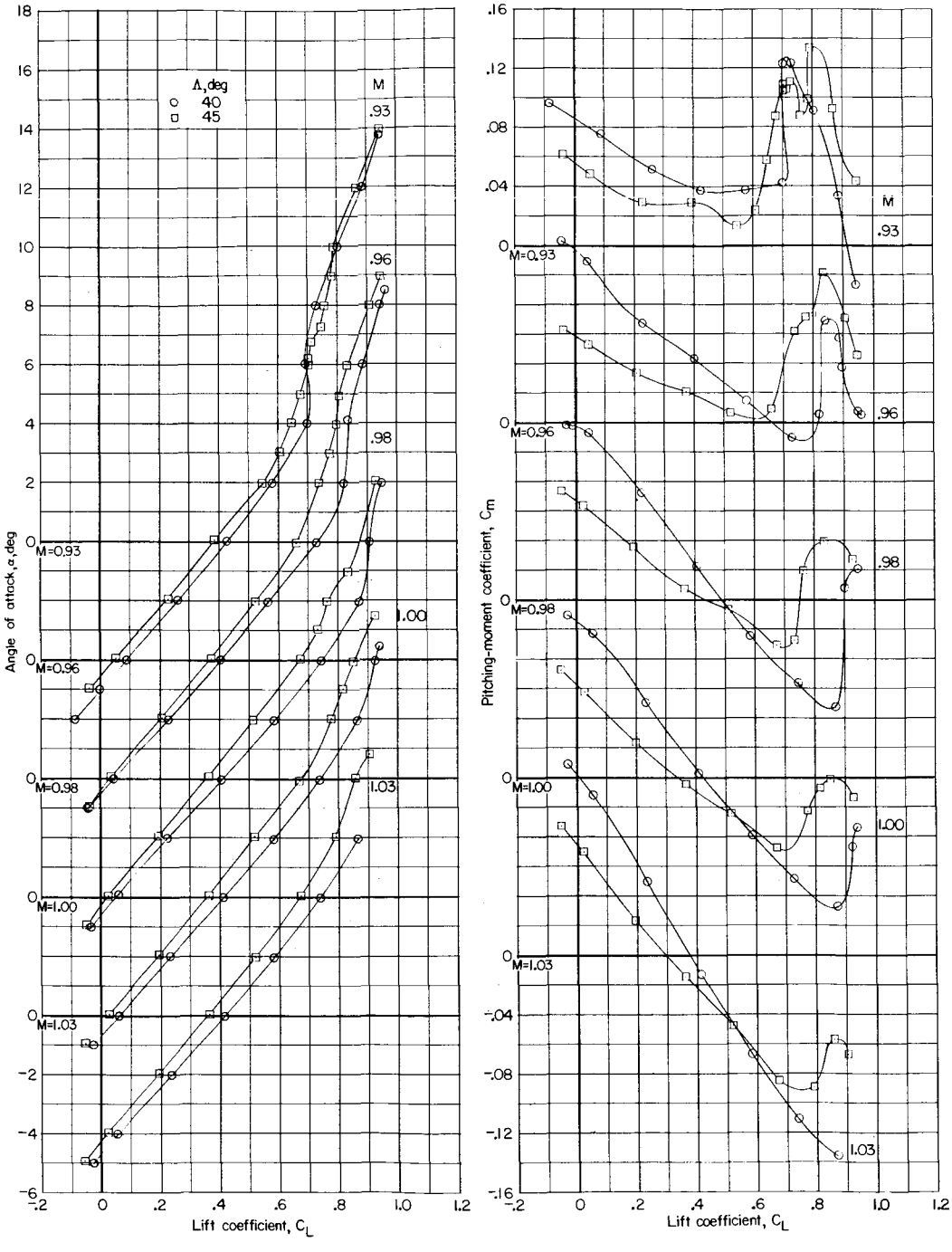

(b) M = 0.93 to 1.03.

Figure 51.- Concluded.

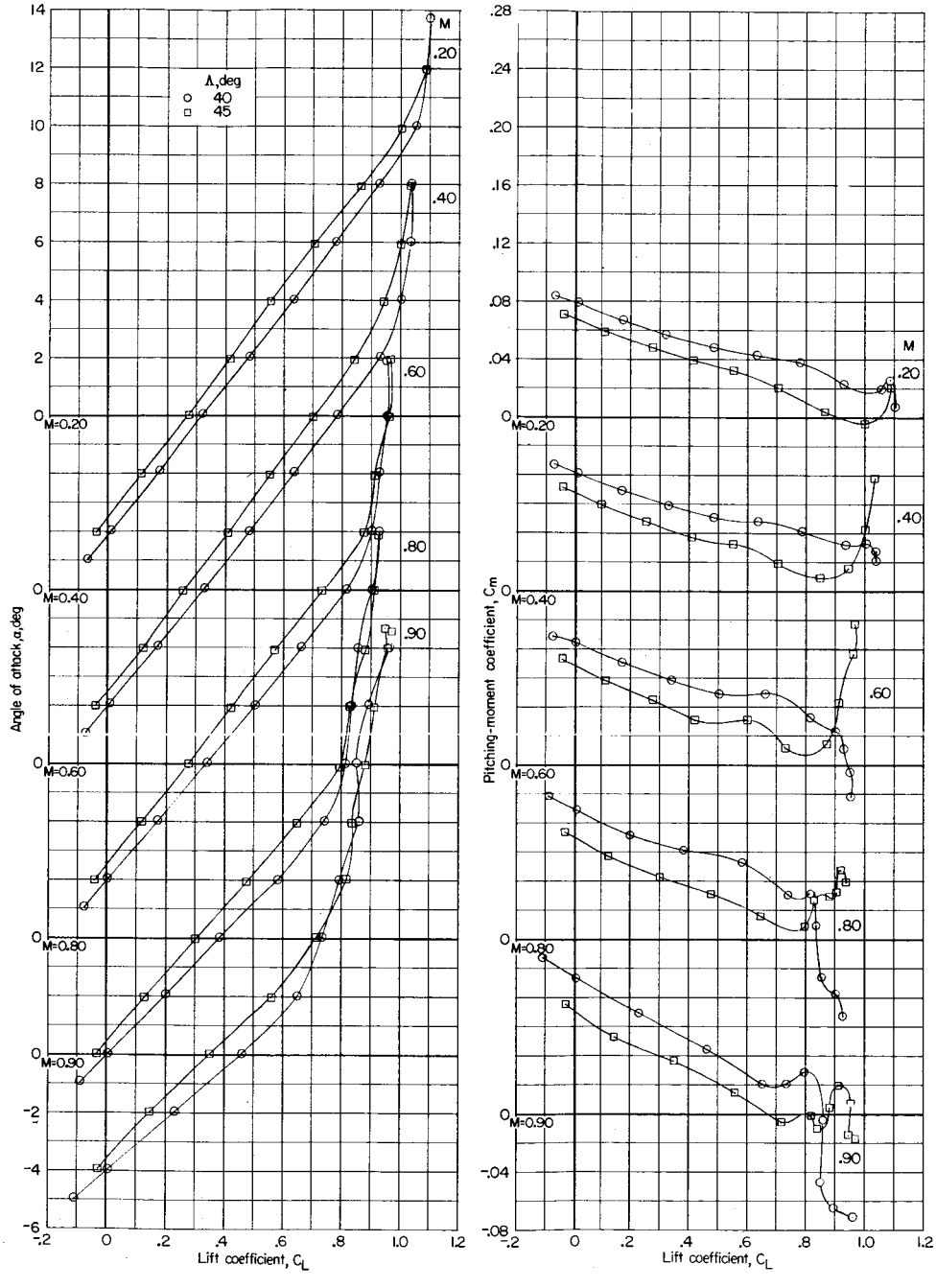

(a) M = 0.20 to 0.90.

Figure 52.- Effect of sweepback angle on aerodynamic lift and pitching-moment characteristics of basic model $(W + W_B + F + F_A + E)$. $\Gamma = 6^\circ$; $\beta = 0^\circ$.

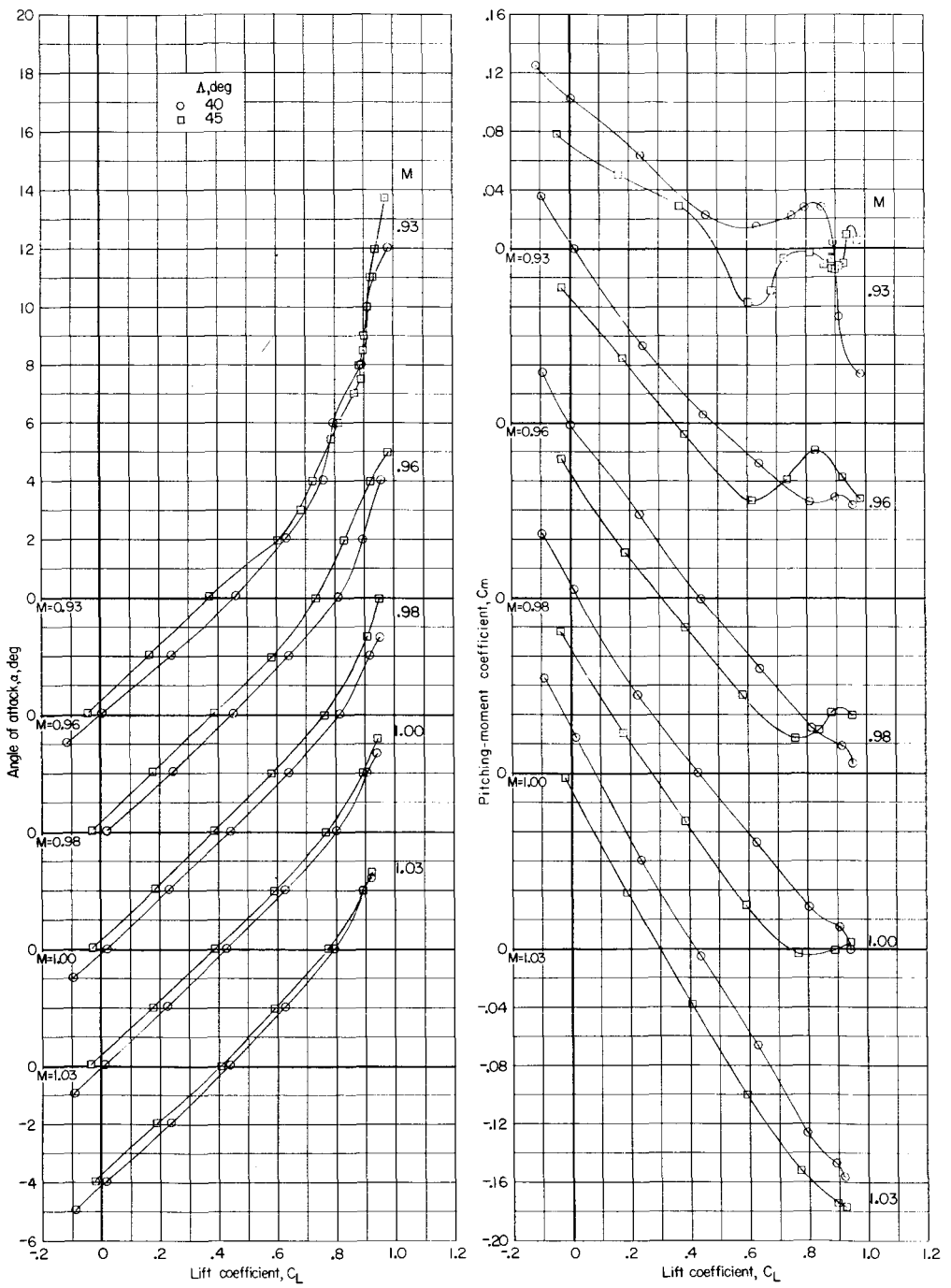

(b) M = 0.93 to 1.03.

Figure 52.- Concluded.

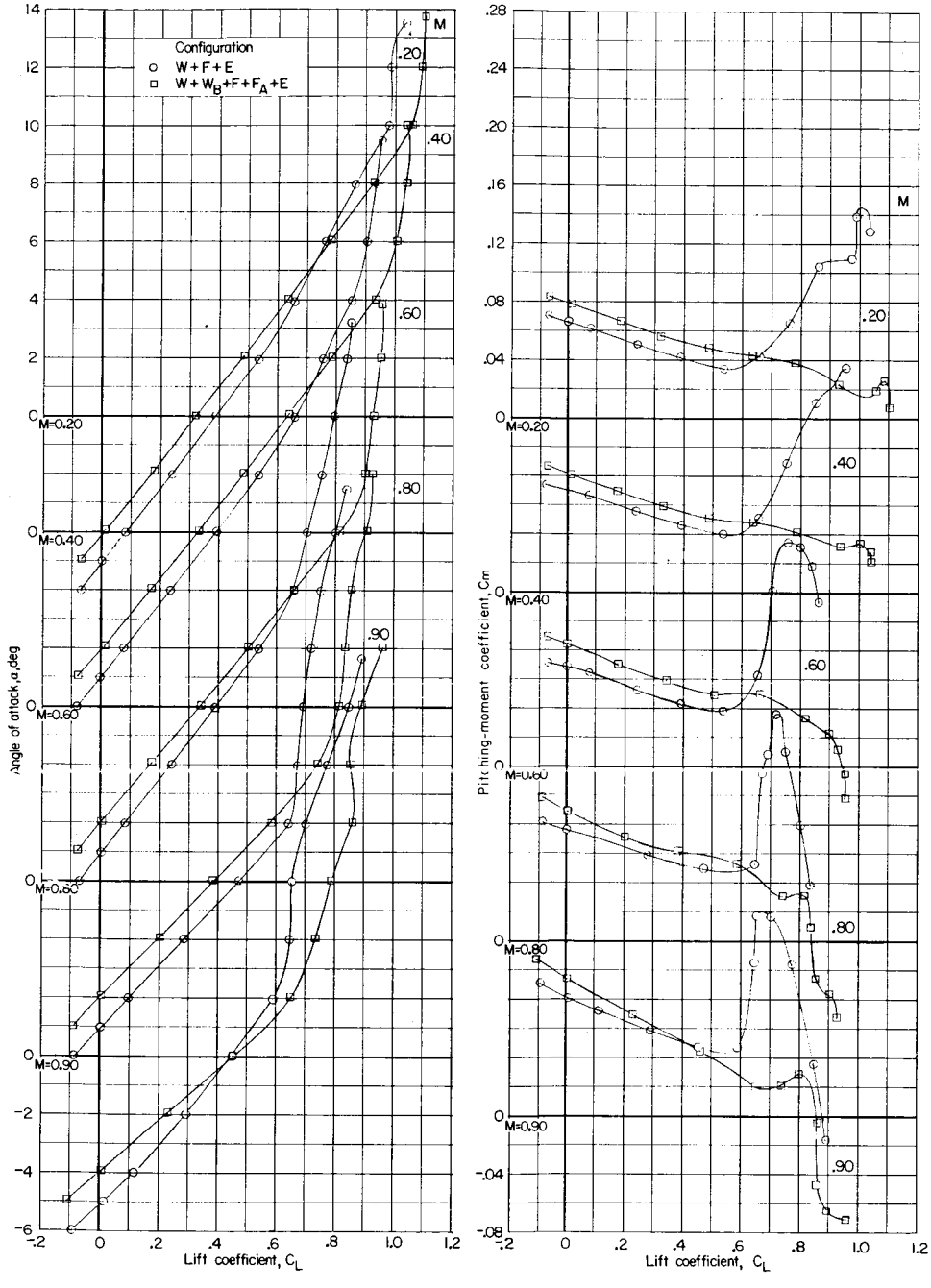

(a) M = 0.20 to 0.90.

Figure 53.- Effect of basic additions on aerodynamic lift and pitching-moment characteristics of basic model. $\Lambda = 40^{\circ}$; $\Gamma = 6^{\circ}$; $\beta = 0^{\circ}$.

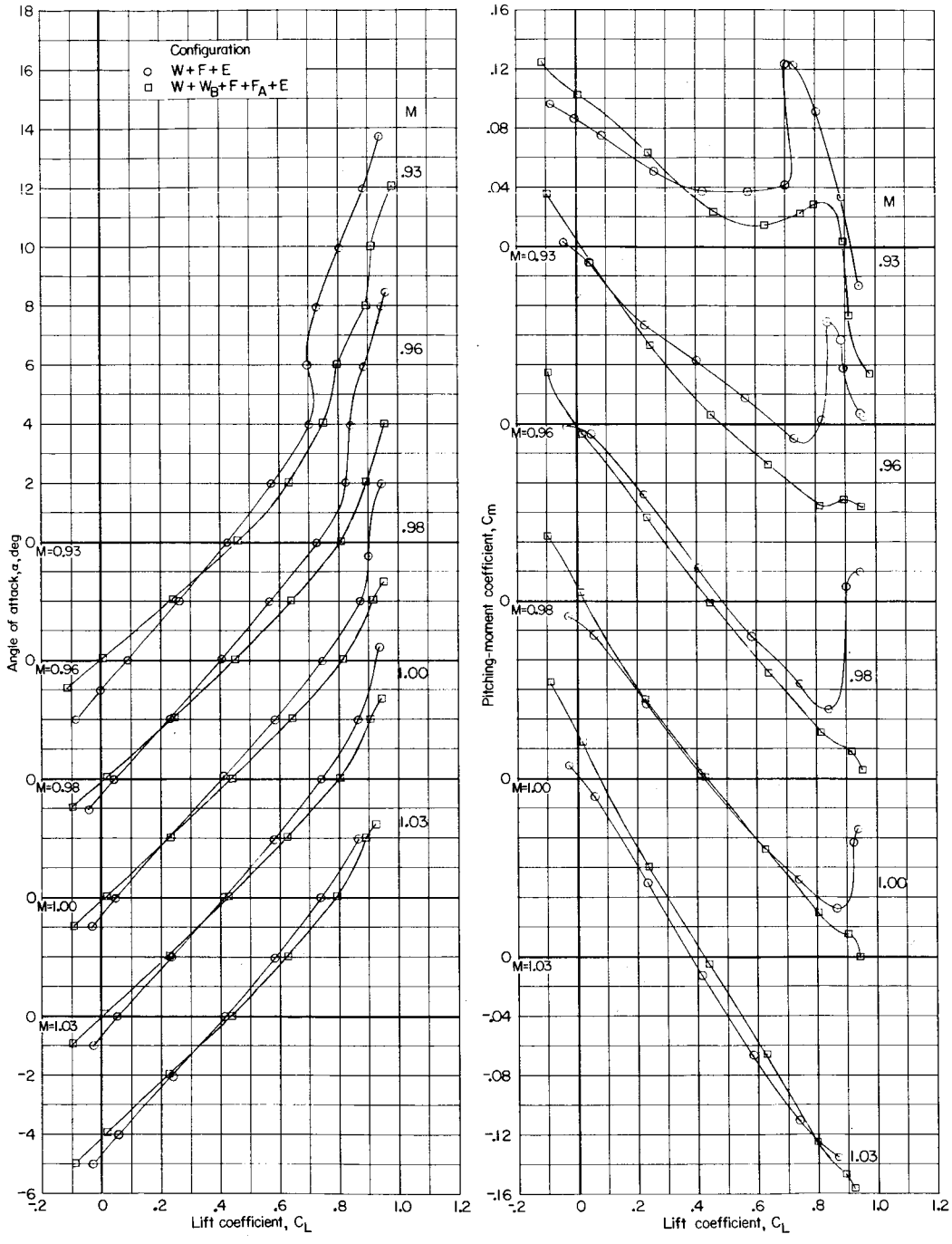

(b) M = 0.93 to 1.03.

Figure 53.- Concluded.

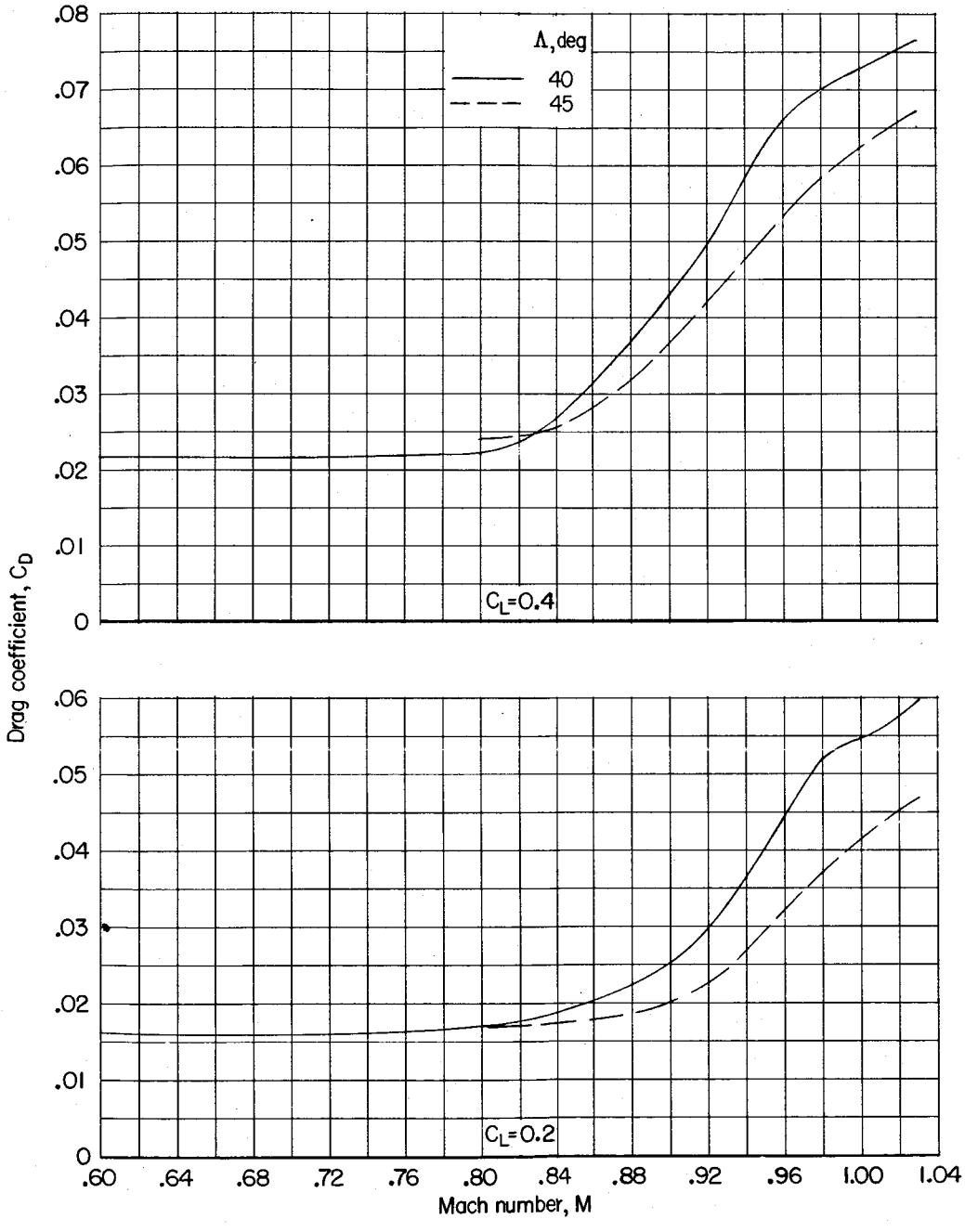

(a) C_D.

Figure 54.- Variation with Mach number of aerodynamic characteristics of basic model without basic additions (W + F + E) with sweepback angles of 40° and 45°. $\Gamma = 6°$; $\beta = 0°$.

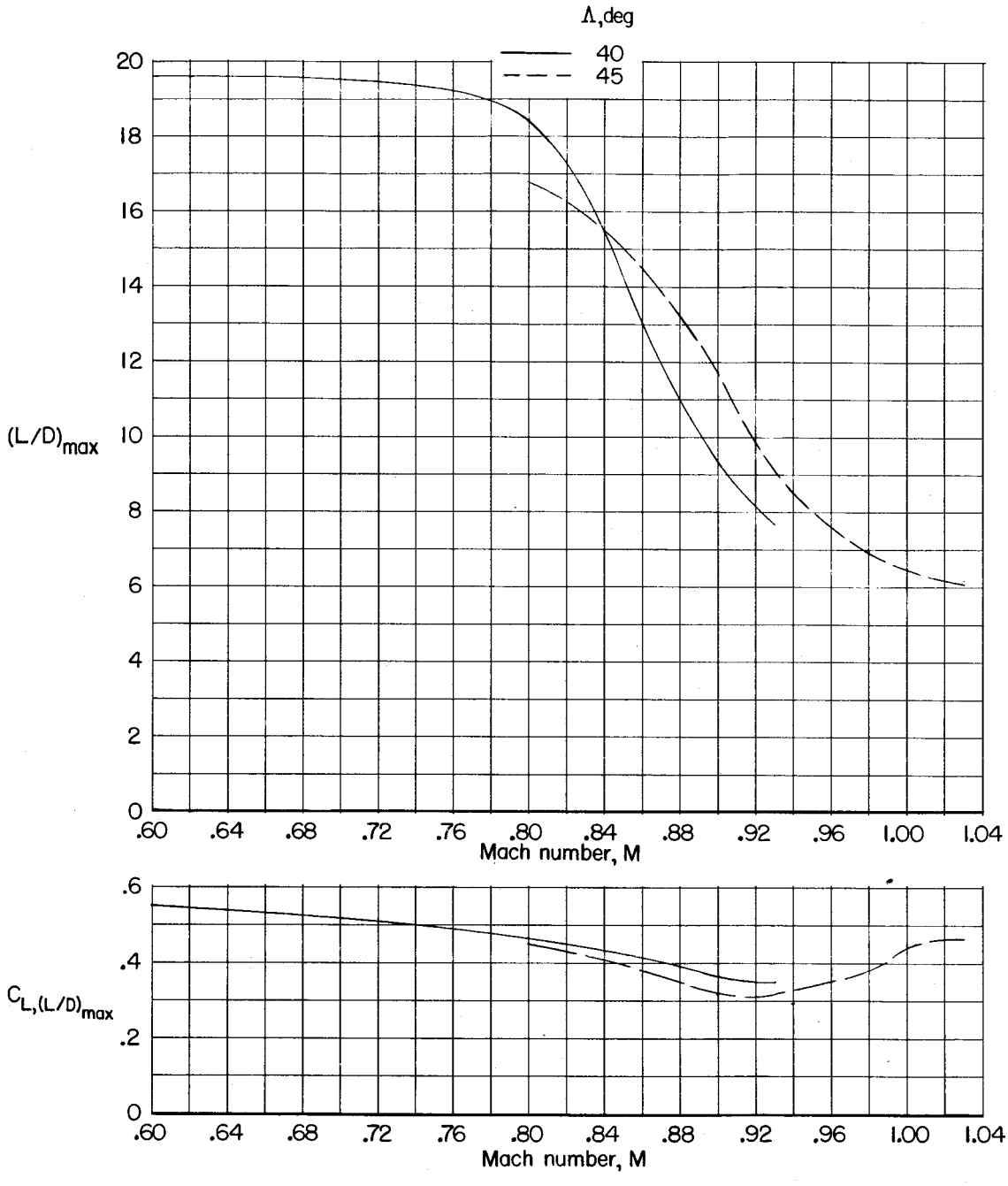

(b) Untrimmed $\left(\frac{L}{D}\right)_{max}$ and C_L at untrimmed $\left(\frac{L}{D}\right)_{max}$.

Figure 54.- Continued.

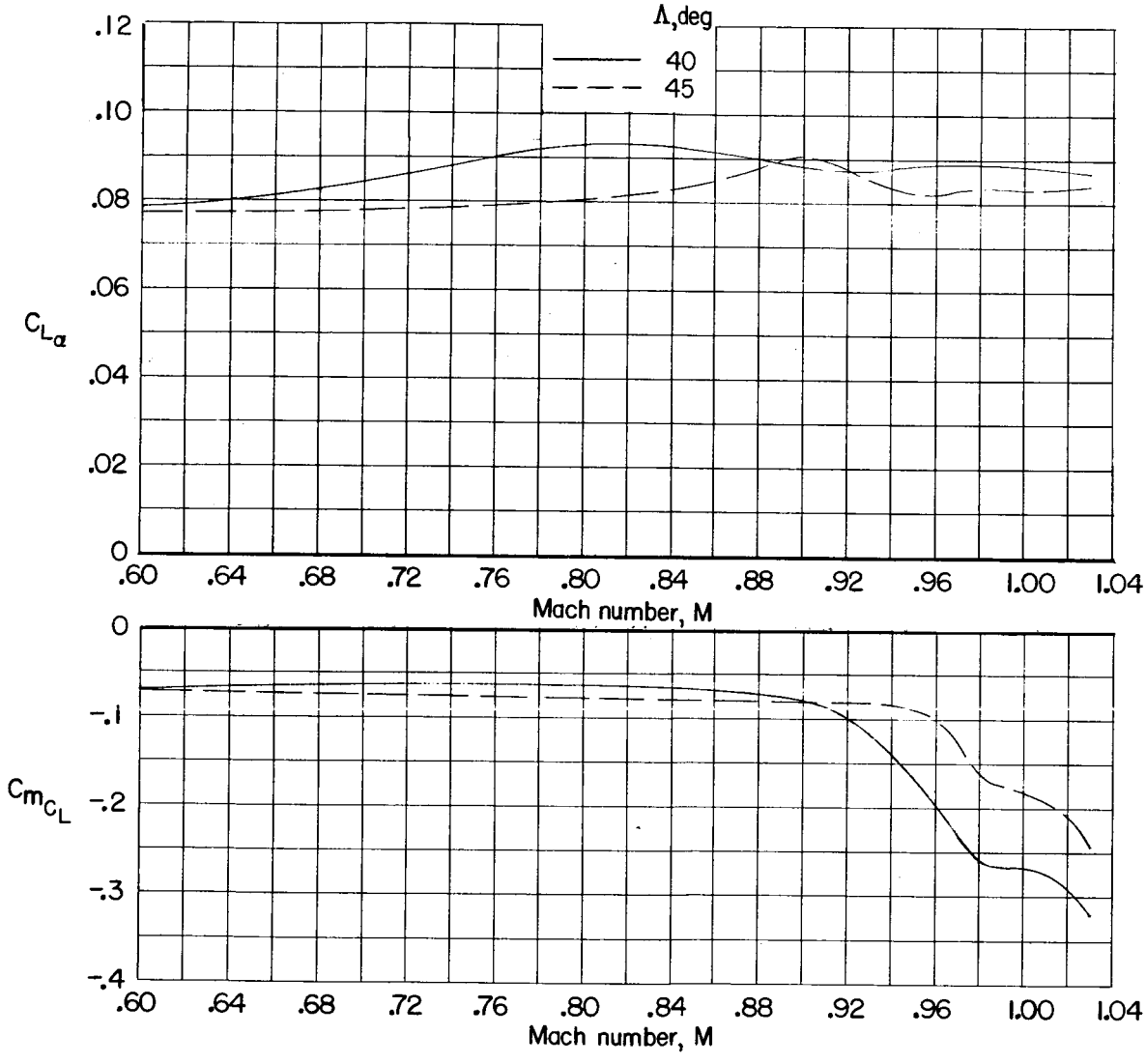

(c) C_{L_α} and $C_{m_{C_L}}$.

Figure 54.- Concluded.

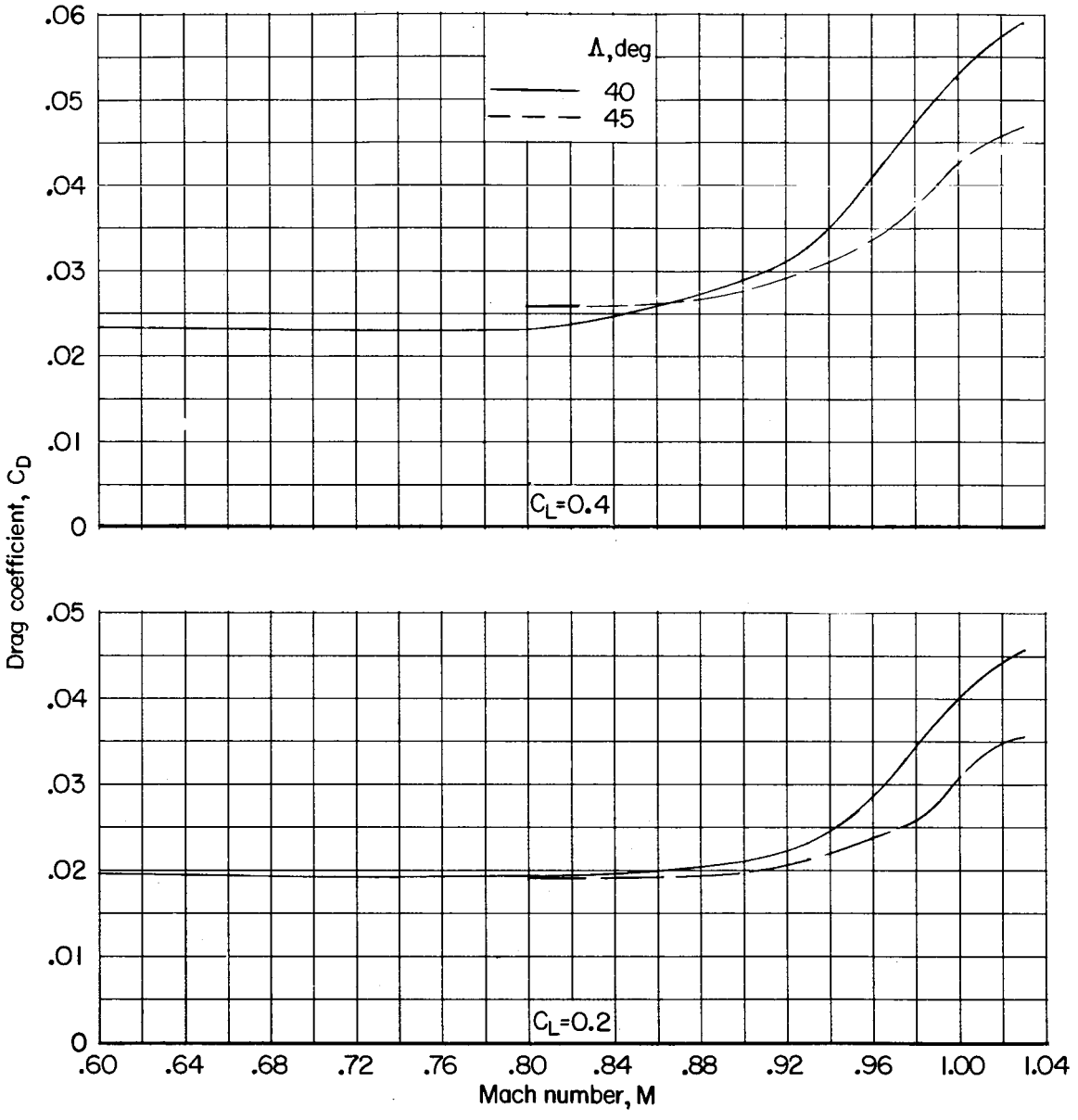

(a) C_D.

Figure 55.- Variation with Mach number of aerodynamic characteristics of basic model $(W + W_B + F + F_A + E)$ with sweepback angles of 40° and 45°. $\Gamma = 6°$; $\beta = 0°$.

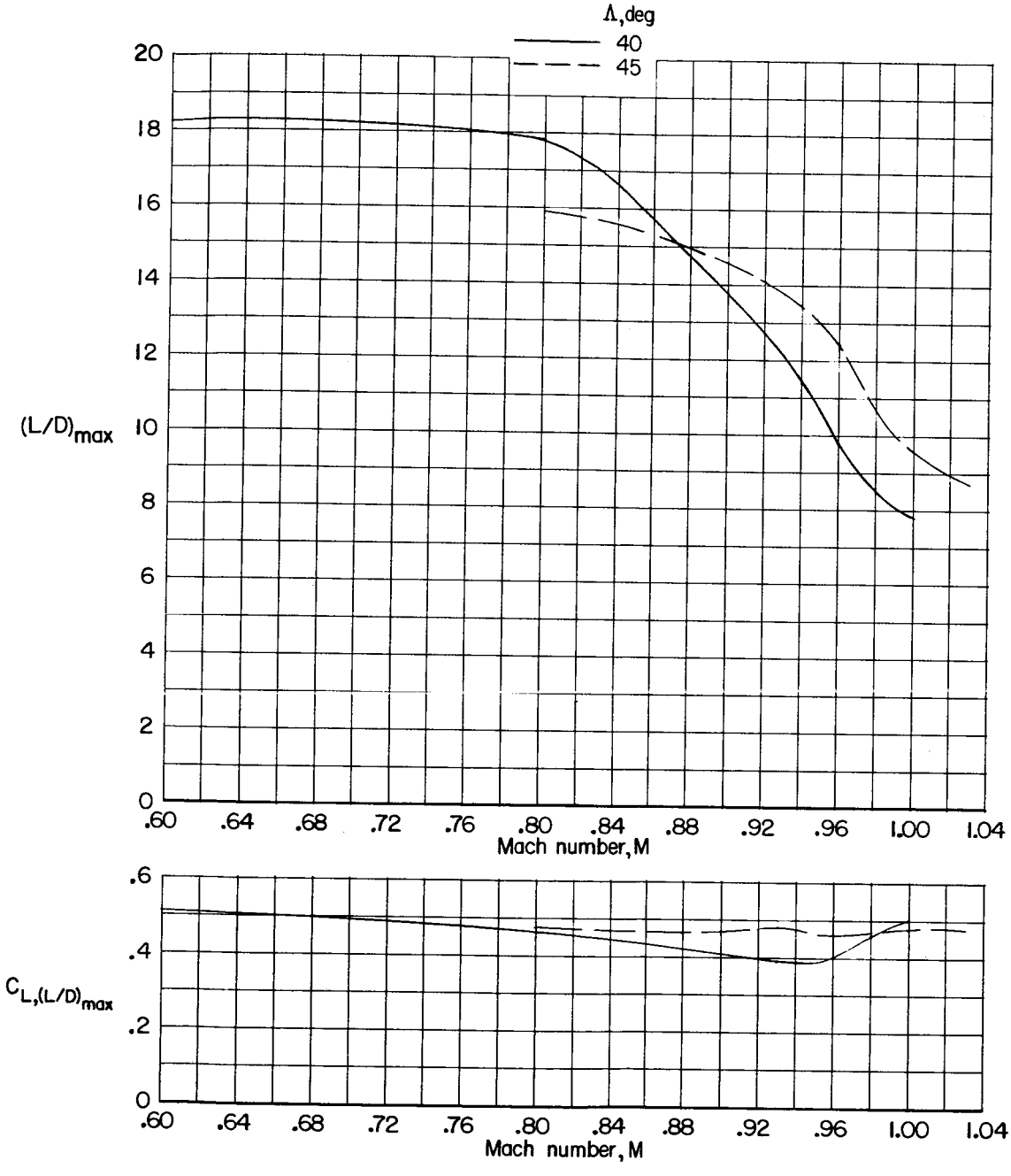

(b) Untrimmed $\left(\frac{L}{D}\right)_{max}$ and C_L at untrimmed $\left(\frac{L}{D}\right)_{max}$.

Figure 55.- Continued.

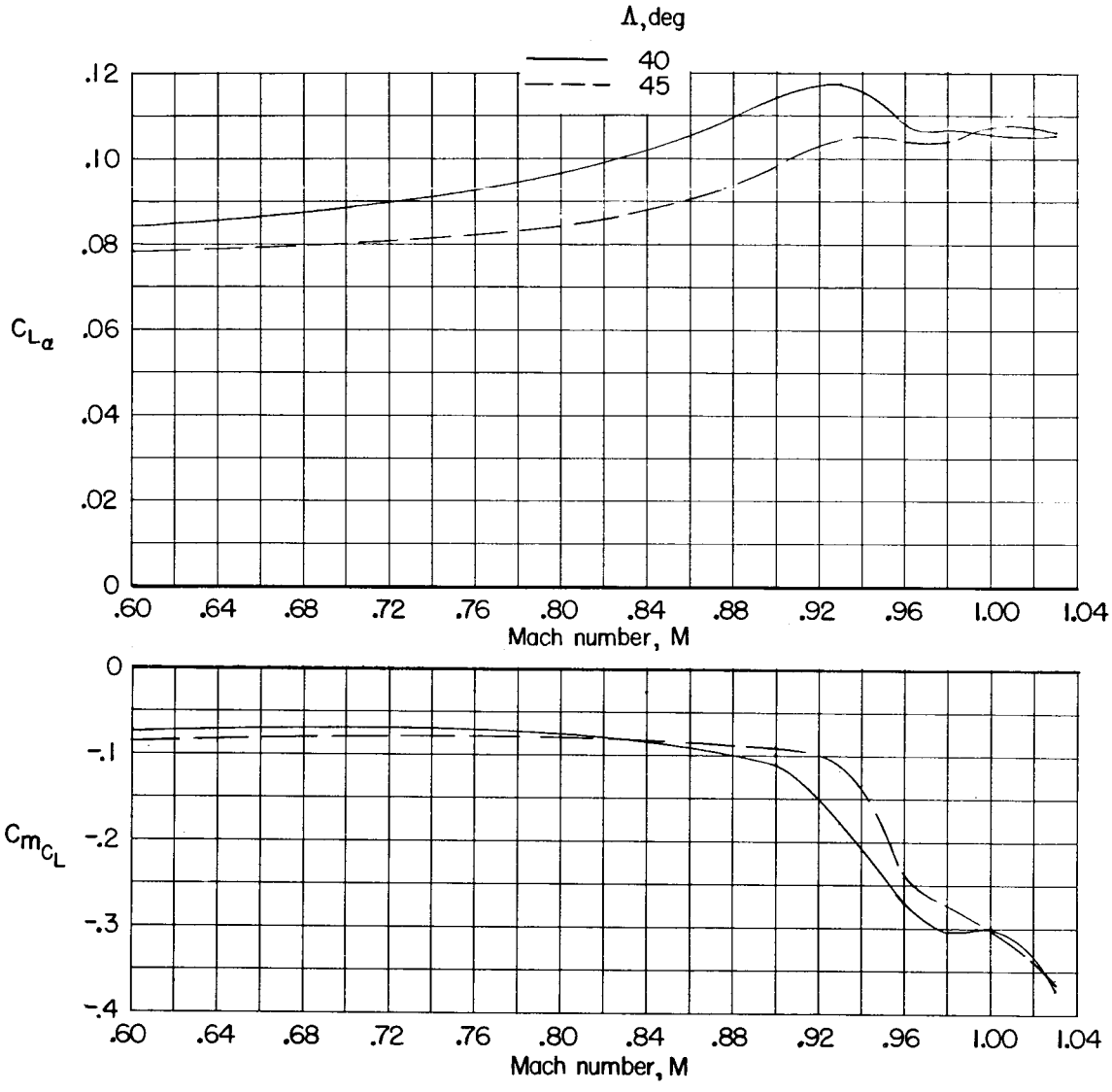

(c) C_{L_α} and $C_{m_{C_L}}$.

Figure 55.- Concluded.

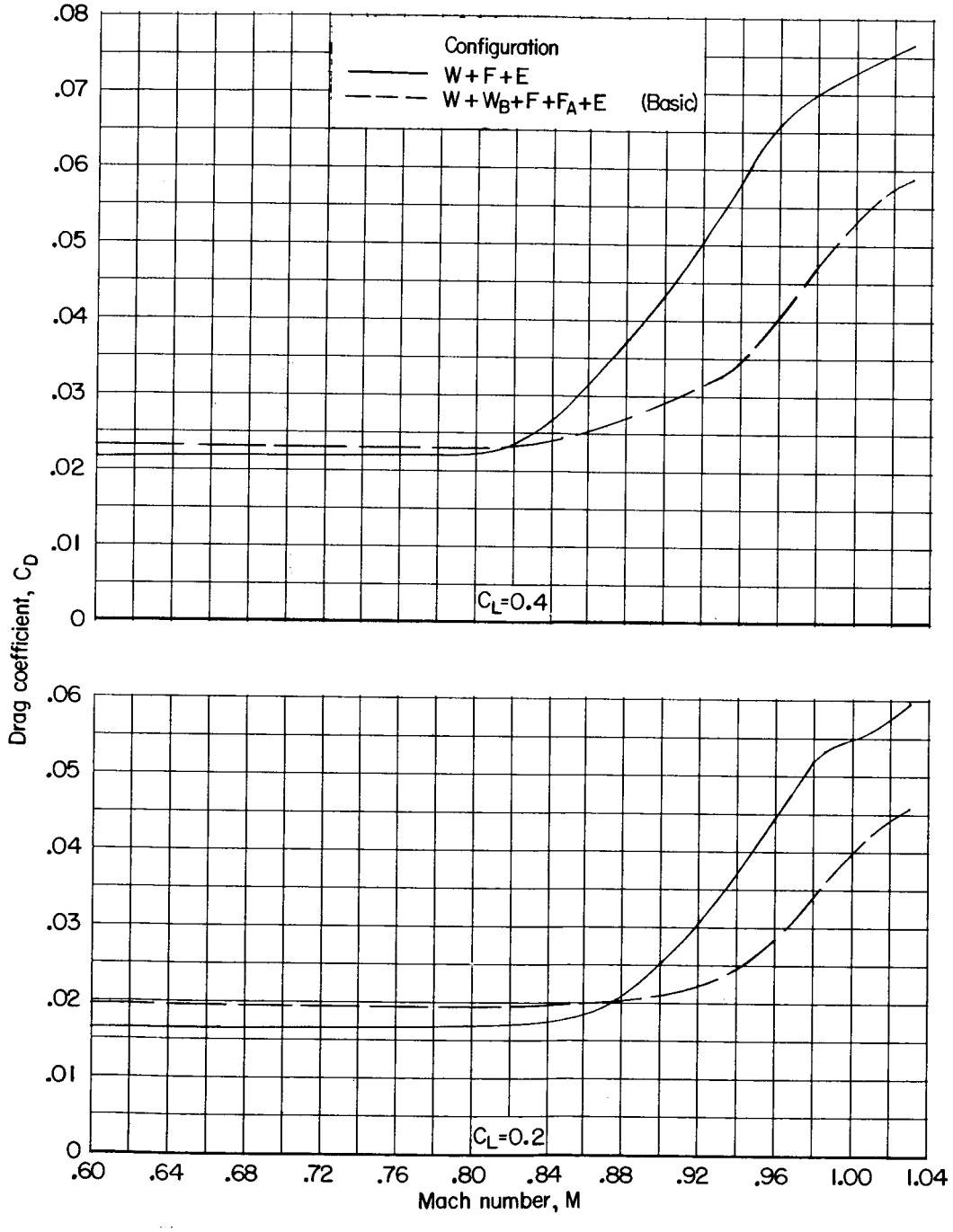

(a) C_D.

Figure 56.- Variation with Mach number of aerodynamic characteristics of model without and with basic additions. $\Lambda = 40^\circ$; $\Gamma = 6^\circ$; $\beta = 0^\circ$.

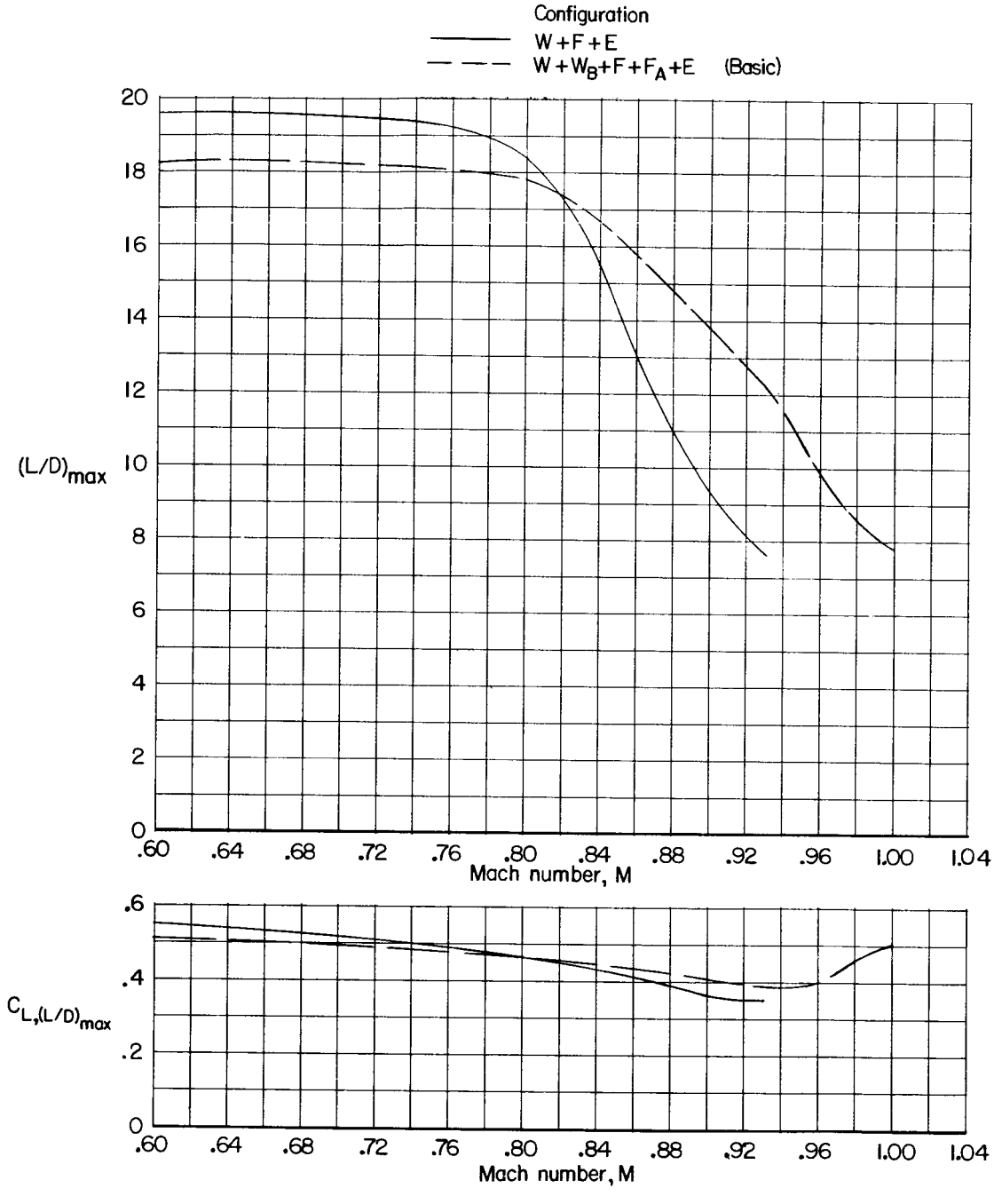

(b) Untrimmed $\left(\frac{L}{D}\right)_{max}$ and C_L at untrimmed $\left(\frac{L}{D}\right)_{max}$.

Figure 56.- Continued.

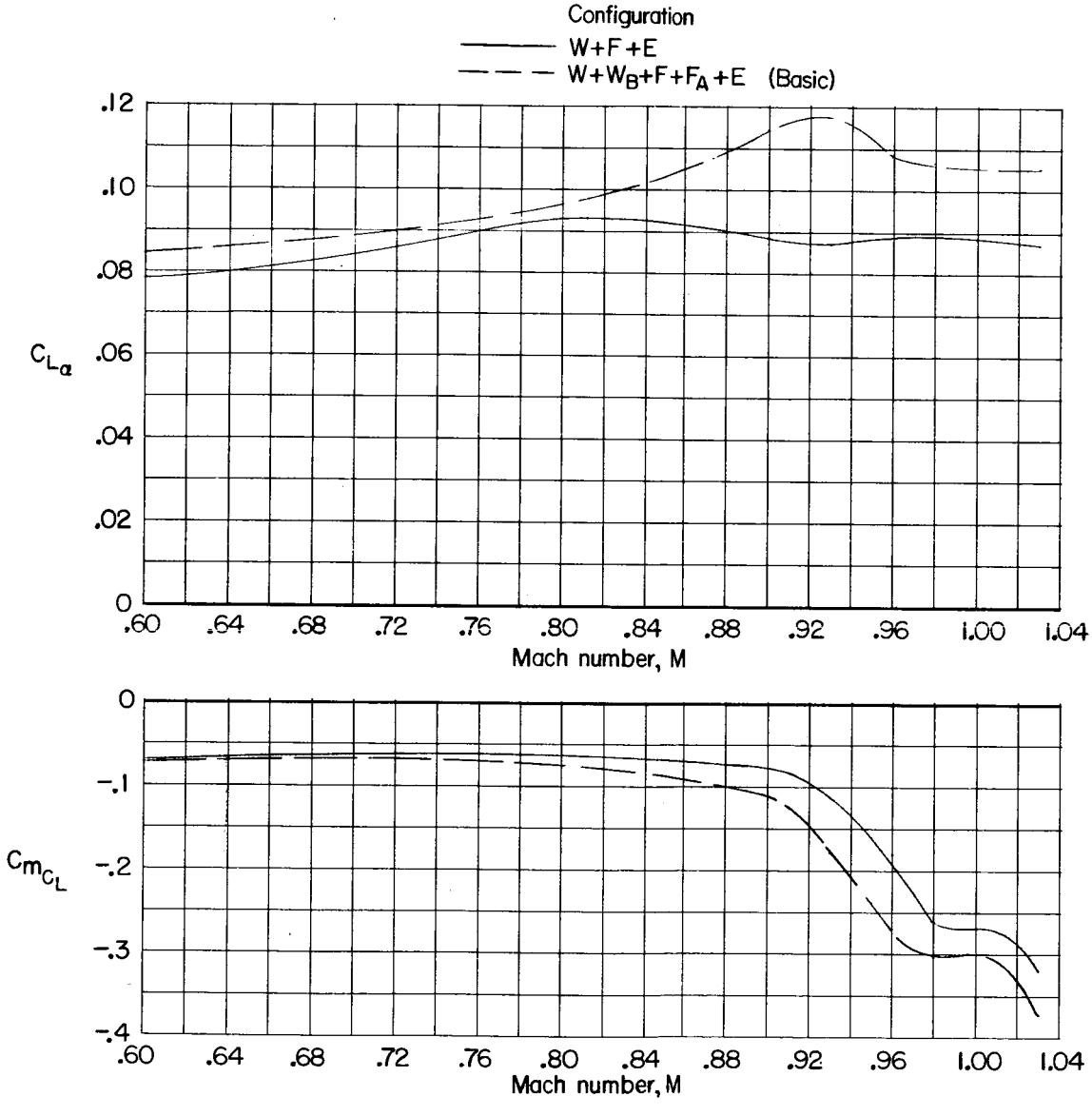

(c) C_{L_α} and $C_{m_{C_L}}$.

Figure 56.- Concluded.